國 立 交 通 大 學

應 用 化 學 研 究 所

博 士 論 文

高效能水溶性量子點之製備與其在生物檢測之應用

Preparation of High Performance Water-Soluble Quantum Dots and Their Applications in Bioassay

研 究 生：黃靜萍

指導教授：陳登銘　博士

李耀坤　博士

中華民國九十七年一月

授權書

（博碩士論文）

本授權書所授權之論文為本人在　國立交通大學　應用化學研究所
無機　組　96 學年度第 2　學期所撰 博士 學位論文 。

論文名稱:

□同意　■不同意

本人具有著作財產權之論文提要，授予國家圖書館、本人畢業學校及行政院國家科學委員會科學技術資料中心，得重製成電子資料檔後收錄於該單位之網路，並與台灣學術網路及科技網路連線，得不限地域時間與次數，以光碟或紙本重製發行。

■同意　□不同意

本人具有著作財產權之論文全文資料，授予行政院國家科學委員會科學技術資料中心，得不限地域時間與次數以微縮、光碟重製後發行，並得享該中心微縮小組製作之研究報告、獎勵代表作、博碩士論文三檔資料等值新台幣伍佰元之服務。本論文因涉及專利等智慧財產權之申請，請將本論文全文延後至民國 _102_ 年 __ 月後再公開。

□同意　■不同意

本人具有著作財產權之論文全文資料，授予教育部指定送繳之圖書館及本人畢業學校圖書館，為學術研究之目的以各種方法重製，或為上述目的再授權他人以各種方法重製，不限時間與地域，惟每人以一份為限。

上述授權內容均無須訂立讓與及授權契約書。依本授權之發行權為非專屬性發行權利。依本授權所為之收錄、重製、發行及學術研發利用均為無償。

指導教授姓名: 陳登銘博士 李耀坤博士

研究生簽名: 黃靜萍　學號: 9318822
(親筆正楷)

日期: 民國 97 年 01 月 21 日

備註: 1. 上述同意與不同意之欄位若未勾選，本人同意視同授權。
2. 授權第二項者，請再交論文一本予承辦人員。
3. 本授權書已於民國 85 年 4 月 10 日送請著委會修正定稿。

簽署人須知

1. 依著作權法的規定，任何單位以網路、光碟與微縮等方式整合國內學術資料，均須先得到著作財產權人授權，請分別在三種利用方式的同意欄內鈎選並填妥各項資料。
2. 所謂非專屬授權是指被授權人所取得的權利並非獨占性的使用權，授權人尚可將相同的權利重複授權給他人使用；反之即為專屬授權，如果您已簽署專屬授權書予其他法人或自然人，請勿簽署本授權書。
3. 授權人的權利與義務:在美國授權博碩士論文予ＵＭＩ公司(博碩士論文全文資料發行公司)製作發行，須交付美金 45 元的出版費，銷售年逾七件以上時得享收入 10%的權利金約美金 20 元；在國內本計畫之經費全數由政府支應，收入亦應歸國庫，為答謝您的支持，科資中心特為您提供新台幣 500 元的等值資料服務(以研究報告、獎勵代表作、博碩士論文三擇為限)，請逕洽本案聯絡人，地址電話詳如第５項。義務方面唯一要注意是，著作人日後不可以主張終止本授權書，但您仍可以授權其他自然人或法人上述的行為。
4. 全國博碩士論文全文資料微縮片整合計畫的宏觀效益:在個人方面，您的論文將可永久保存（微縮技術在理論上可保存八百年，實證已逾百年），也因為您的授權，使得後進得以透過電腦網路與光碟多管道檢索，您的論文將因而被充分利用。在國家總體利益方面，紙本容易因影印而造成裝訂上的傷害，圖書館中孤本的公開陳列與外借也有破損之虞，唯有賴政府全面性的整合，借助科技設備才能一舉完成保存與利用的全方位效益，回憶您過去尋找資料之不便經驗，學弟與學妹確實須要您的論文與授權書。
5. 本案聯絡電話: (02)7377746 江守田、王淑貞地址: 台北市和平東路二段 106 號 17 樓 1702 室

研究生姓名: 黃靜萍 聯絡電話: 0961502571

地址: 屏東市公華街241巷69-1號

國立交通大學

論文口試委員會審定書

本校 應用化學 學系博士班 黃靜萍 君

所提論文 高效能水溶性量子點之製備與其在生物檢測之應用
(Preparation of High Performance Water-Soluble Quantum Dots and Their Applications in Bioassay)

合於博士資格標準、業經本委員會評審認可。

口試委員：

指導教授：

系主任： 教授

中華民國 九十七年01 月 16 日

高效能水溶性量子點之製備與其在生物檢測之應用

研究生:黃靜萍　　指導教授:陳登銘　博士

李耀坤　博士

國立交通大學應用化學所博士班

中文摘要

本論文研究係以水溶性量子點硫醇琥珀酸修飾硒化鎘/硫化鋅製備尿素、葡萄糖及三酸甘油脂等生物分子指示劑，更進一步合成高效能水溶性量子點建立量子點螢光共振能量檢測系統，最終將其應用於生物分子之檢測。

因水溶性量子點螢光強度易受環境中酸鹼值之影響，當量子點暴露於鹼性環境時，其螢光強度隨環境中鹼性強度增加而增強；藉由光譜分析可明顯追蹤其放射光譜產生紅位移之現象，此係因鹼性環境下可減少量子點表面之缺陷與其結構之修飾，造成有效電子-電洞結合率增加所致。利用上述特性，本研究亦探討尿素經尿素酶水解反應後產生鹼性物質，致使螢光產生變化故可藉以分析樣品內尿素之含量。反之，當量子點暴露於酸性環境時，其螢光強度隨酸強度增加而降低，造成其放射光譜產生藍位移之現象，此係酸性環境中量子點表面缺陷增加，而電子-電洞結合率降低所致。另一方面，本研究亦利用葡萄糖氧化酵素催化葡萄糖，因其反應後形成酸性產物，故可藉量子

點之螢光變化分析樣品中葡萄糖含量。為增強量子點之螢光強度及脂質被分析物之偵測，本研究藉由光氧化提升量子點螢光效率，並改善其表面疏水性，以提升脂質被分析物之溶解度；本論文亦藉量子點之光活化以結合解脂酵素水解三酸甘油脂，最終利用螢光強度變化以偵測三酸甘油脂。

本研究結合高分子包覆聚二烯丙基二甲基氯化銨與光活化製程可合成量子效率高達 48%水溶性且放射波長不同範圍之高效能量子點，此高效能之螢光特性可應用於螢光共振能量轉移系統，建立檢測生物分子之分析模型。本研究利用具高正電荷之聚二烯丙基二甲基氯化銨所修飾量子點與類固醇賀爾蒙酵素以自組裝方式形成複合物，結合已標定有機染料四甲基羅達明的膽酸目標物，探討量子點與有機染料間螢光共振能量轉移現象，並掌握膽酸與類固醇賀爾蒙酵素之鍵結能力，以作為生物分子檢測系統之基礎。

Preparation of High Performance Water-Soluble Quantum Dots and Their Applications in Bioassay

Student: Chin-Ping Huang Advisor: Dr. Teng-Ming Chen
Dr. Yaw- Kuen Li

This research focuses on the design and preparation of molecular bioindicators for semi-quantitative determination of urea, glucose, and triglycerides by using water-soluble mercaptosuccinic acid (MSA)-capped CdSe/ZnS quantum dots (QDs) (MSA-QDs). Furthermore, we have also attempted to synthesize high performance water-soluble MSA-QDs and establish a bioassay based on fluorescence resonance energy transfer (FRET) principle that was then utilized in bioassay.

The fluorescence intensity of MSA-QDs, highly sensitive to the acidity/basicity of the environment, was discovered to increase with increasing basicity and a red-shifting in emission wavelength has been observed. This observation was attributed to the reduction of surface defects and modified surface structure of MSA-QDs in a basic environment that further increases the recombination probability of holes and electrons. On the contrary, a blue-shifting in emission wavelength was observed when MSA-QDs was exposed to an acidic environment and the fluorescence intensity was found to decrease with increasing acidity, which is attributed to the surface defects formation and lowering probability of electron-hole recombination. Therefore, the assay of urea and glucose has been demonstrated by monitoring the changes of basicity and acidity, respectively, when urea and glucose are hydrolyzed by urease and glucose oxidase in a series of analytes.

In order to realize the feasibility of detection for lipid analytes, we have improved the fluorescence intensity and activated the surface

hydrophobicity (to enhance the solubility of lipid) of MSA-QDs by carrying out photoactivation under fluorescent lamp irradiation. The assay of triglyceride has been demonstrated by monitoring the change of fluorescence intensity of MSA-QDs when triglyceride is hydrolyzed by lipase in the analytes.

We have also demonstrated that a series of highly efficient, wavelength-tunable or multicolored and poly(diallyldimethylammonium chloride) QDs (PDDA-QDs) with quantum efficiency of ~48% can be synthesized through PDDA capping and photoactivation process. The most challenging task of this research is to investigate and utilize the binding affinity between tetramethylrodamine (TMR)-labeled cholic acid (CA) and self-assembled 5-3-ketosteroid isomerase (KSI) by assuming TMR-CA as the energy donor and PDDA-QDs as the acceptor. Based on the principle of fluorescence resonance energy transfer (FRET) from TMR-CA-KSI to PDDA-QDs, our research results exhibit great potential applications in establishing effective assay systems for quantitative determination of a wide variety of biomolecules.

誌謝

本論文得以順利完成，要感謝許多人給予學生在博士班的學習生涯中不斷的幫助。首先，學生要誠摯地感謝兩位指導教授陳登銘博士與李耀坤博士，這三年來對學生耐心指導與鼓勵，讓學生能順利完成博士學業。從碩士至博士求學期間，陳老師不斷的啟發學生研究精神並給予學生足夠空間與想法進行相關研究，使得學生於材料之研究上有更多更新穎之方向並完成本論文；接下來，要感謝李耀坤老師在學生博士班研究路上不斷的提供學生資源與訓練學生各方面之能力(研究方向思考，數據的判讀，邏輯思考..等)，又加上老師常有獨到之見解，不僅開啟學生之視野，更啟發學生獨立思考之能力。

學生能順利口試而獲得碩士學位，要感謝口試委員們，首先要感謝工研院化工所副所長王先知博士在百忙中抽空給予學生指導與建議，也要感謝張大慈老師與林立元老師給予學生撰寫論文之相關建議，使論文之內容更為嚴謹與充實，再次感謝李積琛老師不僅是學生博士計劃口試也是學生博士口試之口委，李老師提供學生許多材料性質之分析方法與論文之指導。古語說：「以銅為鏡，可以正衣冠，以史為鏡，可以知興替，以人為鏡，可以明得失」。亦有一語: 「舜何人也，宇何人也，有為者，亦若是」。由於有老師所立下之模範，讓學生有學習之榜樣與追逐之目標，奠定學生在學問研究及品德涵養上的基礎，感謝老師不辭辛勞的指導學生。

在研究工作上，首先要感謝陳登銘老師實驗室同學們的支持與鼓勵，李耀坤老師實驗室學長-可欣熱情的提供所合成的蛋白質與分析物，及實驗室同學們的鼓勵；接下來要感謝材料系-蓉萱熱情的幫我利用貴儀相關儀器量測樣品，也教我許多儀器操作，更是我的生活心得分享夥伴陪我度過研究生活中的酸甜苦辣。感謝你們陪伴我度過這段美好的日子，因為有你們，我的生活更多采多姿。

最後，感謝我的父母、家人與未婚夫-建尉，讓我無經濟壓力下完成博士學位，也陪我渡過研究生涯中的高、低潮，並給予精神支持與關懷鼓勵，在此，願將一切榮耀與成就獻給我所深愛的家人。

Contents

中文摘要		ii
Abstract		iv
致謝		vi
Contents		vii
Index of Figures		xi
Index of Tables		xvi
Abbreviations		xvii
Chapter 1	**Background**	**1**
1.1	Properties of Quantum dots	1
1.2	Reviews of the Quantum dots	8
1.2.1	Surface modification of Quantum dots	8
1.2.2	Photoactivation on the Quantum dots	15
1.2.3	Application of the Quantum dots	18
1.3	Motivations	22
1.4	Thesis organization	24
1.5	Reference	26
Chapter 2	**Synthesis the water-soluble CdSe/ZnS quantum dots and their application**	**29**
2.1	Introduction	30

2.2	Materials and Methods	34
2.2.1	Surface modification of Quantum dots	34
2.2.2	Instruments and Chemicals	34
2.2.3	Synthesis of water-soluble MSA-capped CdSe/ZnS QDs	35
2.2.4	Assay conditions and PL measurements for glucose indicator	36
2.3	Results and discussion	36
2.3.1	Optical characterization of MSA capped CdSe/ZnS	36
2.3.2	Influence of pH on luminescence of MSA-CdSe/ZnS	38
2.3.3	Photoluminescence spectroscopy for the detection of urea	40
2.3.4	Influence of GOD on photoluminescence of MSA- QDs	44
2.3.5	Photoluminescent spectroscopy of the detection of glucose	46
2.4	Conclusions	50
2.5	Reference	51
Chapter 3	**Investigation of the photoactivated CdSe/ZnS quantum dots and their application**	**55**
3.1	Introduction	56
3.2	Materials and Methods	58
3.2.1	Instruments and chemicals	58
3.2.2	Photoactivation of CdSe/ZnS QDs	59
3.2.3	Assay conditions and PL measurements	60

3.3	Results and Discussion	61
3.3.1	Characterization of the photoactivation of CdSe/ZnS QDs	61
3.3.2	Influence of pH on the photoluminescence of POD-QDs	65
3.3.3	Photoluminescence spectroscopy for the detection of triglyceride	66
3.4	Conclusion	73
3.5	Reference	74
Chapter 4	**Synthesis and Charac- terization of Poly (diallyldimethylammonium chloride) capped CdSe/ ZnS quantum dots via photoactivation for Fluorescence Resonance Energy Transfer application**	76
4.1	Introduction	77
4.2	Materials and Methods	79
4.2.1	Instruments and chemical	79
4.2.2	Synthesis of the Poly (diallyldimethylammonium chloride) solution (PDDA) capped CdSe/ZnS quantum dots via photoactivation	80
4.2.3	Conditions of the agarose gel electrophoresis	81
4.2.4	Conditions of the Rhodamine X-labeling on Streptavidin	81
4.2.5	Assay condition of the FRET between PDDA-QDs with Rhodamine X-Streptavidin	82
4.3	Results and Discussion	82
4.3.1	Optical properties of the PDDA-QDs via photoactivation	82
4.3.2	Surface and Size Characterization of the PDDA-QDs via photoactivation	88

4.3.3	Fluorescence resonance energy transfer with the PDDA-QDs and SAv-Rhodamine	94
4.4	Conclusions	97
4.5	Reference	99
Chapter 5	**FRET-based biosensing via PDDA-QDs/KSI and Cholic acid-TMR**	101
5.1	Introduction	102
5.2	Materials and Methods	102
5.2.1	Instruments and chemicals	105
5.2.2	Assay condition of the FRET between PDDA-QDs with KSI-TMR	105
5.2.3	Assembly of the KSI-Bound Dye-Labeled analogue with QDs and FRET Quenching Assays	105
5.3	Results and discussion	108
5.3.1	Spectra	108
5.3.2	FRET efficiency between PDDA-QDs with KSI-TMR	109
5.3.3	Assembly of the KSI-Bound Dye-Labeled analogue with QDs and FRET Quenching Assays	111
5.4	Conclusion	117
5.5	Reference	118
Chapter 6	**Conclusion**	120

Index of Figures

Figure 1.1 Represent QDs core materials scaled as a function of their emission wavelength superimposed over the spectrum [3] 1

Figure 1.2 Quantum dots can be synthesized from various types of semiconductor materials (II-VI: CdS, CdSe, CdTeI; III-V: InP, InAsI; IV-VI: PbSeI) characterized by different bulk band gap energies. 2

Figure 1.3 Absorption (upper) and emission (lower) spectra of four CdSe/ZnS qdot samples. 3

Figure 1.4 Nanocrystal surrounded by TOPO chains anchored to its surface 5

Figure 1.5 Bared CdSe QDs and inorganic surface passivation core/shell QDs (a) organic matrix (b) CdS shell (c) ZnS passivation on CdSe surface [13-15] 6

Figure 1.6 Photobleaching curves showing that QDs are several thousand times more photostable than organic dyes (e.g. Texas red) under the same excitation conditions [19] 7

Figure 1.7 Qdot solubilization and functionalization. 9

Figure 1.8 Scheme of the polymer coating procedure. 11

Figure 1.9 Formation of the polymer-QD complex showing an idealized micellar polymer shell (40% octylamine-modified PAA) encapsulating the QDs [34] 12

Figure 1.10 (a) Schematic of the CdSe-ZnS core-shell nanoparticle with dihydrolipoic acid surface capping groups; (b) cartoon of the S-S linked MBP-zb homodimer and detail showing nucleotide and primary amino acid sequences of the C-terminal basic leucine zipper interaction domain. 13

Figure 1.11 Absorption (A) and emission (B) spectra of CdSe@CdS nanocrystals (Cd/Se 8:1) measured after different irradiation times in air. (B): Luminescence spectrum after exposure to light for 15 days [35] 15

Figure 1.12 Suggested schematics of photoinduced luminescence enhancement. 17

Figure 1.13 Scheme of Maltose-Dependent Change in CdSe Emission [42] 19
Figure 1.14 Maltose-dependent fluorescence of complex **1** modified-K46C MBP-MT attached to 3.0-3.5 nm diameter THDA capped CdSe nanoparticles under 363 nm excited) at pH 7.5 (20 mM 3-(*N*-morpholino)propanesulfonic acid, MOPS) 19
Figure 1.15 Principle of Quantum Dots-Based Enzymatic Activity Probes [43] 20
Figure 1.16 Emission spectra of rhodamine-labeled peptide-coated quantum dots 15 min following the addition of collagenase of increasing concentration. 21
Figure 2.1 The structure of MSA assembled on the surface of QD 31
Figure 2.2 (a) The absorption spectrum (b) photoluminescence spectrum of MSA-QDs with different size in 50 mM phosphate buffer solution 37
Figure 2.3 PL spectrum of MSA-QDs at different pH values 39
Figure 2.4 The correlationship between the PL intensity monitored at 586 nm of QDs and pH value 39
Figure 2.5 The variation of PL spectra of urease/QDs with urea concentration. 41
Figure 2.6 The variation of pH value and PL intensity with urea concentration. 42
Figure 2.7 UV-Visible and photoluminescence spectra of the MSA-CdSe/ZnS QDs and GOD. 45
Figure 2.8 The influence of GOD in PL enhancement of MSA-CdSe/ZnS QDs. 45
Figure 2.9 The emission spectra of the assay samples at the end-point of the reaction. 47
Figure 2.10 Correlation between the quench ratio of PL intensity, pH perturbation and the tested glucose concentration. Two assay system, 10 mM and 30 mM phosphate, pH 8.0, were employed. 48
Figure 2.11 Fluorescent photos of the assay samples. Samples were excited by 365 nm sources. 50
Figure 3.1 The scheme of triglyceride indicator by POD-QDs 58
Figure 3.2 The spectrum of 21-Watt fluorescent light 60

Figure 3.3 the PL spectrum of MSA-QDs irradiated under the fluorescent light with different times 62
Figure 3.4 A trend spectrum of the maximum emission peak and the PL intensity under different irradiation times 62
Figure 3.5 The postulate decay route of an exciton generated in CdSe/ ZnS quantum dots [5] 64
Figure 3.6 Comparison of PL spectra of MSA-QDs (—) and POD-QDs (----) under excitation at 365 nm. 65
Figure 3.7 Comparison of PL spectra for POD-QDs as a function of pH. The inset reveals correlation between PL quenching ratio of POD-QDs and pH, 100 $(I_o- I)/I_o$ represents the ratio of PL quenching, I_0 is the PL intensity at 570 nm with pH 8.0, and I is the intensity at emission maximum 66
Figure 3.8 Variation of PL intensity of POD-QDs as a function of tributyrin concentration in 10 *m*M phosphate buffer. 68
Figure 3.9 Absorption spectra of lipase/POD-QDs with different tributyrin concentration (0, 4 and 10 mM) in 10 mM phosphate buffer with pH 8.0. 69
Figure 3.10 Linear correlation between quenching percentage of PL intensity, $[100 (I_0 - I)/I_0]$, and tributyrin concentration. 70
Figure 3.11 Evolution of fluorescence images taken at the end-point of the catalytic hydrolysis of tributyrin in 10 *m*M phosphate buffer under ultraviolet irradiation of 365 nm 72
Figure 4.1 The optical characterization of different capping molecular on QDs, MSA capped (。。。); HDA capped (—); PDDA capped (●●●) under 365 nm excited 84
Figure 4.2 The time evolution of the emission intensity for PDDA-QDs and demonstrates that photoetching or photooxidation of the PDDA-QDs 86
Figure 4.3 The photoluminescence and images (inset) with the multicolor of the PDDA-QDs, which emission peaks centered at 535 nm (Green), 555nm (Yellow) and 580 nm (Red), when these were excited by 365 nm 87

Figure 4.4 The gel electrophoresis of MSA-QD and PDDA-QD were drove by 100 89
Figure 4.5 the multicolor of PDDA-QDs with various sizes. 90
Figure 4.6 Multiple XPS measurements of MSA-QDs (Black line) and PDDA-QDs (Red line) by Mg Kα source 92
Figure 4.7 The appearances of (a) $Cd3d_{5/2}$ at 407 eV (409 eV), $Cd3d_{3/2}$ at 413.8eV (416 eV), (b) Se 3d at 55.1eV (55.9eV), (c) C 1s at 287 eV (288 eV) and (d) O 1s at 533 eV(534 eV) confirmed the existence of Cadmium, selenium, carbon and oxide in both the MSA-QDs (—) and PDDA-QDs (—。—), repecticely 93
Figure 4.8 Fluorescence emission spectra from solutions containing 92 nM PDDA-QD and 0~645 nM SAv-Rhodamine by molar ratio. 95
Figure 4.9 PL and FRET efficiencies as a function of the SAv-Rhodamine/PDDA-QDs molar ratio 96
Figure 4.10 The fluorescence of SAv-Rhodamine/PDDA- QDs with molar ratio (0- 8) under 365 nm excited 97
Figure 5.1 Reaction catalyzed by ketosteroid isomerase. The α proton at C-4 is transferred to the α side of C-6 during the isomerization reaction. 104
Figure 5.2 FRET-based biosensing model via PDDA-QD/KSI and CA –TMR 106
Figure 5.3 Normalized spectra of (a) emission of PDDA-QDs (530 nm) (b) emission of PDDA-QDs (543 nm) (c) absorption of CA-TMR (d) emission of CA-TMR (580 nm) excited 400 nm. 108
Figure 5.4 PL spectrum of the PDDA-QDs (530 nm) donor and TMR dye (580nm) acceptor for each ratio (in titration series KSI-TMR) for the PDDA-QDs-due pairs used 109
Figure 5.5 PL and FRET efficiencies as a function of the KSI-TMR /PDDA-QDs molar ratio 110
Figure 5.6 The emission spectrum observed from a sample containing 0.33 μM PDDA-QDs, 0.33μM PDDA-QDs/ 2.1μM KSI-TMR and 2.1μM KSI-TMR under 400 nm excited 111
Figure 5.7 Emission spectra obtain from 0.495μM PDDA-QDs/ 2.99μM KSI and varying amounts of CA-TMR (0 to 0.89μM) are also shown for comparison. 113

Figure 5.8 The FRET efficiency between PDDA-QDs-KSI and Bile-TMR are obtained from Figure 5.7 113
Figure 5.9 Emission spectra obtain from 0.495μM PDDA-QDs and varying amounts of CA-TMR (0 to 0.77μM) are also shown for comparison. 114
Figure 5.10 The scheme of sensing model with PDDA-QDs/KSI in the mixed solution (CA-TMR and 19NT) 116
Figure 5.11 shows a typical experiment examining changes in the FRET efficiency of 543 nm emitting PDDA-QDs with increasing concentrations of mixed solutions (CA-TMR and 19NT) 116
Figure 6.1 Summaries of the research areas 123

Index of Tables

Table 2.1 Summering the characterizations of optical and size with MSA-QDs 38

Table 2.2 Comparison of performance of different urea sensors 43

Table 3.1 Comparison of performance of different methods for the detection of triglycerides 72

Table 4.1 The binding energy intensity and the atomic amount of MSA-QD and PDDA-QD 94

Abbreviations

Symbol	Full name
19NT	4-Estren-17b-OL-3-ONE
CA	Cholic acid
CdS	Cadium Sulfide
CdSe/ZnS	Cadmium selenide/ Znic Sulfide (core/shell structure)
ConA	Concanavalin A
DHLA	dihydroxylipoic acid
FAD	flavin adenine dinucleotide
F_D	The integrated fluorescence intensity of donor alone (no acceptor present)
F_{DA}	The integrated fluorescence intensity of the donor in the presence of acceptor(s)
FRET	Förster resonance energy transfer
FWHM	Full-width half-maximum
G-25	Sephadex G
GOD	glucose oxidase
HDA	n-hexadecylamine
KSI	△5-3-ketosteroid isomerase
MAA	Mercaptoacetic acid
MBP	Maltose binding protein
MMPs	Matrix metalloproteinases
MPA	Mercaptopropionic acid
MSA	Mercaptosuccinic acid
MSA-QDs	Mercaptosuccinic acid capped quantum dots
NP	Nanoparticle
PAA	Polyacrylic acid

PDDA	Poly (diallyldimethylammonium chloride) solution
PDDA-QDs	Poly (diallyldimethylammonium chloride) solution quantum dots
PL	Photoluminescence
POD-QDs	Photoactivated quantum dots
QDs	Quantum dots
QY	Quantum yield
SA	Stearic acid
SAv	Streptavidin
SCKs	Shell cross-linked knedels
SeO_2	Selenium oxide
TBP	Tri-n-butylphosphine
TEM	Transmission electron microscopy
TMAOH	Tetramethylammonium hydroxide
TMR	Tetramethylrodaminme
TOP	Tri-n-octylphosphine
TOPO	Tri-n-octylphosphine oxide
UV-Vis	Ultraviolet-visible
XPS	X-ray Photoelectron Spectroscopy

Chapter 1 Background

1.1 Properties of Quantum dots

For nanocrystals smaller than the Bohr exciton radius (~ a few nanometers), energy levels are quantized, with values directly related to the Quantum dot size. These phenomenon are called quantum confinement, hence the name "Quantum dots" (QDs). Semiconductor QDs are single crystals a few nanometers in diameter whose size and shape can be precisely controlled by the duration, temperature, and capping ligand molecules used in the synthesis process [1-2]. Otherwise, QDs, also as nanocrystals, are a special class of materials known as semiconductors, which are composed of periodic groups of II-VI, III-V, and IV-VI materials. The various compositions of QDs have shown the emitting from the UV to the infrared range, which depend on the band gap of QDs. Figure 1.1 represent QDs core materials scaled as a function of their emission wavelength superimposed over the spectrum [3].

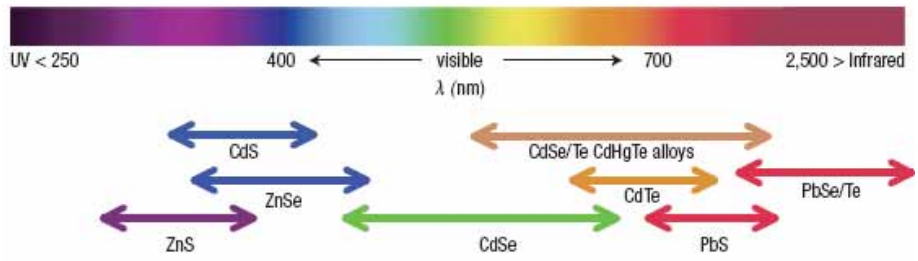

Figure 1.1 Represent QDs core materials scaled as a function of their emission wavelength superimposed over the spectrum [3].

These QDs have composition and size dependent absorption and emission (as shown in Figure 1.2) [3-10]. When absorption a photon with energy above the semiconductor band gap energy would result in the creation of an electron-hole pair (or exciton).

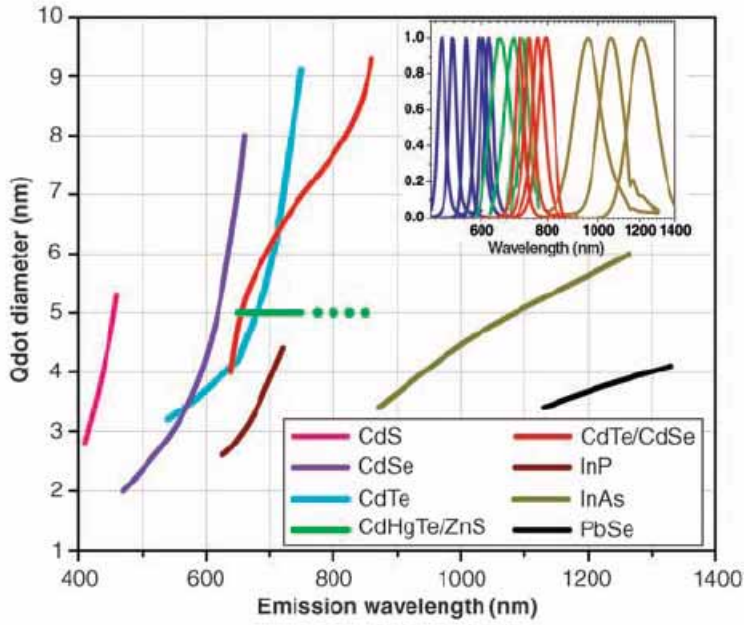

Figure 1.2 Quantum dots can be synthesized from various types of semiconductor materials (II-VI: CdS, CdSe, CdTeI; III-V: InP, InAsI; IV-VI: PbSeI) characterized by different bulk band gap energies. The curves represent experimental data from the literature on the dependence of peak emission wavelength on QDs diameter. The range of emission wavelength is 400 to 1350 nm, with size varying from 2 to 9.5 nm (organic passivation/solubilization layer not included). All spectra are typically around 30 to 50 nm (full width at half maximum). Inset: Representative emission spectra for some materials. Data are from [3-10]. Data for CdHgTe/ZnS have been extrapolated to the maximum emission wavelength obtained in Michalet's group.

According to Figure 1.3 [3], the broading absorption spectrum supported a wide excitation source chose. The radiative recombination of exciton leads to the emission of a photon in a narrow, symmetric energy band (shown in Figure 1.3). Bulk semiconductors only could display a rather uniform absorption spectrum; on the contrary, QDs would appear as a series of overlapping peaks in the absorption range. Owing once more to the discrete nature of electron energy levels in QDs, each peak corresponds to an energy transition between electron-hole (exciton) energy levels.

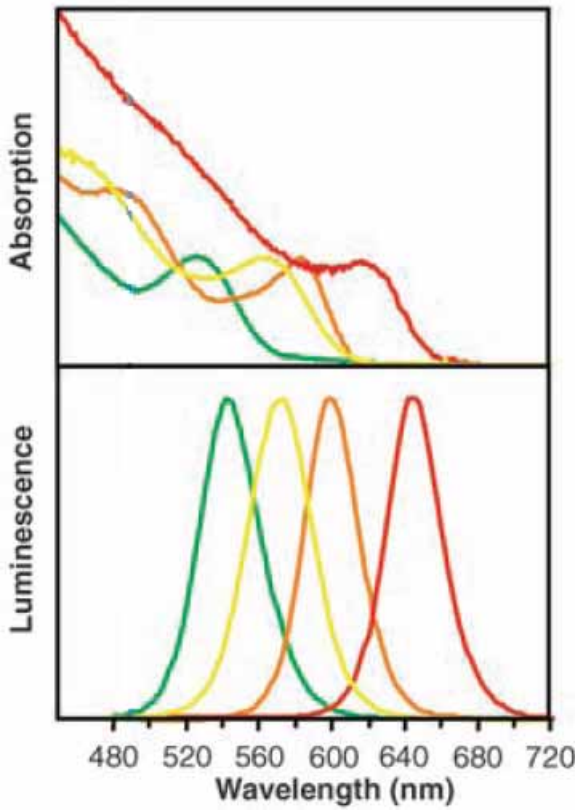

Figure 1.3 Absorption (upper) and emission (lower) spectra of four CdSe/ZnS qdot samples. The blue vertical line indicates the 488-nm line of an argon-ion laser, which can be used to efficiently excite all four types of QDs simultaneously [3].

Furthermore, the QDs would not absorb light that has a wavelength longer than that of the first exciton peak. Therefore, the wavelength of the first exciton peak is a function of the composition and size of the quantum dot. The emission peak is bell-shaped (Gaussian) and occurs at a slightly longer wavelength than the lowest energy exciton peak (absorption peak). Consequently, the fluorescence or absorption could be tunable by synthesized process, such as temperature, growth time et al.

Unfortunately, surface defects in the crystal structure act as temporary traps for the electron or hole, hindering their radiative recombination. If the alternation of trapping and untrapping events results in intermittent fluorescence visible at the single molecule level [11] and reduces the overall quantum yield, which is the ratio of emitted to absorbed photons. Overcoming these shortcomings, and protecting surface atoms from oxidation and other chemical reactions, is to grow a shell of few atomic layers of a material with a larger band gap on top of the nanocrystal core. The properties of core/shell QDs are highly dependant on the inorganic surface passivation and obey the principles of quantum well. Using the organic surfactant (e.g. TOPO or TOP) passivated and stabilized on the CdSe QDs (as shown in Figure 1.4) could not improve the drawback in the fluorescence efficiency [12]. As a result of imperfect surface passivation and rearrangement of the surface atoms, incomplete quantum confinement effect on the surface may takes place. Nevertheless, overcoating nanocrystal core with inorganic materials of higher band offsets has been to improve the photoluminescence quantum yield (QY). It could improve and eliminate

the nonradiative recombination sites on the surface.

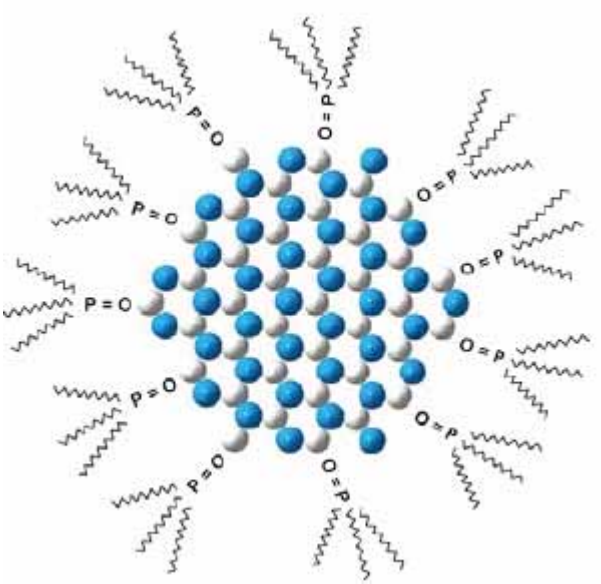

Figure 1.4 Nanocrystal surrounded by TOPO chains anchored to its surface [12].

As illustrated in Figure 1.5 (a-c) [13-15], ZnS or CdS shell capped CdSe QDs would provide higher quantum efficiency and photo stability due to the confinement of the carrier on the edge of the energy band offsets, and consequently reducing the loss of the carrier by trapping or tunneling [13-15]. This shell could be designed carefully to obtain quantum yields close to 90% [16]; this step also enhances QDs photostability by several orders of magnitude relative to conventional dyes [17]. As briefly noted above, QDs are made from inorganic semiconductors and have novel optical properties that can be used to optimize the signal-to-background ratio. Additionally, QDs have very large molar extinction coefficients in the order of $0.5\text{-}5\times10^{6}$ M cm^{-1}[18], which makes them bringhter than organic dye. In photostability, QDs are several thousand times more stable against photobleaching than

organic dyes (shown in Figure 1.6) and are thus well suited for continuous tracking studies over a long period of time [19].

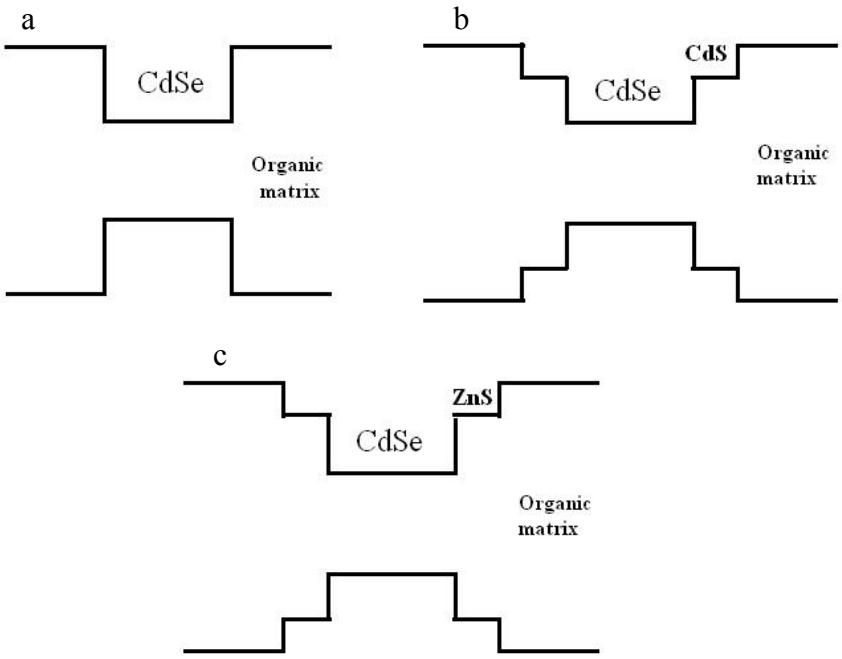

Figure 1.5 Bared CdSe QDs and inorganic surface passivation core/shell QDs (a) organic matrix (b) CdS shell (c) ZnS passivation on CdSe surface [13-15].

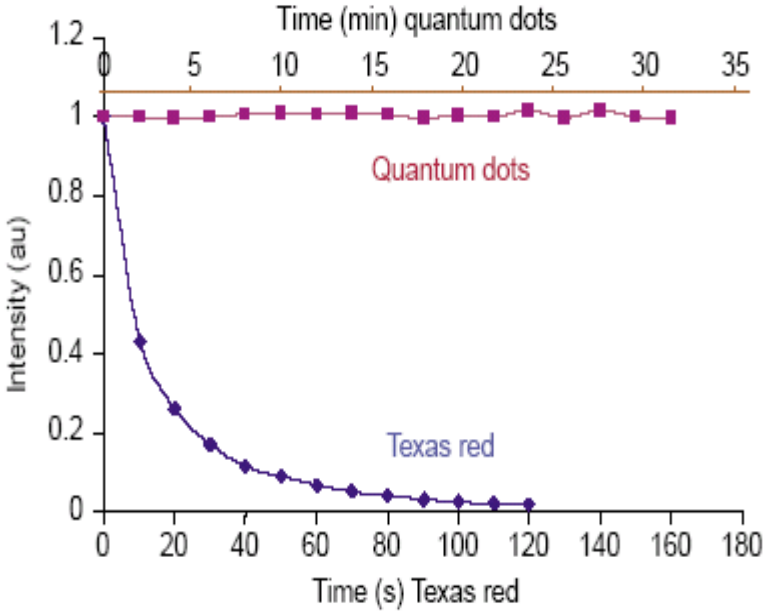

Figure 1.6 Photobleaching curves showing that QDs are several thousand times more photostable than organic dyes (e.g. Texas red) under the same excitation conditions [19].

1.2 Reviews of the Quantum dots

1.2.1 Surface modification of Quantum dots

In traditional methods, QDs could be prepared in the various media, from atomic deposition on solid-phases to colloidal synthesis in aqueous solution. However, the highly homogeneous and crystalline QDs are most important in the synthesis. Previous authors reported the highest quality QDs are typically prepared at elevated temperatures in organic solvents, such as tri-n-octylphosphine oxide (TOPO) and hexadecylamine, all of them are high boiling point bases containing long alkyl chains. These hydrophobic organic molecules serve as the capping agents that coordinate with unsaturated metal atoms on the QDs surface to prevent the formation of bulk semiconductor. Therefore, the organic ligands capped on the QDs surface and are only soluble in hydrophobic solvents, such as chloroform and hexane. For biological application, these hydrophobic QDs must first be made form water-soluble. As a result, different QDs solubilization strategies have been devised over the past few years, including (i) ligand exchange with simple thio-containing molecules [20-21] or more sophisticated ones, such as oligomeric phosphines [22], dendrons[23], and peptides[24]; (ii) encapsulation by a layer of amphiphilic diblock [25] or triblock copolymers[26] or in silica shells [4,27], phospholipid micelles [28], polymer beads [29], polymer shells [30], or amphiphilic polysaccharides [31]; and (iii) combinations of layers of different molecules conferring the required colloidal stability to QDs [3, 32] (as

shown in Figure 1.7).

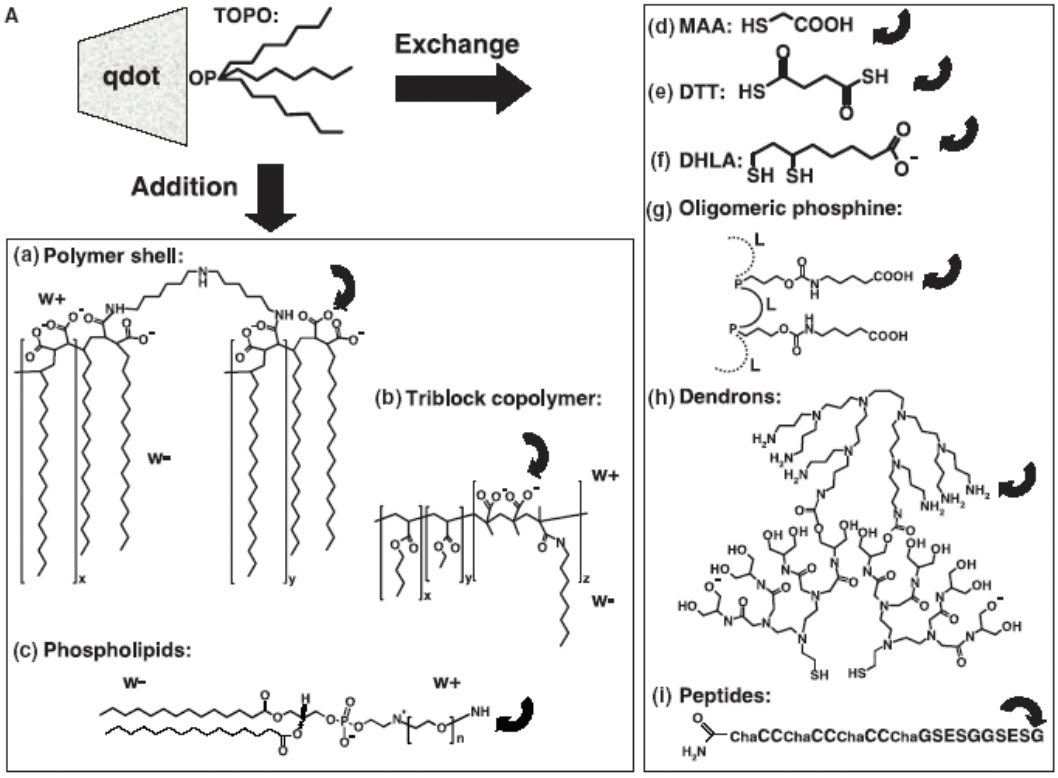

Figure 1.7 Qdot solubilization and functionalization. (A) Surface chemistries. TOPO (trioctylphosphine oxide)– passivated qdots can be solubilized in aqueous buffer by addition of a layer of amphiphilic molecules containing hydrophilic (wt) and hydrophobic (w–) moieties, or by exchange of TOPO with molecules that have a Zncoordinating end (usually a thiol group, SH) and a hydrophilic end. Examples of addition include (a) formation of a cross-linked polymer shell (30), (b) coating with a layer of amphiphilic triblock copolymer (25), and (c) encapsulation in phospholipid micelles (28). Examples of exchange include (d) mercaptoacetic acid (MAA) (20), (e) dithiothreitol (DTT) (21), (f) dihydrolipoic acid (DHLA) (32), (g) oligomeric phosphines (22), (h) cross-linked dendrons (22), and (i) peptides (24). The curved arrow indicates sites available for further functionalization [3].

For describing the above methods, we take some example and reported to depict them. In perceiving of QDs surface modification methods, as elaborated in the previous sections, it is clearly that the water-soluble QDs was prepared mostly by capping with a mercaptocarboxylic acid layer, such as mercaptoacetic acid (MAA), mercaptopropionic acid (MPA), and dihydroxylipoic acid (DHLA) etc. The main reason is that the thio group derivatives as a linkage has higher affinity binding than other functional groups on the QDs. For example, Chan and Nie (1998) [20] reported a method by using mercap toacetic acid for solubilization and covalent protein attachment. Sun (2001) used MSA to replace mercaptoacetic acid because one MSA molecule provides two carboxyl groups that may increase binding number of IgG on each QD [33]. In addition, the MSA layer is expected to reduce passive protein adsorption on QDs. In addition to this general method, the encapsulation on the hydrophobic QDs surface by polymer has recently been developed. Pellegrino (2004) have developed a simple and general strategy for decorating hydrophobic nanocrystals of various materials, such as CoPt, Au, CdSe/ZnS, and Fe_2O_3 with a hydrophilic polymer shell by exploiting the nonspecific hydrophobic interactions between the alkyl chains of poly(maleic anhydride alt-1-tetradecene) and the nanocrystal surfactant molecules . Then, addition of bis(6-aminohexyl)amine results in the cross-linking of the polymer chains around each nanoparticle (Figure 1.8). Therefore, the nanocrystal become soluble into water upon hydrolyzation of the unreacted anhydride groups [30].

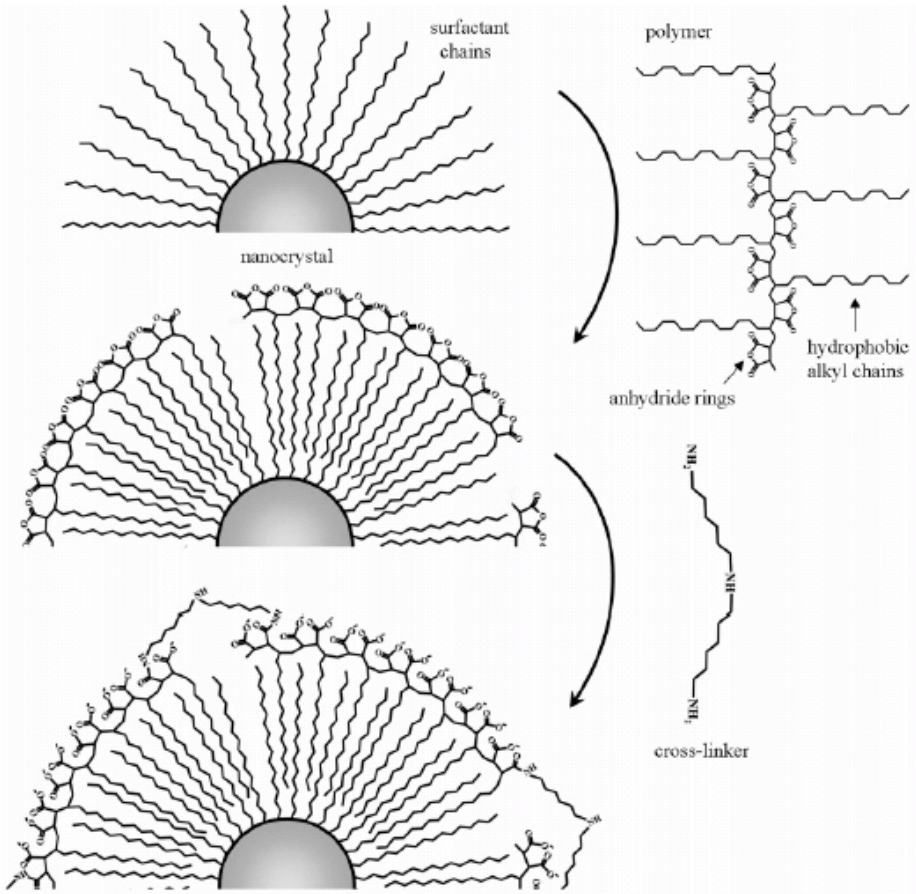

Figure 1.8 Scheme of the polymer coating procedure. The following plausible configuration is then assumed for the polymer coating process: The hydrophobic alkyl chains of the polymer intercalate with the surfactant coating. The anhydride rings are located on the surface of the polymer-coated nanocrystal. The amino end groups of the cross-linker molecule open the rings and link the individual polymer chains. The surface of the polymer shell becomes negatively charged, stabilizing the particles in water by electrostatic repulsion. A structural analysis aimed at determining the detailed conformation of the cross-linked polymer shell is in progress [30].

Petruska (2004) have successfully employed hydrophobically modified polymers to solubilize nanoparticle [34]. Using low-molecular weight polyacrylates modified with octyl chains were developed to stabilize and encapsulate QDs, rendering them soluble in polar media, e.g. water or alcohol. The amphiphilic polymer encases the nanoparticle, creating a micellar shell around QDs. Then, the hydrophobic groups are cross-linked to stabilize the QDs-polymer conjugate for preparing shell cross-linked knedels (SCKs) (as shown in Figure 1.9).

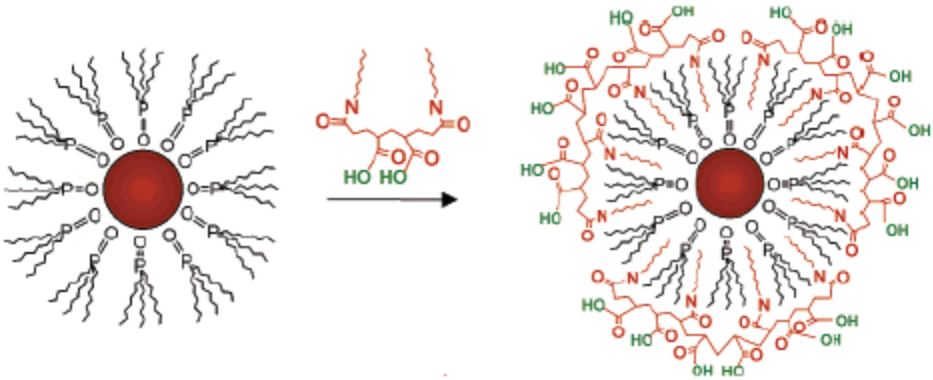

Figure 1.9 Formation of the polymer-QD complex showing an idealized micellar polymer shell (40% octylamine-modified PAA) encapsulating the QDs [34].

Mattoussi (2000) reported the strategy of combining the use of alkyl-COOH capped CdSe/ZnS (Figure 1.10) and two-domain recombinant proteins cloned with a highly charged leucine zipper tail offers several advantages. (1) The alkyl-COOH teriminated capping groups, which permit dispersion of the QDs into water solutions, also provide a surface charge distribution that can promote direct self-assembly with other molecules that have a net positive charge. (2)

The fusion protein approach provides a general and consistent way to prepare a wide selection of biological macromolecules amenable to alterations of the interaction domain, such as charge, size, stability to pH, and temperature [32].

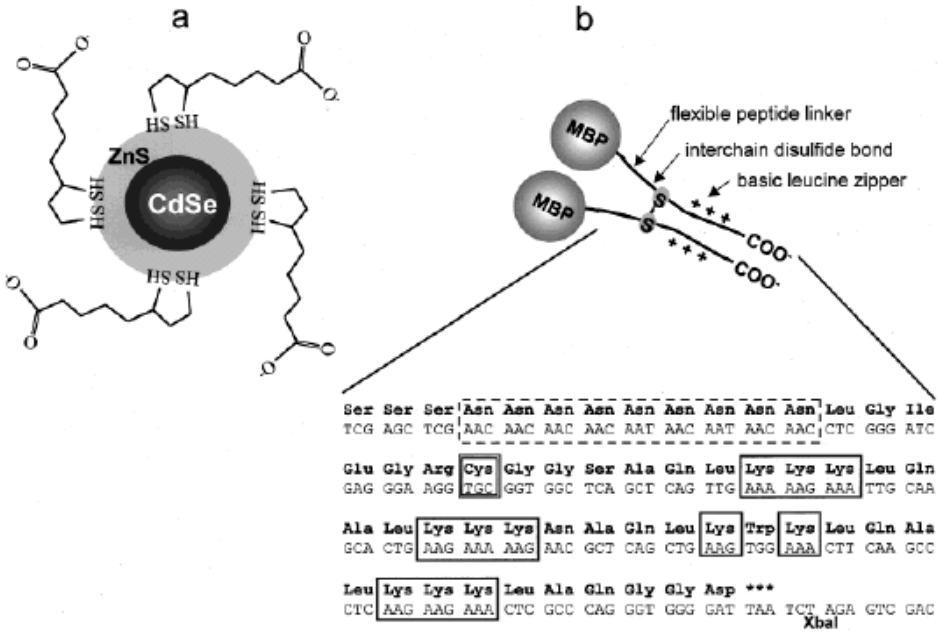

Figure 1.10 (a) Schematic of the CdSe-ZnS core-shell nanoparticle with dihydrolipoic acid surface capping groups; (b) cartoon of the S-S linked MBP-zb homodimer and detail showing nucleotide and primary amino acid sequences of the C-terminal basic leucine zipper interaction domain. Poly-Asn flexible linker is boxed with dashed lines, unique engineered cysteine is double boxed, and lysine residues contributing to net positive charge of leucine zipper are single boxed [32].

Comparing the ligand exchange and polymer encapsulation method, the ligand exchange are wide used into modification QDs surface, because of the surfactant (contain thio group) are cheaper than other polymers and have high binding affinity on the metal atoms. Furthermore, the encapsulation polymer on the hydrophobic surface is easily form the emulsification in the environment. Consequently, most research all like to use the thio derived molecules capping on the QDs surface.

1.2.2 Photoactivation on the Quantum dots

Wang (2004) reported that Mechanism of Strong Luminescence Photo-activation of Citrate-Stabilized Water-Soluble Nanoparticles with CdSe Cores. Using sodium citrate as a stabilizer, CdSe and CdSe/CdS semiconductor nanocrystals have been synthesized in aqueous environment. Unfortunately, these QDs display photoluminescence with very low quantum yields, upon prolonged illumination with visible light, enhancements up to 5000% have been measured. Because of their high surface area, nonradiative recombination at surface sites and surface traps compete with the band-edge emission [35]. Photoactivation of the QDs luminescence, that is, an order of magnitude or more increase of QY, is a new process of preparation of highly luminescent nanocrystal. It is important alternative way to achieve high QY. Figure 1.11 shows several absorption and emission spectra after different irradition times for CdSe/CdS.

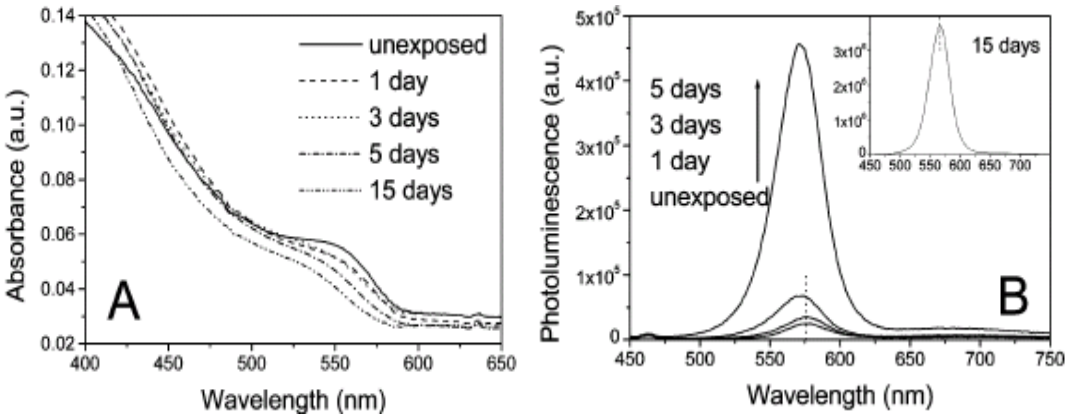

Figure 1.11 Absorption (A) and emission (B) spectra of CdSe@CdS nanocrystals (Cd/Se 8:1) measured after different irradiation times in air. (B): Luminescence spectrum after exposure to light for 15 days [35].

The optical densities of all the samples noticeably decreased during the illumination. The corresponding emission peak grew dramatically, at least 2 orders of magnitude in the peak intensity, retaining about the same peak width of 35-50 nm. It could be observed that light treatment promoted spectral shifts toward shorter wavelengths both in absorption and luminescence, which is consistent with a possible decrease of particle size during illumination. As a result of the photoactivation in CdSe NPs, charge carriers resulting from the absorption of light are trapped into the surface states formed because of the uneven atomic-scale topography of QDs. Additionally, the excitons activate the reactions with oxygen present in the environment, for instance, the transfer of a photoexcited electron to O_2 leading form O_2^-. The remaining hole also trapped on the surface oxidizes the Se to SeO_2.This results in the gradual etched of the unwanted topographic features on the surface and in smooth, highly luminescent QDs where the nonradiative decay of excitons no longer dominates. The mechanism is schematically presented in Figure 1.12. In various possible models of photoactivated luminescence, it is important to perceive the occasion and the consequence of the phenomenon. Jones et al. reported the increase in quantum efficiency up on illumination to chemical changes in the particles due to the redistribution of surfactant molecules on QDs surfaces [36]. Therefore, using photoactivation on QDs could enhance the quantum efficiency, and improve the application in the bioassay system.

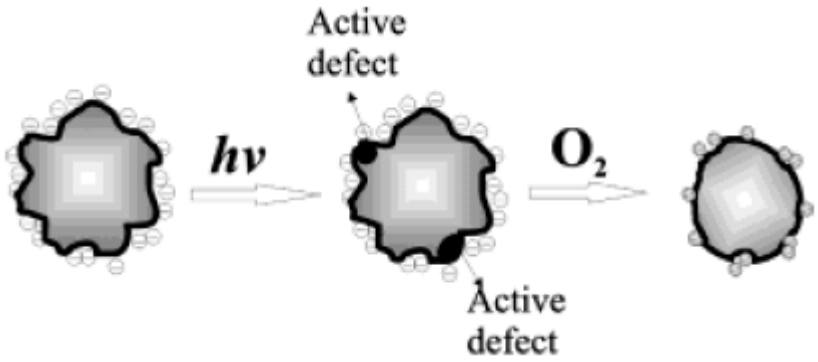

Figure 1.12 Suggested schematics of photoinduced luminescence enhancement. Photoinduced charge carriers are trapped in “roughness states” (active defect) on the surface. Photooxidation eliminates the surface roughness of the NP, i.e., atomic-scale imperfections. This procedure results in reduced-size NPs and yields NPs with reduced surface defects and enhanced photoluminescence [36].

1.2.3 Application of the Quantum dots

Sandros (2005) present a facile, reagentless method for generating protein-based semiconducting nanoparticle sensors for small molecules. Previous author reported that Maltose binding protein (MBP) is typically for biosensor method development. As a result of MBP undergo a reversible, ligand-dependent conformational change. These movements have been harnessed for maltose sensing either by differentially opening/closing motion on the protein surface [37-39], or by using lever-action molecular displacement [40-41]. Hence, Sandros employs the lever-action strategy to alter the interaction between an MBP attached [(tetraamine)(5-maleimido-phenanthroline)ruthenium]-[PF6]2 (**1**) and the surface of a water-soluble CdSe nanoparticle. The system provides reagentless selective detection of maltose by changing the interaction between 1 and CdSe nanoparticle surface in a distance-dependent fashion (as shown in Figure 1.13) [42]. The valence-band hole of the CdSe nanoparticle would be occupied on electron transfer from (**1**), when source excited on the CdSe. Alternatively, electron transfer from (**1**) to the valence band of the CdSe excited state, forming a nonfluorescent CdSe anion, is consistent wuth the decrease in CdSe emission intensity. A 1.4-fold increase in fluorescence intensity was observed upon maltose addition (Figure 1.14). The phenomenon indicated a decrease in the (**1**)-CdSe electron transfer quenching.

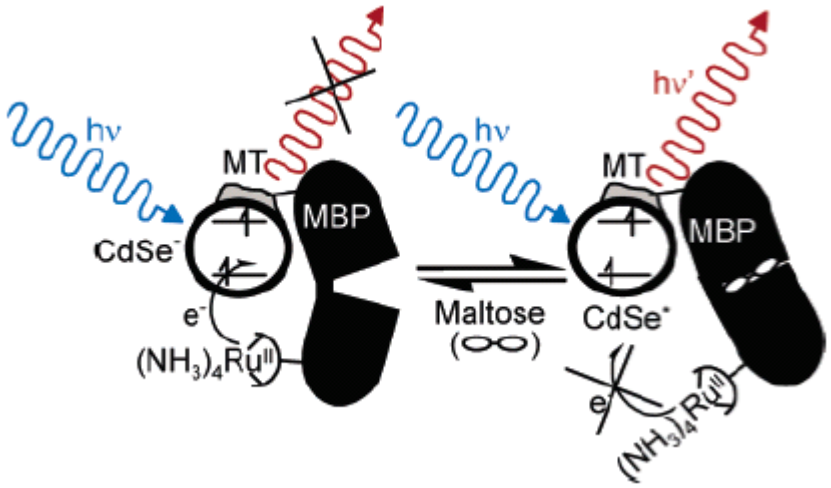

Figure 1.13 Scheme of Maltose-Dependent Change in CdSe Emission [42].

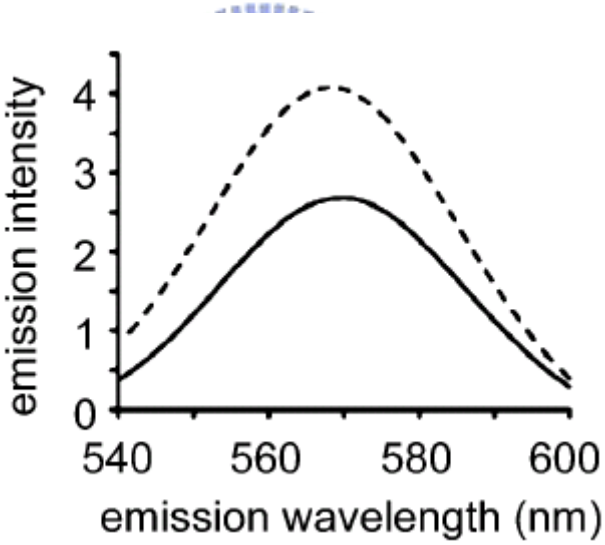

Figure 1.14 Maltose-dependent fluorescence of complex **1** modified-K46C MBP-MT attached to 3.0-3.5 nm diameter THDA capped CdSe nanoparticles under 363 nm excited) at pH 7.5 (20 mM 3-(*N*-morpholino)propanesulfonic acid, MOPS): fluorescence emission spectra of a solution (5 nM biosensor) without (solid line) and with 1 mM maltose (dashed line) [42].

Shi (2006) reported the development of quantum dots FRET-based protease sensors and their application for the measurement of extracellular matrix metalloproteinases (MMPs) activity in normal and cancerous breast cells. The quantum dots based probes were prepared by exchanging the TOPO capping ligands of CdSe/ZnS QDs with tetrapeptide RGDC molecules. The acceptors are rhodamine which be labeled on the peptide molecules by covalent bonding. Upon enzymatic cleavage of the peptide molecules, the rhodamine (acceptor) molecules no longer provided an efficient energy transfer channel to QDs. Therefore, the emission color of the QDs changed back to green (the scheme show in Figure 1.5). The QDs FRET-based enzymatic activity probes were first used to determine the activity of collagenase in solution to test the analytical capabilities of the QDs FRET-based probes in a model system. FRET measurements of the QDs at increasing levels of collagenase in solution are shown in Figure 1. The fluorescence intensity (545 nm) of the QDs increased while the fluorescence intensity of the rhodamine molecules decreased due to the enzymatic cleavage of the RGDC peptide by collagenase [43].

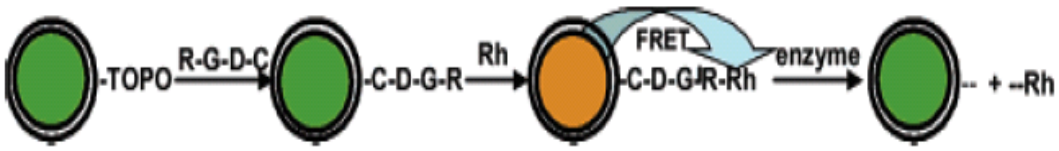

Figure 1.15 Principle of Quantum Dots-Based Enzymatic Activity Probes [43].

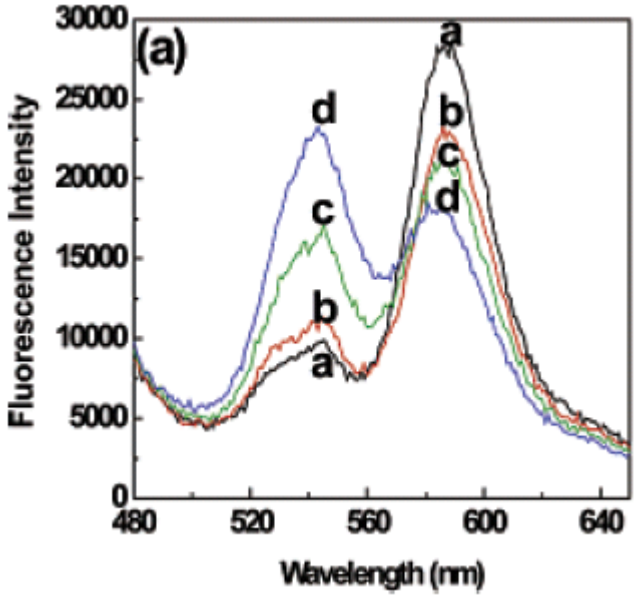

Figure 1.16 Emission spectra of rhodamine-labeled peptide-coated quantum dots 15 min following the addition of collagenase of increasing concentration. (a) 0 μg/mL (black), (b) 0.5 μg/mL (red), (c) 2.5 μg/mL (green), and (d) 5.0 μg/mL (blue) [43].

1.3 Motivations

In this work, we aim to achieve several goals as below: ***First at all, modifying the CdSe/ZnS QDs surface contains carboxyl group and water soluble in aqueous.*** As we have discussed previously, modifiable ligand on the QDs surface, such as ligand exchange by thio group, encapsulation with amphiphilic polymer, and combinations of layers with thio group modified on biomolecular, are also effective for water-soluble QDs and play an important role in the biological or biosensor application area. Among the semiconductor NPs, CdSe or CdSe/ZnS QDs have more advantages in their optical properties, such as tunable photoexcitation depend on the size, high photostability, narrow and symmetric luminescence spectra, and high quantum yield. Therefore, QDs charm many researchers to choose them to apply in the bio-labeling, biosensor (bioindicator), nanodevice, and solar-cell, etc. Recently, the biosensors (bioindicators) are popular in the clinic or portable. However, in the composition of biosensor, they also need complex component, such as sensing area, enzyme immobilized, and circuit designing. For this reason, we propose easily bioindicators, which are urea, glucose, by luminescence intensity of QDs under photoluminescence spectrum instrument monitored. ***Second, to improve the quantum efficiency of water-soluble QDs (MSA-QDs) suit to assay lipid (triglyceride), where the MSA-QDs must be photoactivated through fluorescent lamp and support more hydrophobic site on the QDs surface to soluble the triglyceride.*** As we discussed above, current reviewers suggest that the luminescence intensity of QDs would be

increase around 5000% after photoactivation by UV lamp. However, the QDs could not easily control to keep away the aggregation. In this work, the fluorescent lamp is employed as photoactivation source, which contains wide band spectra, and easily gets high performance luminescence POD-QDs with low aggregation phenomena. The POD-QDs is also employed to apply in the triglyceride sensing through visualizing under 365 nm excited. ***Third, to fabricate and utilize the PDDA-QDs interaction forces to assemble protein molecular assay the bimolecular through fluorescent resonance energy transfer (FRET).*** As we have discussed previous, the water-soluble QDs has lethal shortcoming in the luminescence through ligand exchange, and is not easily applied in the biological. Hence, we propose an easily method to improve QDs luminescence, which contains the photoactivation and polymer capping under the fluorescent lamp irradiation. The high performance water-soluble QDs would be fabricated and realized into the biosensing system through fluorescent resonance energy transfer (FRET).

1.4 Thesis organization

In chapter 1, we are given a background introduction, including the basic concepts, definition and indication of quantum dots properties. Then, we have some reviews on the most representative experiments about application on CdSe or CdSe/ZnS QDs. At least, we will have the motivations of this work and thesis organization.

In chapter 2, we will focus on the fabrication water-soluble QDs, with various emissions, through thio group ligand exchange (MSA-QDs). Then, we demonstrate the urea and glucose bioindicator by MSA-QDs, and investigate the luminescence intensity of MSA-QDs during acid or basic environment. We also provide and explain some phenomena, like surface trap or smoothing QDs surface during ions effect.

In chapter 3, we will improve the luminescence intensity of MSA-QDs through photoactivarion. We also point out the mechanism of photoactivation on the MSA-QDs (POD-QDs). Then, we develop the triglyceride bioindicator by POD-QDs and show the sensitive curve by turning buffer capacity in the environment.

In chapter 4, we will progress the solubility of POD-QDs through Poly (diallyldimethylammonium chloride) solution (PDDA) capped on the MSA-QDs (PDDA-QDs) under fluorescent lamp (intensity 8.5 mW/cm^2) irradiation. Then, we discuss the surface properties of PDDA-QDs, such as charge, size, surface state, and composition, by analytic instrument.

Finally, we develop the FRET system to sense the biomolecule through high performance luminescence PDDA-QDs and organic dye Rhodaminme. Consequently, we discuss the FRET efficiency between PDDA-QDs and Streptavidin-Rhodaminme.

In chapter 5, we develop the FRET based system to assay the biomolecule through high performance luminescence PDDA-QDs and organic dye. First at all, we discuss the binding constant between PDDA-QD/△5-3-ketosteroid isomerase (EC 5.3.3.1) and Cholic acid-tetramethylrodaminme (CA-TMR). Second, we provide the FRET efficiency between the above systems and discuss the energy phenomena between PDDA-QDs and organic dye. Third, we demonstrated the competition reactions, which obtain Cholic-TMR and 4-Estren-17b-OL-3-ONE (19NT), based on the FRET system with PDDA-QDs.

In chapter 6, we will have a brief conclusion of this work.

1.5 Reference

[1] A. P. Alivisatos, *Science*, 271 **(1996)** 933.

[1] X. Michalet, F. F. Pinaud, L. A. Bentolila, J. M. Tsay, S. Doose, J. J. Li, G. Sundaresan, A. M. Wu, S. S. Gambhir, S. Weiss, *Science*, 307 **(2005)** 538.

[2] I. L. Medintz, H. T. Uyeda, E. R. Goldman, *Nature materials*, 4 **(2005)** 435.

[3] M. Bruchez, M. Moronne, P. Gin, S. Weiss, A. P. Alivisatos, *Science*, 281 **(1998)** 2013.

[4] W. W. Yu, J. C. Falkner, B. S. Shih, V. L. Colvin, *Chem. Mater.* 16 **(2004)** 3318.

[5] A. A. Guzelian, U. Banin, A. V. Kadavanich, X. Peng, A. P. Alivisatos, *Appl. Phys. Lett.* 69 **(1996)** 1432.

[6] A. A. Guzelian, *J. Phys. Chem.* 100 **(1996)** 7212.

[7] W. W. Yu, Y. A. Wang, X. Peng, *Chem. Mater.* 15 **(2003)** 4300.

[8] W. W. Yu, L. Qu, W. Guo, X. Peng, *Chem. Mater.* 16 **(2004)** 560.

[9] J. M. Tsay, M. Pflughoefft, L. A. Bentolila, S. Weiss, *J. Am. Chem. Soc.* 126 **(2004)** 1926.

[10] M. Nirmal, *Nature.* 383 **(1996)** 802.

[11] J. K. Lorenz, A. B. Ellis, *J. Am. Chem. Soc.* 120 **(1998)** 10970.

[12] X. Peng, M. C. Schlamp, A. V. Kadavanich, A. P. Alivisatos, *J. Am. Chem. Soc.* 119 (**1997)** 7019.

[13] B. O. Dabbousi, J. Rodriguez-Viejo, F. V. Mikulec, J. R. Heine, H. Mattoussi, R. Ober, K. F. Jensen, M. G. Bawendi, *J. Phys. Chem. B* 101 (**1997)** 9463.

[14] W. Guo, J. J. Li, Y. A. Wang, X. Peng, *J. Am. Chem. Soc.*125 (**2003)** 3901.

[15] P. Reiss, J. Bleuse, A. Pron, *Nano Lett.* 2 **(2002)** 781.

[16] A. Sukhanova, *Anal. Biochem.* 324 **(2004)** 60.

[17] L. CA, W.K. Woo, F.V. Mikulec, M.G. Bawendi, *J Phys Chem B*, 106 **(2002)** 7619.

[18] X. Gao, L. Yang, A. P. John, F. F. Marshall, J. W. Simons , S. Nie, *Current Opinion in Biotechnology* **(2005)** 63.

[19] W. C. W. Chan, S. M. Nie, *Science* 281 **(1998)** 2016.

[20] S. Pathak, S. K. Choi, N. Arnheim, M. E. Thompson, *J. Am. Chem. Soc.* 123 **(2001)** 4103

[21] S. Kim, M. G. Bawendi, *J. Am. Chem. Soc.* 125 **(2003)** 14652.
[22] W. Guo, J. J. Li, Y. A. Wang, X. G. Peng, *Chem. Mater.* 15 **(2003)** 3125.
[23] F. Pinaud, D. King, H. P. Moore, S. Weiss, *J. Am. Chem. Soc.* 126 **(2004)** 6115.
[24] X. Y. Wu et al., *Nature Biotechnol.* 21 **(2003)** 41.
[25] X. Gao, Y. Cui, R. M. Levenson, L. W. K. Chung, S. Nie, *Nature Biotechnol.* 22 **(2004)** 969.
[26] D. Gerion, *J. Phys. Chem. B* 105 **(2001)** 8861.
[27] B. Dubertret, *Science* 298 **(2002)** 1759.
[28] X. Gao, W. C. W. Chan, S. Nie, *J. Biomed. Opt.* 7 **(2002)** 532.
[29] T. Pellegrino, L. Manna, S. Kudera, T. Liedl, D. Koktysh, A. L. Rogach, S. Keller, J. Ra1dler, G. Natile, and W. J. Parak, *Nano Lett.,*4 **(2004)** 703.
[30] F. Osaki, T. Kanamori, S. Sando, T. Sera, Y. Aoyama, *J. Am. Chem. Soc.* 126 **(2004)** 6520.
[31] H. Mattoussi, J. Matthew Mauro, E. R. Goldman, G. P. Anderson, V. C. Sundar, F. V. Mikulec, M. G. Bawendi *J. Am. Chem. Soc.* 122 **(2000)** 12142.
[32] B. Sun, W. Xie, G. Yi , D. Chen , Y. Zhou , J. Cheng, *Journal of Immunological Methods* 249 **(2001)** 85.
[33] M. A. Petruska, A. P. Bartko, V. I. Klimov, *J. Am. Chem. Soc.* 126 (**2004**) 714.
[34] Y. Wang, Z. Tang, M. A. Correa-Duarte, I. Pastoriza-Santos,| M. Giersig, N. A. Kotov, L. M. Liz-Marzan, *J. Phys. Chem. B , 108* (**2004)**15461.
[35] M. Jones, J. Nedeljkovic, R. J. Ellingson, A. J. Nozik, G. Rumbles, *J. Phys. Chem. B , 107* (**2003)** 11346.
[36] G. Gilardi, L. Q. Zhou, L. Hibbert, A. E. Cass, *Anal. Chem.* 66 (**1994)** 3840.
[37] J. S. Marvin, E. E. Corcoran, N. A. Hattangadi, J. V. Zhang, S. A. Gere, H. W. Hellinga, *Proc. Natl. Acad. Sci. U.S.A.* 94 (**1997)** 4366.
[38] S. A. Trammell, H. M. Goldston, P. T. Tran, L. M. Tender, D. W. Conrad, D. E. Benson, H. W. Hellinga, *Bioconjugate Chem.* 12 (**2001)** 643.
[39] D. E. Benson, D. W. Conrad, R. M. De Lorimer, S. A. Tramell, H. W. Hellinga, *Science*, 292 (**2001)** 1641.

[40] M. Fehr, W. Frommer, S. Lalonde, *Proc. Natl. Acad. Sci. U.S.A.* 99 (**2002)** 9846.
[41] M. G. Sandros, D. Gao, D. E. Benson, *J. Am. Chem. Soc.* 127 **(2005)** 12198.
[42] L. Shi, V. De. Paoli, N. Rosenzweig, Z. Rosenzweig, *J. Am. Chem. Soc.* 128 **(2006)** 10378.

Chapter 2 Synthesis the water-soluble CdSe/ZnS quantum dots and their application

Abstract:

The mercaptosuccinic acid (MSA), which contains a thio group and two carboxyl groups, are easily to replace and stablize the surface of QDs. Fluorescence emission wavelength can be tuned by modifying the size of QDs particles, and the type of capping molecules, which are responsible for modification of the surface charges for bimolecular coupling. An original and novel assay system with urease or glucose oxidase (GOD) as a catalyst and CdSe/ZnS quantum dots (QDs) as an indicator has been developed for quantitative analysis of urea or glucose. By mixing urease (or glucose oxidase) and QDs, the determination of urea (or glucose) can be performed in a quantitative manner. The detection is based on the enhancement (or quenching) of QD photoluminescence (PL) intensity, which is correlated to the enzymatic degradation of urea (or glucose). The glucose assay system can also provide convenient way to estimate glucose concentration by visualizing the color change of QDs. These newly developed systems possess many advantages, including simplicity, low cost, high flexibility, and good sensitivity. Furthermore, no chemical modification and enzyme immobilization were needed in this system.

2.1 Introduction

Colloidal semiconductor nanocrystals or quantum dots (QDs) have attracted much interest in the areas of fundamental research and technical applications, because of their tunable photoexcitation depend on the size and emission, which is associated with narrow and symmetric luminescence spectra [1–5]. Advances in surface passivation and additional confinement of excitonic states by coating the native core with a thin layer of a semiconductor with a larger bandgap substantially improve the fluorescence quantum efficiency, such that the resulting core-shell QDs have PL quantum yields that are similar to those of organic dyes [6–14]. Unfortunately, conventional organic dyes used in diagnostics application and biological labeling reagents commonly have characteristics that limit their effectiveness in such applications. Organic fluorophores have narrower excitation bands and broader emission spectra than CdSe QDs. Therefore; QDs have become extremely popular due to their unique optical properties. However, the high quality luminescences QDs were hydrophobic and insoluble into aqueous solution. Using mercaptoacetic acid ligands was one of the first strategies applied to produce water soluble QDs [15]. Since then, a number of other thioalkyl acid ligands including 3-mercaptopropionic acid [16-18] and dihydrolipoic acid [19-21] have been used. Self-assembly of these ligands on the surface of a CdSe/ZnS QD proceeds with a metal − thiol affinity interaction and orients the ligands such that the carboxyl groups are exposed to the surrounding aqueous

solution. Under sufficiently basic conditions, the carboxyl groups are deprotonated and render the QD water-soluble. Other thiol-based approaches have been used, including thioglycerol [22-23], 2-mercaptoethane sulfonate [24], and thiol-terminated polyethylene glycol [25].

In this study, we use the mercaptosuccinic acid (MSA) to replace the hydrophobic surfactant (HDA) on the QDs surface. The structure of MSA assembled on the surface of QD is shown in Figure 2.1 Considering stability, the MSA would be expected to be the stable since it has two ionizable carboxyl groups. Fluorescence emission wavelength can be tuned by modifying the size of QDs particles, and the type of capping molecules, which are responsible for modification of the surface charges for bimolecular coupling. The hybrid systems containing QDs coupled with various bio-molecules stimulate growing interests in the research areas of biotechnology and nanotechnology.

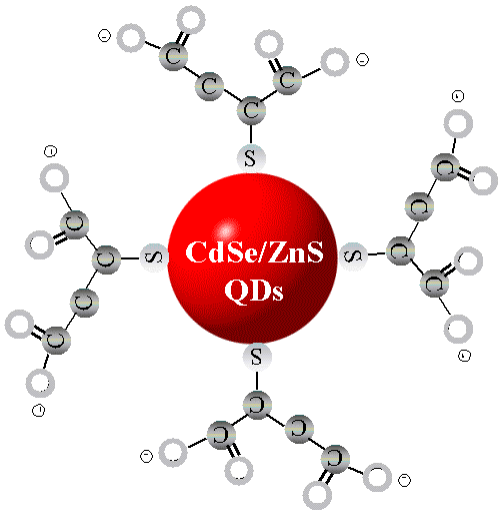

Figure 2.1 The structure of MSA assembled on the surface of QD

Through the bioconjugation of QDs, hybrid materials have demonstrated both unique optical properties of QDs and high specificities toward biomolecules, such as oligonucleotides and proteins [16-18]. In addition to application in imaging, QDs were recently demonstrated to be good “indicators” for enzymatic hydrolysis of paraoxon [26-27]. It was found that a subtle change of the surface property of QDs could result in a dramatic change in their optical properties. In principle, this novel feature of QDs can be extended for detecting specific analytes if appropriate conditions are established.

Urea in blood or in urine is an important substance in the diagnosis of renal and liver diseases. The detection of urea is performed frequently in the medical care. Normal level of urea in serum is in the range of 2.5-6.7 mM. In patients suffering from renal insufficiency, urea concentration in serum may be as high as 30-80 mM. With such a urea level, hemodialysis is required [28]. For urea detection, biosensors based on the potentiometry and amperometry were previously investigated and reported [29-33]. However, the complexity of sensor fabrication is a common drawback often mentioned in the literature.

Determination of glucose concentration takes a relevant place in controlling various food and biotechnological processes as well as in diagnosing many metabolic disorders. Among various methods employed to this aim, the utilization of glucose oxidase (GOD) to produce hydrogen peroxide from glucose and further couple with the applications of potentiometry, amperometry, or optical method to analyze the amount of hydrogen peroxide is the most common strategy [34-36]. Using fluorescence technique it is recently developed an

alternative approach to sense glucose. For example, Schultz and coworkers developed a competitive glucose assay that does not consume glucose by the optical detection [37-38]. The sensing principle was based on fluorescence resonance energy transfer (FRET) between a fluorescence donor and an acceptor, each covalently linked to concanavalin A (ConA) or dextran. The presence of glucose resulted in its competitive binding to ConA consequently released from the dye-labeled dextran, thus, decreased in the FRET efficiency. Although early results of this technique have gained considerable enthusiasm for fluorescence sensing of glucose [38-40], the complexity of chemical modification on protein is an evident drawback. Another case of glucose detection by FRET technique was designed based on spontaneous formation of viologens/pyramine complex, in which the boronic acid-substituted 4,7-phenanthrolinium viologens was used to quench the fluorescence of pyranine. In the presence of glucose, the complex dissociates, resulting in a large increase in the fluorescence [41]. Unfortunately, some complicated procedures are required for synthesizing the counterparts of the complex.

In this study, we describe a simple scheme for preparation of a urea-sensing system, which is composed of water-soluble mercaptosuccinic acid (MSA)-QDs and urease; it allows effective and quantitative detection of urea. Furthermore, a new approach for glucose analysis was designed using QDs as a sensitive “indicator”. An assay system containing glucose oxidase (GOD) and CdSe/ZnS quantum dots (QDs) was developed for quantitative analysis of glucose without chemical modification on protein or QDs.

2.2 Material and Methods

2.2.1 Instruments and Chemicals

A Hitachi U-3010A UV-Visible spectrophotometer and a Jobin-Yvon Spex Fluolog-3 spectrophotometer were used to investigate the fluorescence characteristics of the samples. The pH meter (IQ120) was purchased from IQ Scientific, USA. All chemicals were of analytical grade or highest purity available. Chloroform, methanol (all anhydrous, Aldrich), cadmium oxide (CdO, Aldrich), selenium (Se, Aldrich), tri-n-butylphosphine (TBP, Showa), n-hexadecylamine (HDA, Lancaster), stearic acid (SA, Lancaster), diethyl zinc (1M solution in toluene, Aldrich), sulfur powder (S, Aldrich), D,L-mercaptosuccinic acid (MSA, Acros), and tetramethylammonium hydroxide 25% by weight in methanol (TMAOH, Acros) were used as received. Urease (E.C. 3.5.1.5.), Glucose oxidase (E.C. 1.1.3.4.) and D-glucose were purchased from Sigma.

2.2.2 Synthesis of water-soluble MSA-capped CdSe/ZnS QDs

Luminescent CdSe/ZnS QDs were synthesized according to the previously reported procedures [2, 6, 7]. However, MSA was selected as the surface-capping reagent to form water-soluble QDs. 30 mg of CdSe/ZnS QDs were suspended in 10 mL of methanol and transferred to a reaction vessel. Then, a separated 50 mL methanolic solution of 1M MSA was added to the above-mentioned QD-containing solution

and the pH of the solution was adjusted to 11 with tetramethylammonium hydroxide pentahydrate. The mixture was then refluxed at 60˚C overnight under N_2, and the sample was stored in the dark. The QDs were precipitated with anhydrous ether, centrifuged at 6000 rpm, and the supernatant was decanted to remove the organic solvent. Methanol was added to wash the precipitant four times. The precipitant was re-suspended in a phosphate buffer (10 mM or 30 mM, pH 8.0) and stored in the dark [7,14,42].

2.2.3 Assay conditions and PL measurements for urea indicator

For studying the pH effect on the PL intensity of the MSA-QD, a series of samples with different basicity (pH 8, 8.4, 9.5, 10.3, 11.0, 11.5) were prepared by adding various amount of NaOH (0.1 M) and water to a 200 μl MSA-QDs solution (20 *m*M phosphate buffer, pH 8) to reach a final volume of 300 μl and the amount of MSA- QDs employed was controlled by the absorption at 565 nm with final 0.6 OD. For urea determination, the assay solutions containing urease (1.33 units), MSA-QD (final 0.3 OD observed at 565 nm), and various concentrations of urea (0-120 mM) were prepared in 300 μl of phosphate buffer (20 *m*M, pH 8.0). Reactions were performed for 10 min before spectrophotometric analysis and acidity (pH) measurements. The PL intensity was measured by using the Jobin-Yvon Spex Fluolog-3 spectrophotometer with 365 nm He/Ne light source to excite MSA-QDs.

2.2.4 Assay conditions and PL measurements for glucose indicator

For all tests and reactions, the experiments were repeated at least 3 times to ensure the accuracy of the measurement. To study the effect of pH on the PL intensity of the MSA-CdSe/ZnS QDs, a series of samples with different pH values (pH 3.5~ 11.6) were prepared by adding various amount of HCl (0.1 M) or NaOH (0.1 M) and water to a 200 μL MSA-CdSe/ZnS QDs solution (10 mM phosphate buffer, pH 8.0) to reach a final volume of 300 μL. Glucose oxidase and glucose solution were prepared in high concentration in phosphate buffer (10 mM or 30 mM, pH 8.0) for further study. For all experiments, the total volume of the sample was 300μL and the amount of MSA-CdSe/ZnS QDs employed was controlled by the absorption at 574 nm with final 0.3 OD. For assay system, glucose oxidase (13.5 units) was added to the solution containing QDs and various concentration of glucose. Reactions were performed for 30 min before spectrophotometric analysis and acidity (pH) measurements. The PL intensity was monitored at 586 nm through out all experiments. The Jobin-Yvon Spex Fluolog-3 spectrophotometer with excitation wavelength set at 365 nm (He/Ne light source) was employed.

2.3 Results and discussion

2.3.1 Optical characterization of MSA capped CdSe/ZnS

The water-soluble, MSA functionalized, CdSe/ZnS QDs were

successfully synthesized according to the protocol described in the ***Material and Methods***. The optical properties of MSA-QDs in 50 mM phosphate buffer solution are shown in Figure 2.2 (a-b). The data are summarized in Table 2.1. The optical properties of MSA-QDs have significantly red-shift (~5 nm), which cause from trap-states on the QDs surface, as compared with the HDA capped QDs. Additionally, the photoluminescence peaks are symmetric and, unlike the organic dye, does not exhibit red tails. Full width at half-maximum (FWHM) of 25 nm ± 5 nm are obtained, enabling effective distinction between different colors emission. The narrow emission spectrum indicated that high degree of monodispersity of QDs was present. In the urea and glucose indicator application, we used the MSA-QDs with a characteristic peak at 560 nm (574 nm) and a narrow emission band centered at 580 nm (586 nm), respectively.

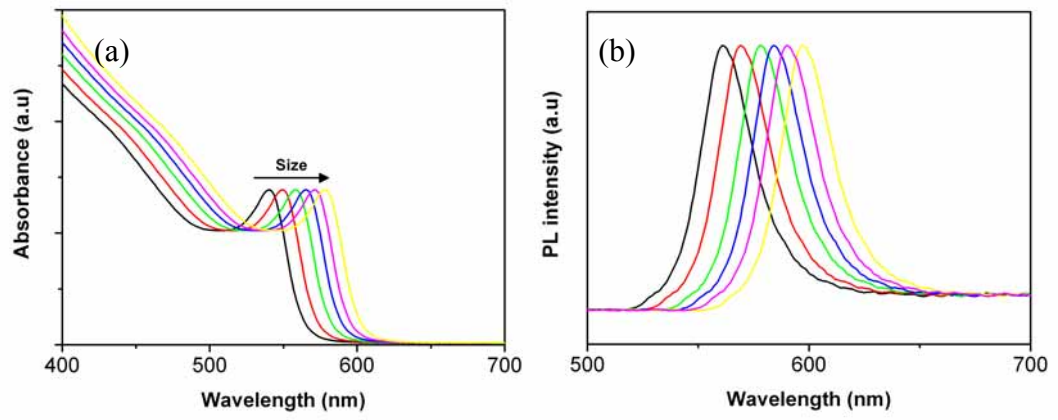

Figure 2.2 (a) The absorption spectrum (b) photoluminescence spectrum of MSA-QDs with different size in 50 mM phosphate buffer solution

Table 2.1 Summering the characterizations of optical and size with MSA-QDs

Size of the MSA-QDs (nm)	Absorption peak (nm)	Emission peak (nm)
2.85	540	561
2.89	549	569
2.94	558	578
2.98	565	584
3.01	572	590
3.05	579	597

2.3.2 Influence of pH on luminescence of MSA-CdSe/ZnS

It has been proposed that the PL intensity of water-soluble MSA-QDs was sensitive to acidity (or basicity) of the environment [38]. Our investigation confirmed this finding. A series of fluorescence spectra of QDs in different pH conditions (3.5 – 11.6) were measured and the results showed that the PL intensity and the emission spectra were significantly perturbed by pH condition. As pH value varied from 8.3 to 3.5, the PL intensity of QDs was quenched and the emission spectrum was blue-shifted (Figure 2.3). The quenching phenomenon and the blue-shifted of emission peak (~10 nm) were very likely due to the etching process occurring on the surface of QDs. On the other hand, the PL intensity was found to increase when the pH was increased from 8.3 to 11.6 (Figure 2.3). The observed PL enhancement might result from the reduction of non-radiative recombination by minimizing the surface defects of QDs, which consequently confined the wave function of electron-hole pairs inside the nanocrystals. Figure 2.4

exhibited the PL intensity of QDs, which was found to linearly correlate to the pH value with a factor of approximately 5000 cps/pH unit.

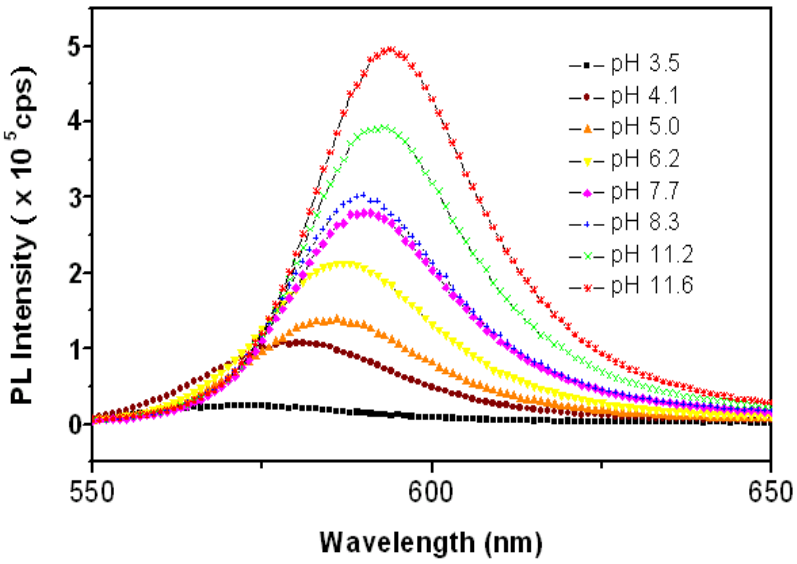

Figure 2.3 PL spectrum of MSA-QDs at different pH values.

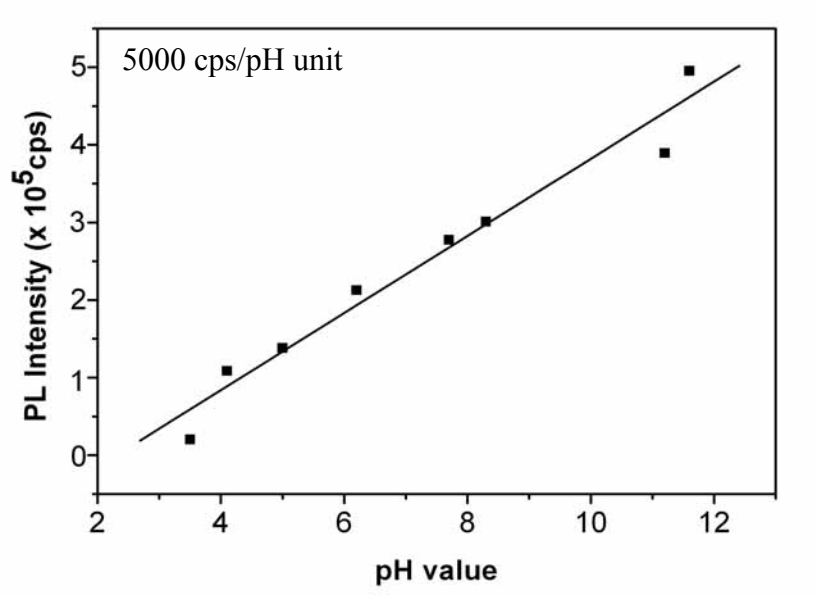

Figure 2.4 The correlation between pH value and the PL intensity monitored at 586 nm of QDs

2.3.3 Photoluminescence spectroscopy for the detection of urea

CdSe/ZnS QDs are potentially useful in sensor design, as they possess a significant response in fluorescence and a high surface/volume ratio. Since the PL intensity of QDs was found to correlate with the acidity (or basicity) of the environment, it was expected that QDs could be used as an indicator in monitoring biochemical reactions associated with pH change. For examining the feasibility of such an application, we have designed a system of enzymatic analysis of urea. Since the urease-catalyzed hydrolysis of urea releases NH_4^+, OH^- and HCO_3^- ions as products (see equation 1), the pH value of the assayed sample gradually increases as the urea degradation occurs.

$$(NH_2)_2CO + 3\ H_2O \xrightarrow{urease} 2NH_4^+ + OH^- + HCO_3^- \qquad (1)$$

Figure 2.5 exhibits the variation of PL intensity of MSA-QDs as a function of urea concentrations (0~120 *m*M) under urease catalysis in 20 *m*M phosphate buffer with pH 8.0. The emission spectra were recorded using the excitation wavelength (λ_{ex}) of 365 nm. The results indicated that the PL intensity of MSA-QDs was enhanced with increasing urea concentration. Figure 2.6 was plotted by the ratio of PL enhancement, $(I-I_o)/I_o$, versus urea concentration. An approximately linear relationship can be observed with the urea concentration lower than 100 *m*M. Since the PL intensity is perturbed by the acidity, it is of interest to measure both the change of PL intensity and the final

acidity of a reaction, simultaneously. The response of acidity measured by pH meter was found to be linear at low urea concentration (0-15 *m*M) and to maintain at pH 9.5 when the substrate concentration was higher than 20 *m*M. However, interestingly, the PL intensity of MSA-QDs showed approximately linear response for urea concentration up to 100 *m*M. Clearly, when the acidity of an assay system approaches its thermodynamic steady-state, the micro-environment of MSA-QDs is continuously changed. One of the possible situations is that the MSA moiety on the surface of QD may be removed through the substitution reaction of hydroxide, which is produced from the urea degradation. Consequently, the PL intensity is enhanced owing to the increased amount of less MSA-coated QDs, which has been shown to be stronger in fluorescence intensity [15,39].

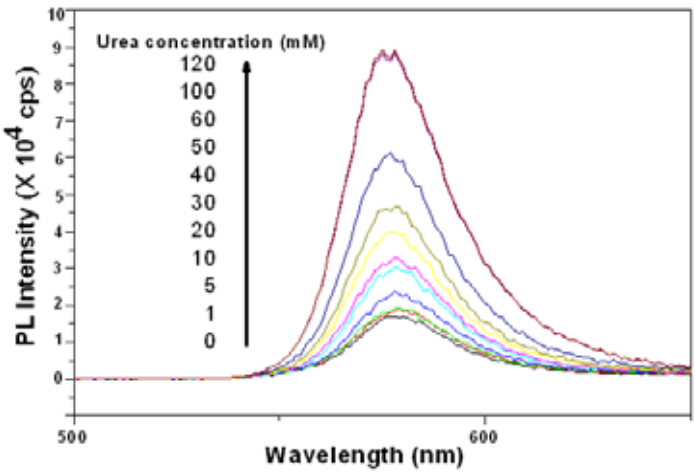

Figure 2.5 The variation of PL spectra of urease/QDs with urea concentration. Reactions took place in 20 mM pH 8.0 buffer. Note that, the spectra obtained from the reactions with 100 and 120 mM of urea are nearly superimposed.

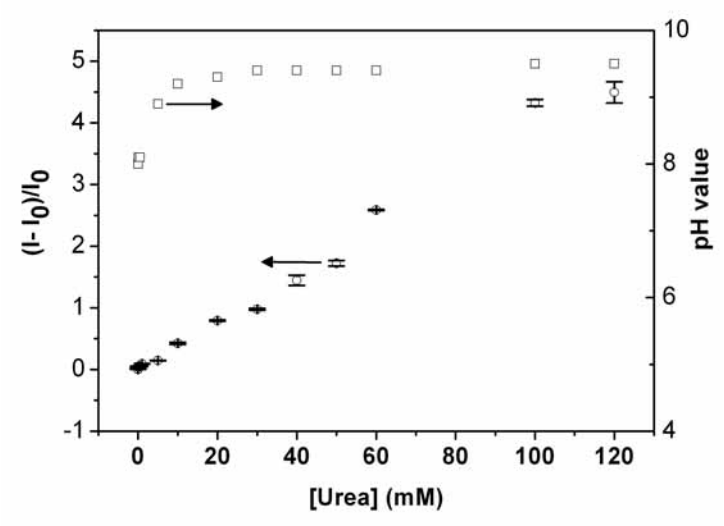

Figure 2.6 The variation of pH value and PL intensity with urea concentration. Urea was analyzed by the urease/QDs sensing system in 20 mM pH 8.0 buffer, in which the pH value (□) and the PL perturbation (■) were determined. I_o and I represent the PL intensity of MSA-QDs observed at 580 nm with the reaction at zero time and at the end-point, respectively.

In order to evaluate other possible interferences in this system, urease, urea, NaCl, and NH_4^+ were incubated with MSA-QDs separately. No significant perturbation on PL intensity was observed (data not shown) when urease, urea, NaCl and NH_4^+ were added up to 2.5 units and 100 *m*M, 1000 *m*M, 20 *m*M, respectively. We concluded that the change of PL intensity of our system is indeed solely owing to the product(s) of the catalytic reaction. With this newly developed system, urea concentration can be analyzed in a broad range (0.01 to 100 *m*M). The designed system is very promising for urea analysis in biological systems as compared with many other currently existing methods. Table 2.2 summarizes the detection limits of urea with various methodologies

including amperometry, potentiometry and optical spectroscopy and the present study. Clearly, the current method exhibits great potential for urea sensing with a wide detection range.

Table 2.2 Comparison of performance of different urea sensors.

Type	Sensing matrix	Linear range (mM)	Limiting detection (mM)	Ref
Amperometry	Polytoluidine blue film	0.02-0.8	0.02	[29]
	PVC ammonium electrode	15- 80	15	[30]
Potentiometry	PNVK/SA/urease LB film	0.5-68	0.5	[31]
	Polyvinylalcohol / 2-fluoro-1-methylpyridiniumtoluene-4-sulphonate/urease	0.089-1.1	0.089	[32]
	Urease+ polyurethane-acrylate	0.2-6	0.2	[33]
Optical	Urea/MSA-QDs	0.01-120	0.01	This study

2.3.4 Influence of GOD on photoluminescence of MSA- QDs

For understanding the possible influence of GOD on the PL intensity of QDs, the fluorescence of GOD was investigated. With excitation at 365 nm, a broad fluorescence spectrum (410 to 600 nm) with two peaks centered at 450 and 520 nm was observed. These characteristic bands confirmed the presence of flavin adenine dinucleotide (FAD, a prosthetic group) in GOD [45-49]. Since the emission spectrum of FAD was observed to overlap with the absorption band of QDs, the fluorescence resonance energy transfer (FRET) should be taken into account in the assay system (Shown in Figure 2.7). A simple examination was performed to evaluate the influence of GOD to the PL intensity of QDs. As anticipated, the presence of GOD significantly enhanced the PL intensity of QDs. Figure 2.8 demonstrated such linear relationship with the increment of 2300 cps per unit of GOD. Although the PL enhancement may not be solely due to the process of FRET, it is closely related to the presence of GOD.

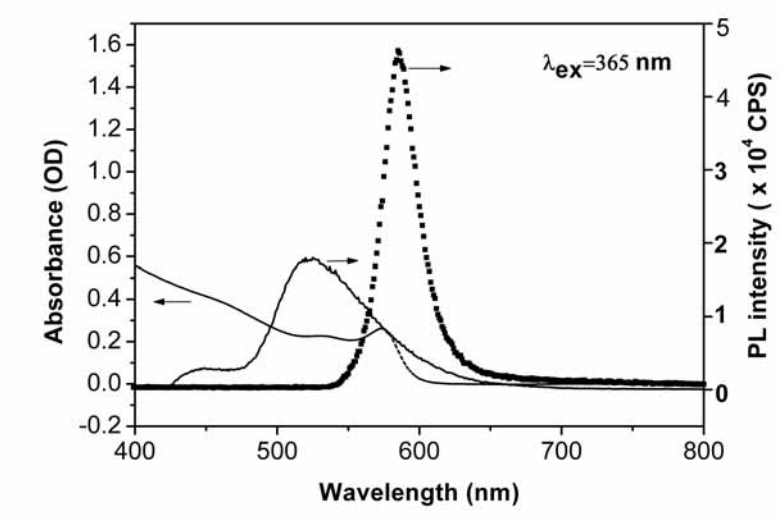

Figure 2.7 UV-Visible and photoluminescence spectra of the MSA-CdSe/ZnS QDs and GOD. The spectra drew by dash line, dot line, and solid line, were the absorption spectrum of QDs, emission spectrum of QDs, and emission spectrum of GOD, respectively. All measurements were performed in 10 mM phosphate, pH 8.0. The excitation wavelength was 365 nm.

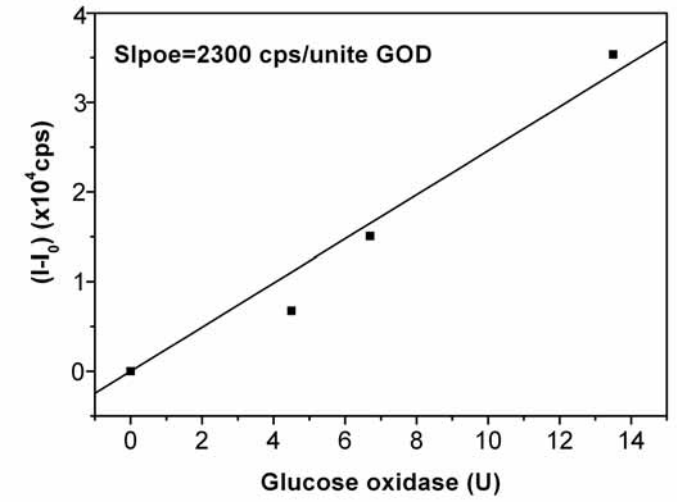

Figure 2.8 The influence of GOD in PL enhancement of MSA-CdSe/ZnS QDs. The enhancement of PL intensity was linear to the added GOD.

2.3.5 Photoluminescent spectroscopy of the detection of glucose

Since the PL intensity of QDs was found to be sensitively influenced by the acidity (or basicity) of the environment, we proposed that the MSA-CdSe/ZnS QDs should be potentially useful for assays that produce acidic or basic product. To examine the feasibility of such proposal, we designed an assay system specifically for glucose analysis. In this system, GOD was used to catalyze the oxidation of glucose to release H_2O_2 and gluconolactone. The latter was then rapidly hydrolyzed to form D-gluconic acid and, consequently, lowered the pH value of the assay system. The catalytic reactions can be depicted in equations (1) and (2) as represented below

$$\text{D-glucose} + O_2 \xrightarrow{GOD} \text{D-gluconolactone} + H_2O_2 \qquad (1)$$

$$\text{D-gluconolactone} + H_2O \rightarrow \text{D-gluconic acid} \qquad (2)$$

Figure 2.9 exhibited the variation of fluorescence spectra of various assay reactions as a function of glucose concentration (0.2 to 10 mM). Note that, the fluorescence spectra, with excitation at 365 nm, were taken at the end-point of the enzymatic reaction that occurred in 10 mM of phosphate buffer, pH 8.0. The quenching of PL intensity of MSA-CdSe/ZnS QDs was observed with increasing glucose concentration. The catalytic oxidation of glucose also resulted in spectral shifts toward shorter wavelengths in the PL spectra. Since acids were found to be able to slowly etch QDs [49], the blue-shifted emission spectra were presumably attributed to the particle size reduction as more acid was produced.

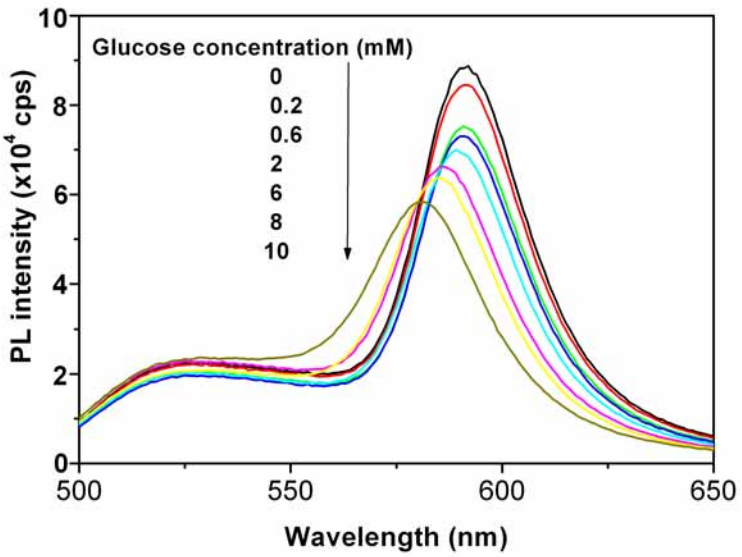

Figure 2.9 The emission spectra of the assay samples at the end-point of the reaction. The assay system contained GOD, QDs, and the tested glucose with concentration 0, 0.2, 0.6, 2, 6, 8, 10 mM. Reactions were performed at 10 mM phosphate buffer, pH 8.0 for 30 min. The emission spectra were recorded under excitation with 365 nm lights.

Figure 2.10 represented the experiments of PL quenching and the pH values as a function of glucose concentrations oxidized in two different buffer systems, 10 mM and 30 mM phosphate, pH 8.0. The data obtained from the assay system of 10 mM phosphate, pH 8.0 were directly derived from Figure 2.7. The quench ratio of PL intensity was defined as 100 $(I_o\text{-}I)/I_o$, where I_o and I represented the PL intensity of QDs observed at 586 nm with the reaction at zero time and at end-point, respectively. When the assays were performed in 10 mM phosphate, the quench ratio of PL intensity, $[(I_o\text{-}I)/I_o]$, was found to be proportional to glucose concentration in the range of 0.2 to 10 mM, while at higher glucose concentration (>15 mM) the quenching effect was leveled-off

(data not shown), suggesting that the capacity of QDs be insufficient to reveal the existing acid.

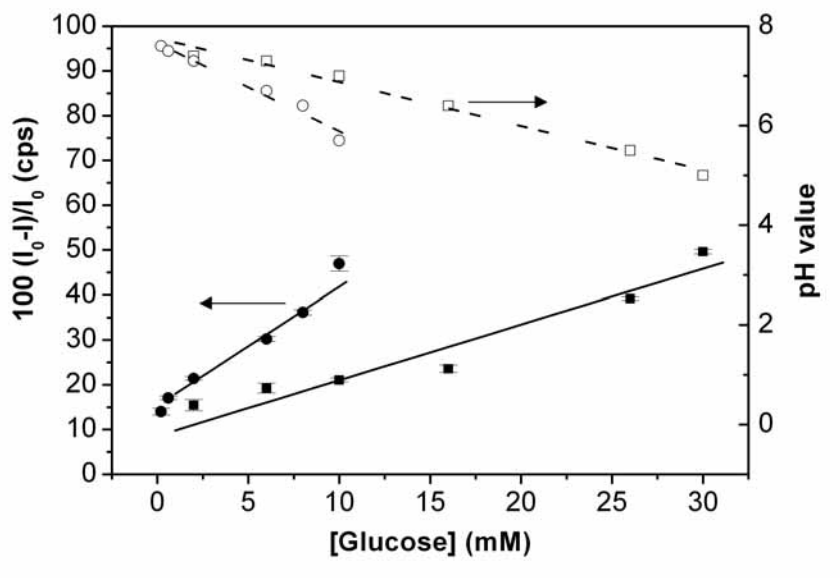

Figure 2.10 Correlation between the quench ratio of PL intensity, pH perturbation and the tested glucose concentration. Two assay system, 10 mM and 30 mM phosphate, pH 8.0, were employed. The data obtained from the assay system using 10 mM phosphate were directly derived from fig.6. The quench ration of PL intensity was defined as 100 $(I_o\text{-}I)/I_o$, where I_o and I represented the PL intensity of QDs observed at 586 nm with the reaction at zero time and at end-point, respectively. The data shown by open circle (○) and open square (□) were the pH measurements of the reactions assayed in 10 mM and 30 mM phosphate, respectively. The data shown by filled circle (●) and filled square (■) were the quench ratio of PL intensity obtained in 10 mM and 30 mM phosphate system, respectively.

To solve such a problem, one could use higher concentration of QDs. Alternatively, increasing buffer concentration was suggested. For that, the gluconic acid produced at early stage of reaction will be consumed by the buffer and allow QDs to effectively function as an indicator to track and reveal the later stage of reaction. The assay system using 30 mM phosphate, pH 8.0 was found to be suitable for glucose concentration ranging from 2 to 30 mM. The pH value of each reaction in both the 10 mM and 30 mM buffer systems also consistently showed the correlation between the fluorescence quenching and the amount of glucose measurement.

Our assay system can also provide a convenient way for the determination of glucose concentration by visualizing color change of QDs fluorescence. Figure 2.11 exhibited series of fluorescence images for various glucose analytes obtained from 0 to 14 mM in the 10 mM buffer system. The fluorescence of the reaction samples, irradiated with 365 nm light, resulted in the color change from pale orange to bright, yellowish green when glucose concentration was increased from 0 to 14 mM. Two breaking points between 0.6 mM to 2 mM and 10 mM to 12 mM were clearly observed, respectively. With appropriate control of the buffer system, it is feasible to develop a simple assay kit for semi-quantitative determination of glucose without using expensive instrumental setup.

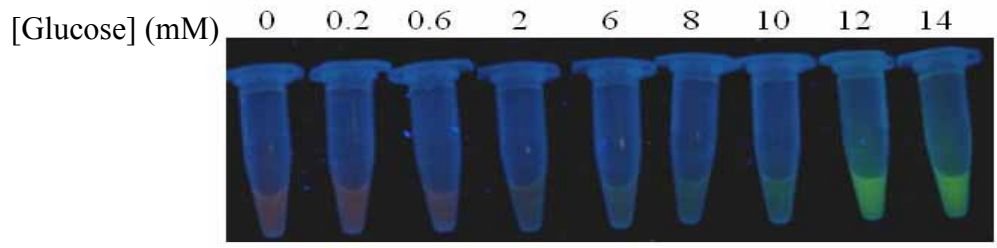

Figure 2.11 Fluorescent photos of the assay samples. Samples were excited by 365 nm sources. The assay conditions were identical to those described in Fig. 2.9.

2.4 Conclusions

We have demonstrated that the water-soluble MSA-QDs can be utilized as a reliable agent for the enzymatic determination of urea and glucose concentration. The MSA-QDs exhibit linear response in PL intensity when urea with concentration ranging from 0.01 to 100 *m*M was analyzed. Additionally, with this new approach, glucose can be successfully analyzed with wide range of concentration. As compared with other urea and glucose sensors (indicator) reported in the literature, the MSA-QD-based biosensor exhibits several advantages, such as the ease of its fabrication, low cost, no enzyme immobilization process required, high flexibility, and good sensitivity. It offers a persuasive way to determine the urea and glucose concentration without using complicate instrumental application.

2.5 Reference:

[1] A.P. Alivisatos, *Science* 271 **(1996)** 933.

[2] X.G. Peng, L. Manna, W.D. Yang, J. Wickham, E. Scher, A. Kadavanich, A. P. Alivisatos, *Nature* 404 **(2000)** 59.

[3] W. Huynh, X. G. Peng, A. P. Alivisatos, *Adv. Mater.* 11 **(1999)** 923.

[4] H. Mattoussi, L. H. Radzilowski, B. O. Dabbousi, E. L. Thomas, M. G. Bawendi, M. F. Rubner, *J. Appl. Phys.* 83 **(1998)** 7965.

[5] H. Mattoussi, I. L. Medintz, A. R. Clapp, E. R. Goldman, J. K. Jaiswal, S. M. Simon, J.M. Mauro, *J. Assoc. Lab. Automation* 9 **(2004)** 28.

[6] A. M. Hines, P. Guyot-Sionnest, *J. Phys. Chem.* 100 **(1996)** 468.

[7] B. O. Dabbousi, J. Rodriguez-Viejo, F. V. Mikulec, J. R. Heine, H. Mattoussi, R. Ober, K. F. Jensen, M. G. Bawendi, *J. Phys. Chem. B* 101 **(1997)** 9463.

[8] Z. A. Peng, X. G. Peng, *J. Am. Chem. Soc.* 123 **(2001)** 183.

[9] A. R. Kortan, R. Hull, R. L. Opila, M. G. Bawendi, M. L. Steigerwald, P. J. Carroll, L. E. Brus, *J. Am. Chem. Soc.* 112 **(1990)** 1327.

[10] Y. Tian, T. Newton, N. A. Kotov, D. M. Guldi, J. H. Fendler, *J. Phys. Chem.* 100 **(1996)** 8927.

[11] X. Peng, M. C. Schalamp, A. V. Kadavanich, A. P. Alvisatos, *J. Am. Chem. Soc.* 119 **(1997)** 7019.

[12] M. Danek, K. F. Jensen, C. B. Murray, M. G. Bawendi, *Chem. Mater.* 8 **(1996)** 173.

[13] D. Gerion, F. Pinard, S. C. William, W. J. Parak, D. Zanchet, S. Weiss, A. P. Alivisatos, *J. Phys. Chem. B* 105 **(2001)** 8861.

[14] J. Aldana, Y. A. Wang, X. Peng, *J. Am. Chem. Soc.* 123 **(2001)** 8844.

[15] W. C. W. Chan, S. Nie, *Science* 281**(1998)** 2016.

[16] G. P. Mitchell, C. A Mirkin, R. L. Letsinger, *J. Am. Chem. Soc.* 121 **(1999)** 8122.

[17] D. Zhou, J. D. Piper, C. Abell, D. Klenerman, D. J. Kang, Y. Ying, *Chem. Commun.* **(2005)** 4807.

[18] G. Gill, I. Willner, I. Shweky, U. Banin, *J. Phys. Chem. B* 109 **(2005)** 23715.

[19] E. R. Goldman, A. R. Clapp, G. P. Anderson, H. T. Uyeda, J. M. Mauro, I. L. Medintz, H. Mattoussi, *Anal. Chem.* 76 **(2004)** 684.

[20] E. R. Goldman, I. L. Medintz, J. L. Whitley, A. Hayhurst, A. R. Clapp, H. T. Uyeda, J. R. Deschamps, M. E. Lassman, H. Mattoussi, *J. Am. Chem. Soc.* 127 **(2005)** 6744.

[21] I. L. Medintz, A. R. Clapp, H. Mattoussi, E. R. Goldman, G. Fisher, J. M. Mauro, *Nat. Mater.* 2 **(2003)** 630.

[22] N. Murase, M. Gao, *Mater. Lett.* 58 **(2004)** 3898.

[23] Y. Chen, Z. Rosenzweig, *Anal. Chem.* 74 **(2002)** 5132.

[24] W. J. Jin, M. T. FernNndez-ArgOelles, J. M. Costa-FernNndez, R. Pereiro, A. Sanz-Medel, *Chem. Commun.* **(2005)** 883.

[25] H. T. Uyeda, I. L. Medintz, J. K. Jaiswal, S. M. Simon, H. Mattoussi, *J. Am.Chem. Soc.* 127 **(2005)** 3870.

[26] X. Ji, J. Zheng, J. Xu, V. K. Rastogi, T. C. Cheng, *J. Phys. Chem. B* 109 **(2003)** 3793.

[27] J. C. Chen, J. C. Chou, T. P. Sun, S. K. Hsiung, *Sensor. Actuators B*. 91 **(2003)** 213180.

[28] I. Vostiar, J. Tkac, E. Sturdik, P. Gemeiner, *Bioelectrochemistry* 56 **(2002)** 234113.

[29] L. Campanella, F. Mazzei, M. P. Sammartino, M. Tommassetti, *Bioelectrochem. Bioenerg.* 23 **(1990)** 195.

[30] R. Singhal, A. Gambhir, M. K. Pandey, S. Annapoorni, B. D. Malhotra, 231 *Biosens. Bioelectron.* 17 **(2002)** 697.

[31] A. Sehigutollari, A. H. Uslan, *Talanta* 57 **(2002)** 1039.

[32] F. Mizutani, S. Yabuki, Y. Sato, *Biosens. Bioelectron.* 12 **(1007)** 321.

[33] M. Lepore, M. Portaccio, E. D. Tommasi, P. De Luca, U. Bencivenga, P. Maiuri, D. G. Mita, *J. Mol. Cata. B: Enzymatic*, 31 **(2004)** 151.

[34] H. Yang, Y. Zhu, *Anal. Chimica Acta*, 554 **(2005)** 92.

[35] K. Y. Park, S. B. Choi, M. Lee, B. K. Sohn, S.Y. Choi, *Sensors and Actuators B*, 83 **(2002)** 90.

[36] R. Ballerstadt, J. S. Schultz, *Methods Biotechnol*, 7 **(2000)** 89.

[37] V. M. Staiano, M. Rossi, S. D. Auria1, *Journal of Fluorescence*, 14 **(2004)** 491.

[38] R. J. Russell, M. V. Pishko, *Anal. Chem.*, 71 **(1999)** 3126.

[39] R. Ballerstadt, J. S. Schultz, *Anal. Chem.*, 72 **(2000)** 4185.

[40] J. T. Suri, D. B. Cordes, F. E. Cappuccio, R. A. Wessling, B. Singaram, *Langmuir* 19 **(2003)** 5145.

[41] C. P. Huang, H. W. Liu, C. Y. Tsao, L. T. Yin, S. F. Chiu, T. M. Chen, *Sensors Actuators B*, 108 **(2005)** 713.

[42] Y. Wang, Z. Tang, M. A. Correa-Duarte, I. P. Santos, M. Giersig, N. A. Kotov, L. M. Liz-Marzan, *J. Phys. Chem. B,* 108 **(2004)** 15461.

[43] S. F. Wuister, C. De Donega, M. A. Meijerink, *J. Phys. Chem. B* 108 **(2004)** 17393.

[44] P. Audebert, C. Demaille, C. Sanches, *Chemical materials*, 5 **(1993)** 911.

[45] C. Haouz, C. Twist, A. M. Zentz, S. P. de Kersabiec, B. Alpert, *Chemical Physics Letters,* 294 **(1998)** 197.

[46] S. K. Haq, M. D. F. Ahmad, R. H. Khan, *Biochemical and Biophysical Research Communications,* 303 **(2003)** 685.

[47] A. M. Hartnett, C. M. Ingersoll, G. A. Baker, F. V. Bright, *Analytical Chemistry*, 71 **(1999)** 1215.

[48] P. Malgorzata, *Materials Science*, 21 **(2003)** 398.

[49] X. Gao, W. C. W. Chan, S. Nie, *Journal of Biomedical Optics*, 7 **(2002)** 532.

Chapter 3 Investigation of the photoactivated CdSe/ZnS quantum dots and their application

Abstract:

The MSA-QDs also have high stability in the aqueous environment, but low luminescence QY is often observed in its, mainly due to the non-radiative recombination of the electron-hole pair at surface sites and surface traps competing with band-edge emission. In order to improve the fluorescence of QDs in sensing application, the process of photoactivation was shown to enhance the photoluminescence (PL) of QDs. In this study, we demonstrated a simple assay system containing lipase and photoactivated luminescent CdSe/ZnS quantum dots (QDs) for the quantitative detection of triglycerides. Photoactivated CdSe/ZnS QDs function as a sensitive "indicator" to reveal the minute acidity change of the assay system resulting from the enzymatic hydrolysis of triglycerides. The assay system also provides a convenient way to estimate triglyceride concentration by visualizing the color change of the QDs fluorescence. As compared to most of the existing methods, the system reported herein possessed many advantages, including simplicity, low cost, high flexibility, and high sensitivity. Furthermore, no complicated chemical modification or enzyme immobilization is needed.

3.1 Introduction

Quantum dots (QDs) have unique optical properties in comparison with traditional organic dyes, due to quantum-size confinement effects, including high fluorescence quantum yield (QY), narrow full-width half-maximum (FWHM), size- and composition-tunable emission, and less susceptibility to photobleaching [1]. Unfortunately, low luminescence QY is often observed in as-prepared nanoparticles, mainly due to the non-radiative recombination of the electron-hole pair at surface sites and surface traps competing with band-edge emission. This displeasing property is particularly found in the water-soluble QDs capping with thiol group [2,3]. Very recently, the process of photoactivation was shown to enhance the photoluminescence (PL) of QDs [4]. When a QDs-containing solution was illuminated with light (254~600 nm), the surface selenium atoms on CdSe QDs were susceptibly oxidized to form selenium oxide and further to liberate Cd^{2+} ions in solution. Thus, the net reaction is reasonably assumed to be as that given in the following equation 1 [4-6].

$$CdSe + 3/2O_2 + 2H^+ \xrightarrow{h\nu} Cd^{2+} + SeO_2 + H_2O \qquad (1)$$

The effect of light irradiation promoting the formation of both electrons and holes on QD surface and consequently enhancing the QY of QDs have been actively investigated by many groups [4-11]. This phenomenon was further verified by the surface-related emission by Maenosono et al. [11]. Because of the strong fluorescence feature, the

photoactivated QDs (POD-QDs) are potentially useful for chemical and biochemical sensing. Such an application was demonstrated in designing a sensitive probe for cyanide in aqueous solution [1, 12].

The quantitative determination of triglycerides is an important issue in many fields such as food and oil-refining industries and medical examination. Methods to fulfill this need are available. The common protocol involves the utilization of lipase or saponification to breakdown triglycerides to release glycerol as well as fatty acids and further couple with potentiometry, surface acoustic wave, or optical tool for quantitative assessment [13-16]. The optical method is generally employed to analyze the amount of hydrogen peroxide [13] or NADH [14], which is produced from glycerol with many steps of enzymatic reactions. All of these methods conceal significant drawbacks such as the demand of enzyme immobilization and/or the requirement of several enzymes for catalysis. For example, the method of potentiometry requires a sensing matrix, an enzyme immobilization process and a read-out circuit system [15] and the spectrophotometric method, on basis of NADH detection, needs several enzymes including lipase, glycerol kinase, pyruvate kinase, and lactate dehydrogenases for consecutive catalytic reactions. To improve those traditional detections, we have developed and report herein a simple detection system (Figure 3.1) by coupling the applications of lipase and POD-QDs, in which POD-QDs serve as an excellent indicator to monitor the minute pH perturbation due to the formation of fatty acids.

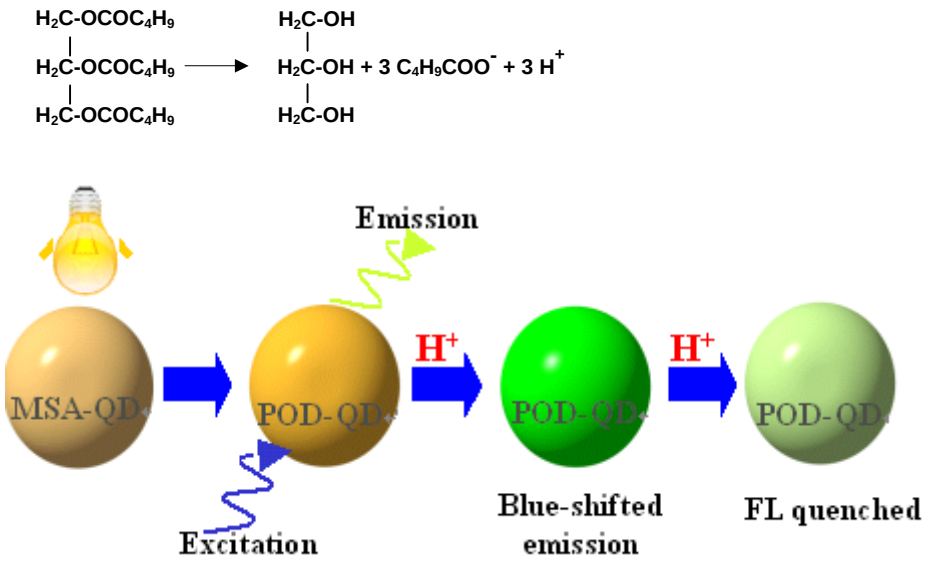

Figure 3.1 The scheme of triglyceride indicator by POD-QDs

3.2 Materials and Methods

3.2.1 Instruments and chemicals

A Hitachi U-3010A UV-Visible spectrophotometer and a Jobin-Yvon Spex Fluolog-3 spectrophotometer were used to investigate the fluorescence characteristics of the samples. Transmission electron microscopy (TEM) measurements were performed by using a Philips TECNAI model 20 electron microscopes operated at 200 kV. TEM samples were prepared by dropping diluted solutions of POD-QD nanocrystals onto 200-mesh carbon-coated copper grids with the excessive solvent immediately evaporated. All chemicals were of analytical grade or the highest purity available. Chloroform, methanol, diethyl zinc (1M solution in toluene), cadmium oxide, selenium, and sulfur powder were purchased from

Aldrich. *n*-Hexadecylamine (HDA) and stearic acid (SA) were obtained from Lancaster. tri-*n*-Butylphosphine (TBP) was purchased from Showa. D,L-Mercaptosuccinic acid (MSA) and 25 wt% tetramethylammonium hydroxide (TMAOH) in methanol were from Acros. A porcine pancreas lipase (E.C. 3.1.1.3) and tributyrin were purchased from Sigma.

3.2.2 Photoactivation of CdSe/ZnS QDs

Luminescent CdSe/ZnS QDs were synthesized according to the previously reported procedures [17-18]. However**,** MSA was selected as the surface-capping reagent to form water-soluble QDs. 30 mg of CdSe/ZnS QDs was suspended in 10 mL of methanol in which a separated 50 mL methanolic solution of 1 M MSA was then added. The pH of the resulting solution was adjusted to 11.0 by adding tetramethylammonium hydroxide pentahydrate. The mixture was kept in dark and refluxed at 60˚C overnight under N_2. When the reaction was completed, the MSA-QDs were precipitated with anhydrous ether and further collected by centrifugation. Methanol (10 ml each time) was employed to wash the precipitated QDs four times. The MSA-QDs were then re-dissolved in a phosphate buffer (5, 10 and 20 mM, pH 8.0) [6,19]. To perform the photoactivation, MSA-QDs were illuminated with a 21-Watt fluorescent light (intensity 8.5 mW/cm^2) for a series of times at ambient temperature. The spectrum of fluorescent light was shown in Figure 3.2. The photoactivated QDs were then obtained by centrifugation (10,600 x g) for 10 min and re-dissolved in 5

mM, 10 mM and 20 mM phosphate buffer for further experiments, respectively.

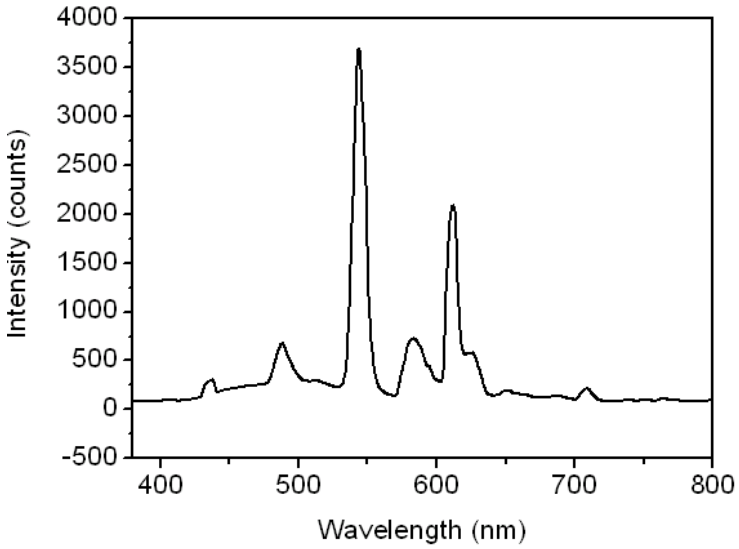

Figure 3.2 The spectrum of 21-Watt fluorescent light

3.2.3 Assay conditions and PL measurements

All experiments were repeated at least three times to ensure the accuracy of the measurements. To study the effect of acidity on the photoluminescence (PL) intensity of POD-QDs, a series of samples with different pH values (5.0~8.0) were prepared by adding various amounts of HCl (0.1 M) and water to a 200 μL solution (10 mM phosphate buffer, pH 8.0) to obtain a final volume of 300 μL. Reactions were performed for 10 min before spectrophotometric analysis and acidity (or pH) measurements. High concentration of lipase was prepared in various phosphate buffers (5 mM, 10 mM, and 20 mM, all pH 8.0). Tributyrin (340 mM) was prepared in ethanol as a stock solution for further study. For all experiments, the total volume of the

sample was 300 μL and the amount of POD-QDs employed was controlled at the final concentration with absorption of 0.1 OD measured at 565 nm. For the assay system, solutions containing 75 units of lipase (100 – 400 units/mg), POD-QDs, and various amounts of tributyrin (0 – 25 mM) were prepared in 5 mM, 10 mM and 20 mM phosphate buffer (pH 8.0). The enzymatic reaction was completed in 10 min and then subject to spectrophotometric analysis and pH measurements. The PL intensity was measured by using a He/Ne laser light source with wavelength of 365 nm to excite the QDs.

3.3 Results and Discussion

3.3.1 Characterization of the photoactivation of CdSe/ZnS QDs

The POD-QDs were successfully prepared according to the protocol described in the section of *Materials and Methods*. The increase in irradiation times at MSA-QDs induced a blue-shift of photoluminescence spectrum, that is, a decrease in size of MSA-QDs ; naoparticles photoactivated during the sunlight irradiation would enhance the PL intensity and restructure the QDs surface. Figure 3.3 shows the PL spectrum of MSA-QDs irradiated under the fluorescent light with different times. The results indicated that the POD-QDs (19 hr irradiated) exhibited a 100-fold stronger luminescence and a distinct blue-shifted (~10 nm) spectrum as compared with that of MSA-QDs (0 hr irradiated). Figure 3.4 shows a trend spectrum of the maximum emission peak and the PL intensity under different irradiation times.

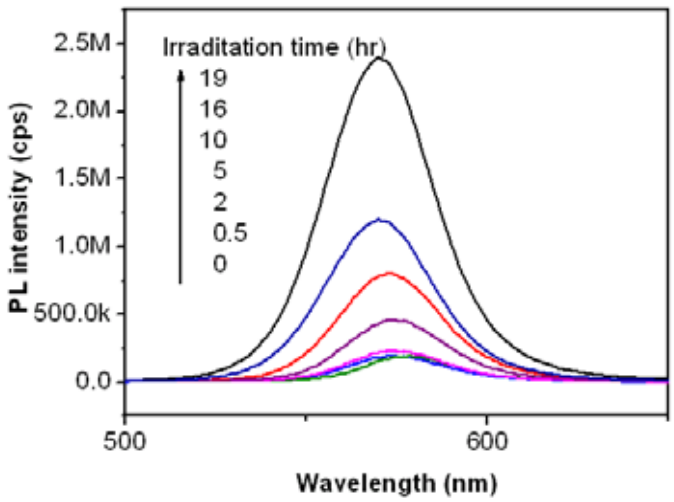

Figure 3.3 the PL spectrum of MSA-QDs irradiated under the fluorescent light with different times.

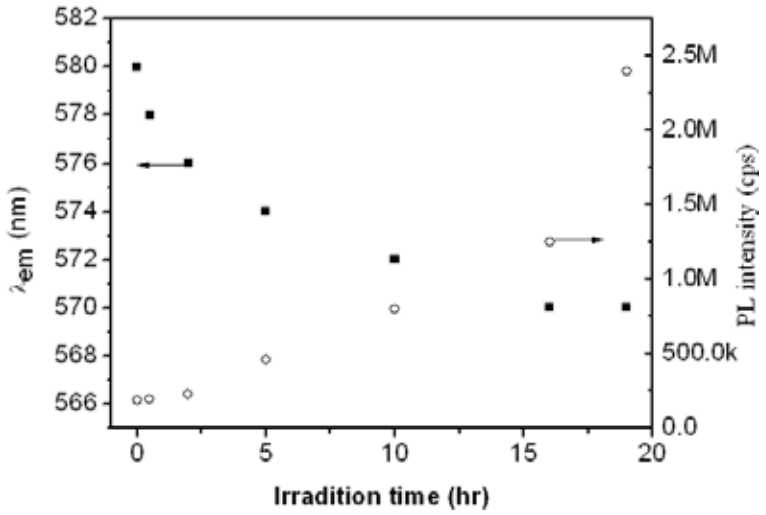

Figure 3.4 A trend spectrum of the maximum emission peak and the PL intensity under different irradiation times.

Observations of the bleaching and blue shift of the exciton PL have been reported in CdSe and CdSe/ZnS quantum dots exposed to intense illumination [5,8]. Previous authors indicated that photobleaching was found to occur about 4 times faster in air than in N_2. In addition, the photoluminescence in air was reported to be initially more intense than

that in N_2, which was possibly caused by oxygen quenching of the deep trap emission [20]. Moreover, partially reversible photodarkening has also been observed in CdSe cluster that was attributed to their temporary charging, which would quench the emission with efficient nonradiative Auger recombination of the e^--h^+ pair induced by the excess charge. According to the postulate decay route of an exciton generated in CdSe/ZnS by Jones reported, an alternative relaxation route involves the formation of nonradiative surface states consisting of trapped electrons or holes that have already been mentioned with regard to peak energies (shown in Figure 3.5). When the photoactivation lengthening of the PL decay result from an increase in the lifetimes of the nonradiative trap states caused by a light-induced rearrangement of surfactant molecules that serve to stabilize the electron or hole traps [5]. If lengthening the average trap state lifetime will increase the chance that thermalization may back to an emitting 1> state and consequently lead to the observed photoenhancement effect. In the triglyceride indicator application, the POD-QDs has many advantages than MSA-QDs, such as: high luminescence; easily mixed with triglyceride, which contain oil phase; easily monitored the photoluminescence by eyes. As a result of Figure 3.6 , the POD-QDs exhibited a 100-fold stronger luminescence and a distinct blue-shifted (~10 nm) spectrum as compared with that of MSA-QDs. The particle size of QDs was estimated to be 2.8 ± 0.4 nm by transmission electron microscopy (TEM) (Figure 3.6, upper right inset). Narrow emission bands centered at 580 nm (MSA-QDs) and 570nm (POD-QDs) were observed when the QDs were excited with a 365 nm He/Ne light source. The significant

effects on photoenhancement as well as the blue-shift feature of the POD-QDs are attributed to the photoactivation, which normally involves, at least, two processes that combined the above description reasons. First, the photoinduced charge carriers are trapped in "roughness states" on the QDs surface. Second, the photooxidation eliminates the surface roughness of the QDs. These processes result in smoothing the surface as well as reducing the size of QDs and consequently enhance the photoluminescence of QDs [2,7].

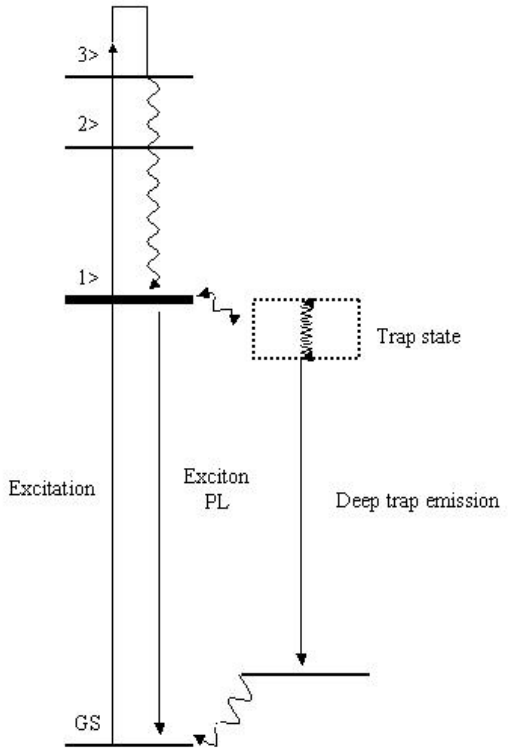

Figure 3.5 The postulate decay route of an exciton generated in CdSe/ ZnS quantum dots [5]

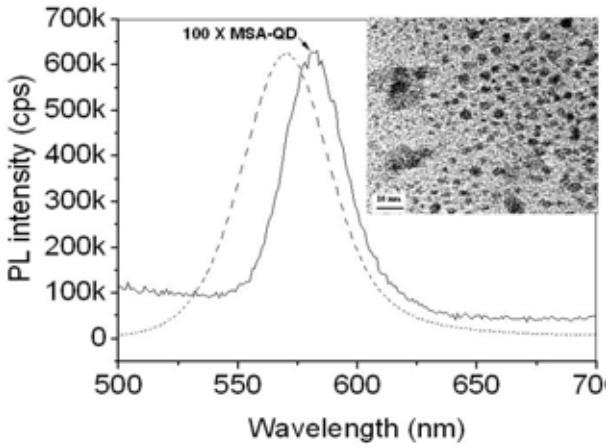

Figure 3.6 Comparison of PL spectra of MSA-QDs (—) and POD-QDs (----) under excitation at 365 nm. The PL intensity of MSA-QDs was magnified 100X. The inset shows TEM images of POD-QDs whose average diameter was estimated to be 2.8 ± 0.4 nm.

3.3.2 Influence of pH on the photoluminescence of POD-QDs

Previous studies have indicated that the PL intensity of water-soluble MSA-QDs is sensitive to the acidity or basicity of a solution [21,22]. As anticipated, this feature was maintained in the case of POD-QDs. As the pH value varied from 8.0 to 5.0, the PL intensity of the QDs was quenched and the emission spectrum was blue-shifted for 10 nm (as shown in Figure 3.7). It is plausible to assume that the quenching phenomenon and the blue-shift of the emission spectra are due to the acidic etching process occurring on the surface of POD-QDs. Consequently, the number of hole-traps on the particle surface was increased and the PL intensity was diminished. We also confirmed the quenching ratio of the PL intensity exhibited a linear response to the acidity of the solution (shown in Figure 3.7,

upper right inset)

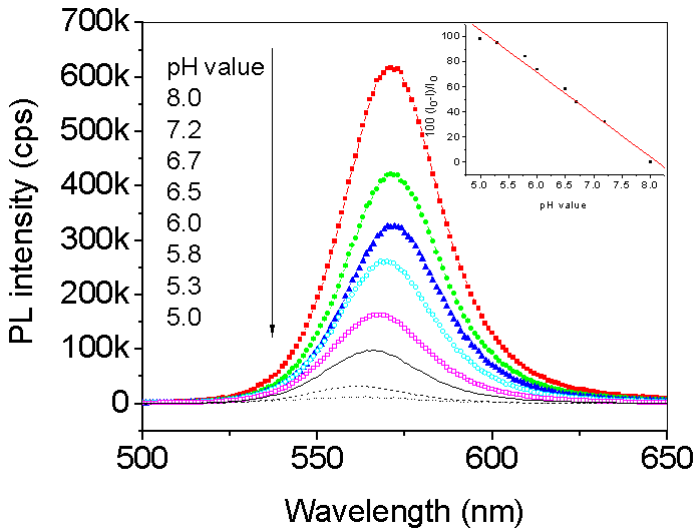

Figure 3.7 Comparison of PL spectra for POD-QDs as a function of pH. The inset reveals correlation between PL quenching ratio of POD-QDs and pH, 100 $(I_o- I)/I_o$ represents the ratio of PL quenching, I_0 is the PL intensity at 570 nm with pH 8.0, and I is the intensity at emission maximum.

3.3.3 Photoluminescence spectroscopy for the detection of triglyceride

Since the PL intensity of QDs is highly sensitive to acidity, we proposed that the POD-QDs should be potentially useful for many biochemical assays that generate acidic or basic products. To examine the feasibility of this proposal, an assay system for triglyceride analysis was established. Tributyrin, a glycerol tributyrate, can be hydrolyzed by lipase to produce glycerol and butyric acid. The general underlying biocatalyzed chemical reaction on which this

operation is based can be described as the follows:

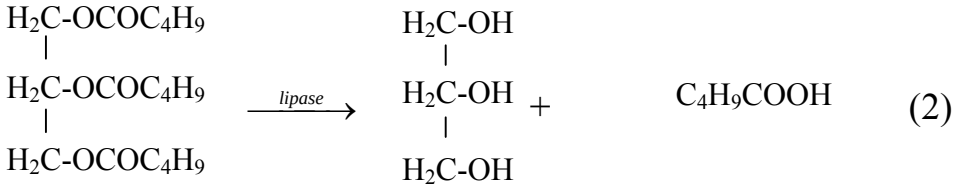

(2)

(Tributyrin) (Glycerol) (Butyric acid)

The pH of the solution changes with the fatty acid produced [23]. The POD-QDs are potentially useful in indicator design-as they are significantly responsive under fluorescence and have a high surface/volume ratio. Although the lipase-catalyzed hydrolysis of tributyrin releases glycerol and fatty acid as products (see equation 2), the pH value of the assayed sample gradually decreases with the degradation of tributyrin. By controlling the initial concentration of employed buffer, the pH condition of a solution can be continuously perturbed by the formation of fatty acid. As demonstrated in Figure 3.8, the variations in fluorescence spectra and the PL intensity of POD-QDs were observed as a function of tributyrin concentration catalyzed to the end point by lipase. The maximal emission peaks were gradually blue-shifted from 570 nm to 560 nm when 0 to 25 mM of tributyrin solution samples were tested. The PL intensity of POD-QDs was increasingly quenched as the concentration of the employed tributyrin was increased. Apparently, the fatty acid, produced as a result of the lipase catalysis, perturbed the acidity of the

assay system and thus influenced the luminescence property of QDs. The blue-shifted PL spectra indicated a trend of decreasing particle size [7].

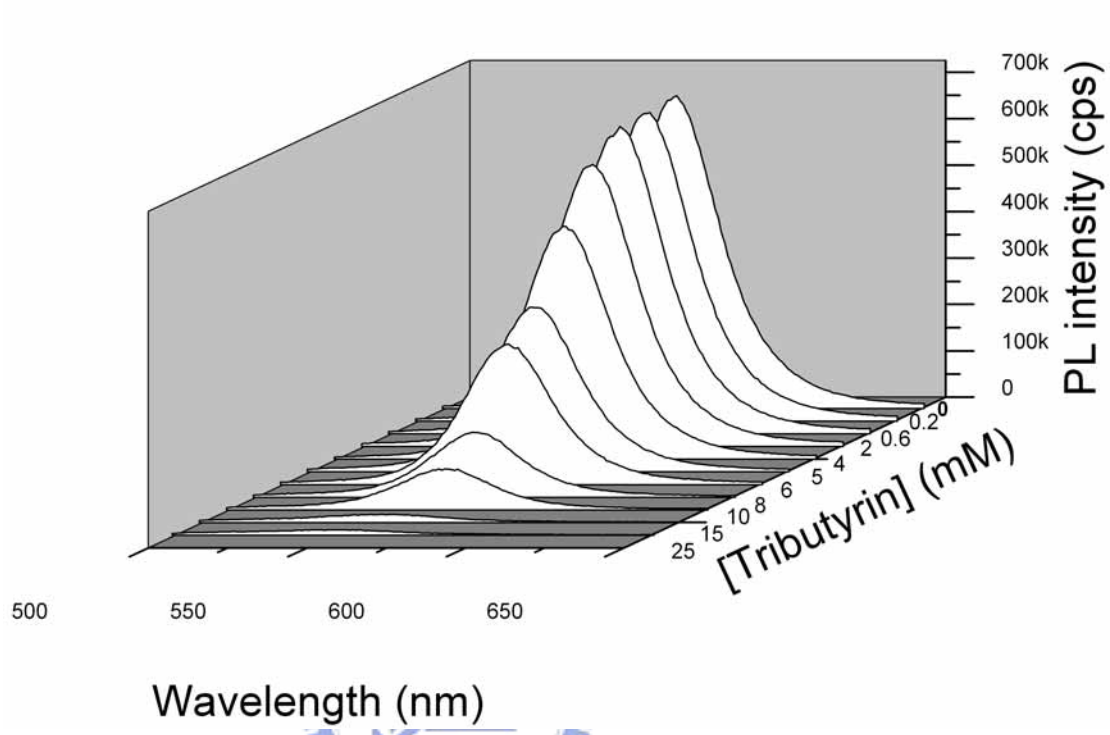

Figure 3.8 Variation of PL intensity of POD-QDs as a function of tributyrin concentration in 10 *m*M phosphate buffer. The PL spectra were recorded at excitation wavelength of 365 nm.

Additionally, Figure 3.9 shows the absorption spectra of lipase/POD-QDs with different tributyrin concentrations (0, 4 and 10 mM) in a 10 mM phosphate buffer with pH 8.0. The slight scattering phenomenon, which results from lipase, tributyrin, and solvent, influences the smoothing of the absorption spectra. It can also be observed that the lipase-catalyzed hydrolysis promoted spectral shifts toward shorter wavelengths in the case of both absorption and luminescence, which is consistent with a possible decrease in particle

size during fatty acid production [16].

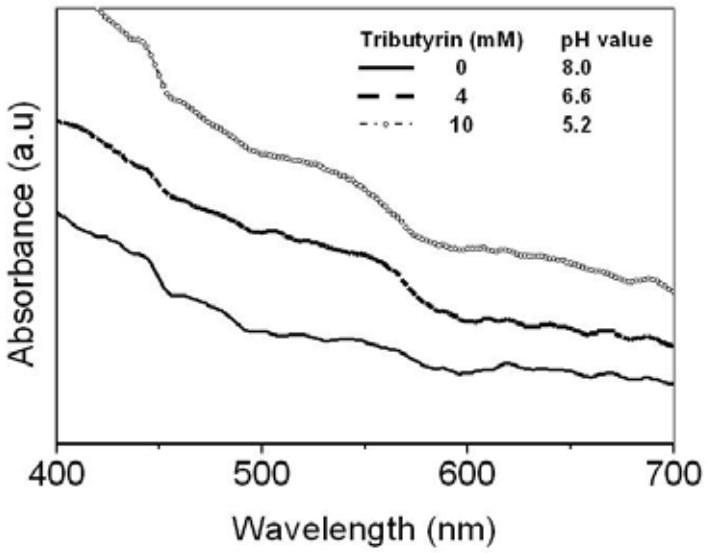

Figure 3.9 Absorption spectra of lipase/POD-QDs with different tributyrin concentration (0, 4 and 10 mM) in 10 mM phosphate buffer with pH 8.0. The assay system obtained in 0 mM (—), 4 mM (---) and 10 mM (oooo) tributyrin with lipase/POD-QDs.

Figure 3.10 plots the quenching ratio of the PL intensity, $100[(I_o-I)/I_o]$, against the concentration of tributyrin. The assays were performed separately in 5, 10, 20 mM of phosphate buffer (pH 8.0), respectively. Since the PL intensity is perturbed by the presence of fatty acid, it is of interest to measure both the change in the PL quenching ratio and the final acidity of the reaction products simultaneously. The down right inset of Figure 3.10 exhibits the responses of pH change and the quenching ratio of PL intensity as a function of tributyrin concentrations hydrolyzed in 5 mM phosphate buffer. Though the pH response showed a good linear correlation at higher tributyrin concentration (0.6 ~ 6 mM), no significant pH change

was observed at lower concentration level (< 0.6 *m*M), which can be rationalized by considering that at [tributyrin] < 0.6mM the proton released can be effectively neutralized by the strong buffering capacity of phosphate buffer solution and thus the observed pH change is negligible.

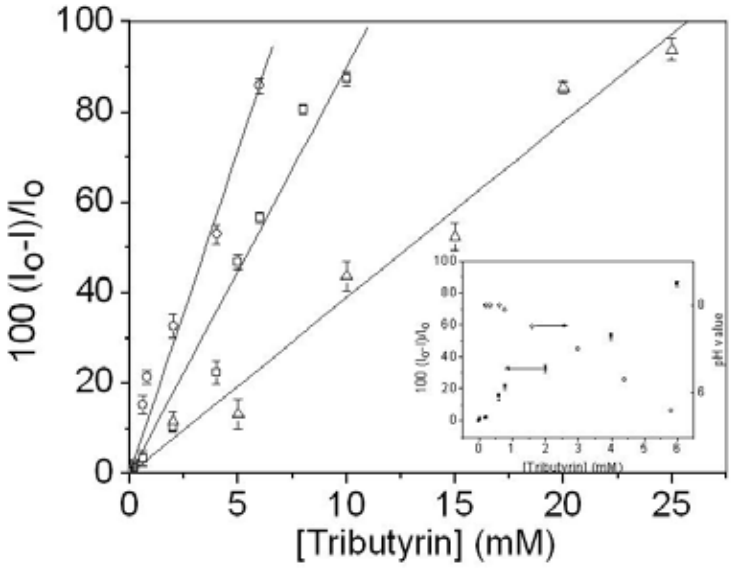

Figure 3.10 Linear correlation between quenching percentage of PL intensity, [100 (I_0 - I)/I_0], and tributyrin concentration. Quenching ratio of PL intensity obtained in phosphate systems of 5-mM (◯), 10-mM (□) and 20-mM (Δ). The inset exhibits the responses of pH change and the quenching ratio of PL intensity as a function of tributyrin concentrations hydrolyzed in 5 mM phosphate buffer.

However, the quenching ratio of PL intensity showed a linear response to triglyceride concentration in the range of 0.02 – 6 mM (correlation coefficient R = 0.986). As a matter of fact, the linearity was not preserved when 8 mM of tributyrin was examined under the same condition, suggesting that the capacity of QDs was insufficient to reflect the existing acid. To overcome and solve this problem, one

could use higher concentration of POD-QDs. Alternatively, the buffer concentration could be adjusted. In principle, the butyric acid produced at the early stage of the reaction will be consumed by the buffer and allow POD-QDs to effectively reveal the acidity of the reaction in late stage. By tuning the buffer capacity of the assay system, the wide-range concentration of triglyceride can be accurately measured. As shown in Figure 3.10, the 10-mM and 20-mM buffer systems are appropriate for the quantitative detection of tributyrin in the range of 0.2 – 10 (correlation coefficient R = 0.979) and 2 – 20 mM (correlation coefficient R = 0.988), respectively. The assay system also provides a convenient way to estimate triglyceride concentration by visualizing the color change of the QDs fluorescence with naked eyes. When the sample with tributyrin concentration higher than 5 mM was assayed in the 10-mM phosphate system, the luminescence of the QDs became almost colorless; whereas, at low concentration level, the yellow fluorescence can be clearly observed (Figure 3.11). It is also feasible to determine tributyrin concentration in other ranges when phosphate buffer with different concentration is selected.

The designed system is promising for triglycerides analysis as compared with many other currently existing methods. Table 1 summarizes the detection limits of triglycerides with various methods including potentiometry, surface acoustic wave, optical spectroscopy and the present study. Our new approach exhibits great potential in triglycerides sensing not only for its simplicity of preparation but also the improvement in sensitivity of detection.

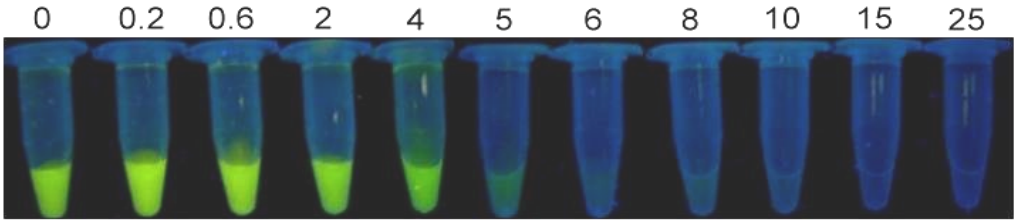

Figure 3.11 Evolution of fluorescence images taken at the end-point of the catalytic hydrolysis of tributyrin in 10 *m*M phosphate buffer under ultraviolet irradiation of 365 nm.

Table 3.1Comparison of performance of different methods for the detection of triglycerides.

Type	Sensing Matrix	Enzyme	Linear range (mM)	Limitation of detection (mM)	Reference
Potentiometry	Porous silicon from p-type (1 0 0) crystalline silicon	Lipase	6 – 30	> 5	[15]
	Silicon nitride	Lipase	5 – 15	5	[21]
Surface Acoustic wave	Pt-electrodes detection cell	Lipase	----	5.46	[16]
Optical method	Quinonemonoimine (A_{abs}=510 nm)	Lipase glycerol kinase 1-α-glycerol kinase Peroxidase	0 – 13.6	1.5	[13]
	NADH (A_{abs}=340 nm)	Lipase glycerol kinase pyruvate kinase lactate dehydrogenase	0.5 – 10	0.5	[14]
	Lipase/POD-QDs	Lipase	0-25	0.02*	This work

* The detection limit of this study was suggested on the basis of the lowest concentration of triglycerin yielding reliable measurements.

3.4 Conclusions

This investigation demonstrated an assay system containing POD-QDs and lipase for the quantitative analysis of triglyceride. With this new approach, triglyceride in a wide range of concentration can be successfully analyzed. As compared to traditional triglyceride assay methods, the POD-QDs-based detection exhibits several advantages, such as ease of reagent preparation, low cost, no enzymatic immobilization, high flexibility, and good sensitivity. The newly developed method can quantitatively determine triglyceride without using multiple enzymes and/or complicated instrument setup.

3.5 Reference

[1] W. J. Jin, M. T. Fernandez-Arguelles, J. M. Costa-Fernandez, A. Sanz-Medel, R. Pereiro, *Chem. Commun.* **(2005)** 883.

[2] J. A. Kloepfer, S. E. Bradforth, J. L. Nadeau, *J. Phys. Chem. B.* 109 **(2005)** 9996.

[3] S. F. Wuister, C. M. Donega, A. Meijerink, *J. Phys. Chem. B.* 108 **(2004)** 17393.

[4] T. Torimoto, S. Murakami, M. Sakuraoka, K. Iwasaki, K. Okazaki, T. Shibayama, B. Ohtani, *J. Phys. Chem. B.* 110 **(2006)** 13314.

[5] M. Jones, J. Nedeljkovic, R. J. Ellingson, A. J. Nozik, G. Rumbles, *J. Phys. Chem. B.* 107 **(2003)** 11346.

[6] J. Aldana, Y. A. Wang, X. Peng, *J. Am. Chem. Soc.* 123 **(2001)** 8844.

[7] Y. Wang, Z. Tang, M. A. Correa-Duarte, I. Pastoriza-Santos, M. Giersig, Nicholas A. Kotov, and L. M. Liz-Marzan, *J. Phys. Chem. B.* 108 **(2004)**15461.

[8] W. G. J. H. M. Sark, P. L. T. M. Frederix, D. J. V. Heuvel, and H. C. Gerritsen, *J. Phys. Chem. B.* 105 **(2001)** 8281.

[9] L. Manna, E. C. Scher, L-S. Li, and A. P. Alivisatos, *J. Am. Chem. Soc.* 124 **(2002)** 7136.

[10]J. A. Gaunt, A. E. Knight, S. A. Windsor, and V. Chechik, *J. Coll. Inter. Sci.* 290 **(2005)** 437.

[11]S. Maenosono, N. Eiha, Y. Yamaguchi, *J. Phys. Chem. B.* 107 **(2003)** 2645.

[12]W. J. Jin, J. M. Costa-Fernandez, R. Pereiro, A. Sanz-Medel, *Anal.*

Chim. Acta. 522 **(2004)** 1.

[13]P. Fossati and L. Prencipe, *Clinc. Chem.* 28 **(1982)** 2077.

[14]G. Bucolo and H. David, *Clin. Chem.* 19 **(1973)** 476.

[15]R. R. K. Reddy, I. Basu, E. Bhattacharya, A. Chadha, *Curr. Appl. Phys.* 3 **(2003)** 155.

[16]K. Ge, D. Liu, K. Chen, L. Nie, S. Yao, *Anal. Biochem.* 226 **(1995)** 207.

[17]X. G. Peng, L. Manna, W. D.Yang, J. Wickham, E. Scher, A. Kadavanich, A. P. Alivisatos, *Nature.* 404 **(2000)** 59.

[18]W. C. W. Chan , S. M. Nie, *Science.* 281**(1998)** 2016.

[19]C-P. Huang, Y-K. Li, T-M. Chen, *Biosens. Bioelectron.* 22 **(2007)** 1835.

[20]N. V. Soloviev, A. Eichhofer, D. Fenske, U. Banin, *J. Am. Chem.Soc. 123* (**2001)** 2354.

[21]X. Gao, W. C. W. Chan, S. Nie, *J. Biomedical. Optics.* 7 **(2002)** 532.

[22]Basu, R. V. Subramanian, A. Mathew, A. M. Kayastha, A. Chadha, E. Bhattacharya, *Sens. Actuators B.* 107 **(2005)** 418.

[23]Amjad Y. Nazzal, Lianhua. Qu, Xiaogang. Peng, Min. Xiao, *Nano Lett.*, 3 **(2003)** 819.

Chapter 4 Synthesis and Characterization of Poly (diallyldimethylammonium chloride)-capped CdSe/ZnS quantum dots with photoactivation for Fluorescence Resonance Energy Transfer application

Abstract:

A new synthetic method that allows simultaneous in situ encapsulation and photoenhancement of QDs by Poly (diallyldimethylammonium chloride) (PDDA) with D, L-Mercaptosuccinic acid (MSA) interaction under fluorescent lamp (intensity 8.5 mW/cm^2) treatment at room temperature, 26 hours. The quantum yield of PDDA-QDs would be improved into 48% to compare with MSA-QDs (0.6%). By the new synthetic method, the multicolor PDDA-QDs are easily to make with high photoluminescence, quantum yield, and well distribution. Using photoluminescence spectrophotometer, Agarose Gel Electrophoresis, Transmission electron microscopy, and Auger Electron Microprobe investigated the surface characterization (including: fluorescence, charge, size and binding energy) in PDDA-QDs and MSA-QDs, respectively. Furthermore, the PDDA-QDs supported the high luminescence and surface charge with Streptavidin-Rhodamine to realize the Fluorescence Resonance Energy Transfer (FRET) model with organic dye (Rhodamine). In this study, the high throughput and high luminescence PDDA-QDs possesses many advantages, including simplicity, high luminescence, and stability.

4.1 Introduction

Quantum dots are currently an active subject of investigation in nanoscience and nanotechnology. Hence, the luminescence of water-soluble QDs improved to be popular in the recent research. At present, the synthetic methods of the water-soluble QDs have several shortcomings: it is cost consuming, still complicated, and low luminescence. The encapsulation of QDs and their primary ligands with macromolecules such as lipids and polymers preserves their quantum yield (QY) [1]; however, the emulsion phenomenon of the QDs does not avoid and the ligands are not easy to get. In additionally, the thiols group is the most utilized ligands for stabilizing QDs, and they have been used almost exclusively in the biotechnology studied [2-5]. Nevertheless, the thio-coated CdSe/ZnS nanocrystals have shown very profound photochemical instability in solution. Unfortunately, the stability of thiol-stabilized nanocrystals used, especially in the case of semiconductor nanocrystals, is not satisfactory mainly due to the photooxidation of the nanocrystal/ligands complex [6-10]. The unstable nature of these nanocrystals makes it hard to reproduce applying for chemical and biochemical procedures to them. Then, the thio-coated QDs would trap the hole on the surface and reduce the luminescence efficiency [6-7]. Therefore, photoenhancement of CdSe or CdSe/ZnS QDs photoluminescence has been reported previously in aqueous solution, thin films, and monolayers by photoactivated [11-14]. Previous author reported that the intensity of exciton PL in hexadecylamine (HDA)-capped QDs was found to increase under broad-band (400-490

nm) illumination [15]. Additionally, the exciton PL peak underwent a blue shift and a narrowing with subsequent rebroadening. The PL enhancement was due to the photoinduced the QDs could rearrange the surfactant molecules that serve to stabilize the e^- or h^+ traps on the QDs surface [11-14].

Herein we report a new synthetic method that allows simultaneous in situ encapsulation and photoenhancement of QDs by Poly (diallyldimethylammonium chloride) (PDDA) with D, L-Mercaptosuccinic acid (MSA) interaction and fluorescent lamp (intensity 8.5 mW/cm^2) treatment. This method avoids the aggregation after photoactivated and preserves the stability of QDs with high Q.Y. Hence, instead of using thiols as capping agent, we introduce the PDDA surrounding on QDs by electrostatic interaction with MSA. The PDDA served both as a stabilizer to disperse QDs and as a linker for absorption with biomolecules. Immediately, the photoactivation improved the luminescence efficiency and reduced the surface defects to decrease the nonradiation recombination [16]. It was found that the obtained PDDA-QDs exhibited high photoluminescence intensity and good dispersion property in the solution. Beside, the quantum yield of PDDA-QDs would be improved into 48% to compare with MSA-QDs (0.6%) as measured using the procedure described by Williams et al [17]. Consequently, we investigated and compared the surface characterization (including: charge, binding energy), photoluminescence and size distribution in the PDDA-QDs and MSA-QDs. Furthermore, the PDDA-QDs supported the high luminescence and surface charge with Streptavidin-Rhodamine to realize the Fluorescence Resonance Energy

Transfer (FRET) model with organic dye (Rhodamine). The organic dyes are easily covalent attached at a specific residue of a streptavidin (SAv). Dye-labeled SAv is allowed to self-assemble around the PDDA- QDs surface through electrostatic interaction. Using the steady-state fluorescence spectra were collected from the PDDA-QDs and SAv-TMR interaction along with the spectra of the individual donor and acceptor species as direct excitation controls. Through the imaging demonstrated and fluorescence spectra, we found the characterization of FRET between these dyes and the PDDA-QDs. Thus, we hereby reported the preparation of the high throughput and high luminescence water-soluble QDs by PDDA capped with photoactivation. As compared to most of the existing method, our synthetic method reported herein possesses many advantages, including simplicity, high luminescence, and stability.

4.2 *Materials and Methods*

4.2.1 Instruments and chemicals

A Hitachi U-3010A UV-visible spectrophotometer and a Jobin-Yvon Spex Fluolog-3 spectrophotometer were used to investigate the fluorescence characteristics of the samples. Transmission electron microscopy was performed on a Philips TECNAI 20 microscope operating at 200 kV. The samples were prepared by dropping diluted solutions of PDDA-QD nanocrystals onto 200-mesh carbon-coated copper grids. Samples for XPS were deposited the MSA-QDs and PDDA-QDs solution onto the wafer. Then, the sample were exposed under the nitrogen and stored in the dark environment to remove the

solvent. XPS was performed on a VG Scientific,Microlab 350 spectrometer using Al Kα excitation. All chemicals were of analytical grade or the highest purity available. Chloroform, methanol, diethyl zinc (1M solution in toluene), cadmium oxide, selenium, and sulfur powder were purchased from Aldrich. *n*-Hexadecylamine (HDA) and stearic acid (SA) were obtained from Lancaster. tri-*n*-Butylphosphine (TBP) was from Showa. D, L-Mercaptosuccinic acid (MSA), and 25% (by weight) of tetramethylammonium hydroxide (TMAOH) in methanol were from Acros. The 20% (by weight) of Poly (diallyldimethylammonium chloride) solution (PDDA) was from Aldrich-sigma. Rhodamine Red-X, succinimidyl ester 5-isomer was obtained from Molecular Probes. Streptavidin was from sigma.

4.2.2 Synthesis of the Poly (diallyldimethylammonium chloride) solution (PDDA) capped CdSe/ZnS quantum dots with photoactivation

Luminescent HDA capping CdSe/ZnS QDs were synthesized according to the previously reported procedure [18-19]. However**,** MSA was selected as the surface-capping reagent to form water-soluble QDs. 2 ml CdSe/ZnS QDs (21.6 M) was suspended in 20 mL of chloroform in which a separated 1 mL methanolic solution of 1 M MSA was then added. The pH of the resulting solution was adjusted to 11.0 by adding tetramethylammonium hydroxide pentahydrate. The mixture was kept in dark and refluxed at 30˚C overnight under N_2. When reaction was completed, the MSA-QDs were precipitated with 25 ml methanol and 10 ml acetone and further collected by centrifugation (4185 xg). Methanol

(7 ml each time) and acetone (3 ml each time) were employed to wash the precipitated QDs ten times, 5 mines. The MSA-QDs were then re-dissolved in a phosphate buffer (100 mM, pH 8.0). Then, 1 ml re-dispersed MSA-CdSe/ZnS solution with OD= 1 was dropped into 0.5 ml PDDA solution (17.8mg/ml) under an ultrasonicwave. To perform the high luminescence efficiency PDDA-QDs, the synthesis process were illuminated with 21 W table lamp (intensity 8.5 mW/cm^2) for 24 h at ambient temperature. The PDDA-QDs were then obtained by centrifugation (10600 xg) for 10 min and re-dissolved in 100 mM phosphate buffer.

4.2.3 Conditions of the agarose gel electrophoresis

Measurements were carried out on agarose gels prepared at 0.5 % in TAE migration buffer (0.4 M TRIS, 0.01 M EDTA, 1.142% acetic acid, pH 10.0). The operation voltage is 100 V. After a 30 min run, the bands were detected by illuminating the gel with the light.

4.2.4 Conditions of the Rhodamine X-labeling on Streptavidin

1 mg of Rhodamine X was dissolved into 0.5 ml anhydrous DMF and added to 0.25 mg of Streptavidin dissolved in 1 ml of 0.1 mM sodium bicarbonate buffer (pH 8.5). The mixed solution was incubated while agitated 1 hour at room temperature, and then added 0.1 mL of freshly prepared 1.5 M hydroxylamine (pH 8.5) to quench the reaction after 1 hour. The Sephadex G (G-25) separated the dye-labeling streptavidin

from unreacted labeling reagent.

4.2.5 Assay condition of the FRET between PDDA-QDs with Rhodamine X-Streptavidin

FRET investigated by reacting 3 μl aliquots PDDA-QDs (3.85μM) solution with 0~70 μl SAv-Rhodamine (0.95μM) in 10 mM phosphate buffer solution, pH 8.0. After 1 hour of incubation time, the reaction mixtures were diluted to 103 μl in PB buffer, and the resulting solutions were placed in 1 cm path length quartz curvettes for photolumiscence measurement.

4.3 Results and Discussion

4.3.1 Optical properties of the PDDA-QDs with photoactivation

Previous investigations indicated that the capping molecular or photoactivation affected the characterization of photoluminescence of QDs [20-22]. Additionally, traditional water-soluble QDs synthetic methods were almost through the thio group surfactant substituted from their primary ligand (TOPO or HDA). Unfortunately, low luminescence QY is often observed in as-prepared nanoparticles, mainly due to the non-radiative recombination of the electron-hole pair at surface site and surface trap competing with band-edge emission. This displeasing property is particularly found in the water-soluble QDs capping with thiol group [5-6]. Very recently, the process of photoactivation was shown to enhance the photoluminescence (PL) of QDs [8]. Additionally, the

polymer molecular capped also eliminate the defects and traps on the QDs surface to increase the recombination of electron and hole [16]. Consequently, our investigation confirmed these finding and design the high luminescence water-soluble PDDA-QDs. Previous authors provided that different capping agents would affect the luminescience properties of QDs [20]. Nevertheless, the PDDA-QDs would be through repleasing the hydrophobic capping agent (HDA) with MSA and absorbing PDDA under photoactivation on the QDs. Figure 4.1 shows that the optical characterization of different capping molecular on QDs with or without photoactivation. Narrow emission bands centered at 562 nm (MSA-QDs) and 557nm (HDA-QDs) were observed when the QDs were excited with a 365 nm He/Ne source. The significant effects on photoluminescence as well as the low QE and red-shift (~5 nm) features of the MSA-QDs are attributed to the trap-states, which normally involves, at least, two reasons. First, the hole is trapped on a thiol molecule; radiative recombination of the exciton is not possible, resulting in a strongly reduced QE. Second, the red-shift observed when thiols adsorb may be due to an increase in the delocalization of the hole wave function due to the availability of new accessible energy states on the adsorbed chalcogenide atoms [7][20].

Hence, these particularly characteristics in the synthetic water-soluble QDs through thio groups capped are easily to production and not useful in biological. However, in this investigation, using the PDDA, absorbed on the MSA-QDs surface under light-trement, could improve the shortcomings (only thio capped QDs), such as the luminescence; Quantum yield; traps on the surface. Figure 4.1 shows

the narrow emission band of the PDDA-QDs centered at 533 nm (excited at 365 nm). Significantly, the results represent that the PL intensity and the emission spectrum were clearly enhancement (200 fold) and blue-shifted (~29 nm) comparing with MSA-QDs and PDDA-QDs, respectively. Upon the light irradiation in ambient environment, the PDDA-QDs has high QY (~48%) and showed significantly blue-shifted from 562 to 533 nm in their emission peak wavelength, indicating that the size of QDs were getting smaller as result of the photo-etching [8].

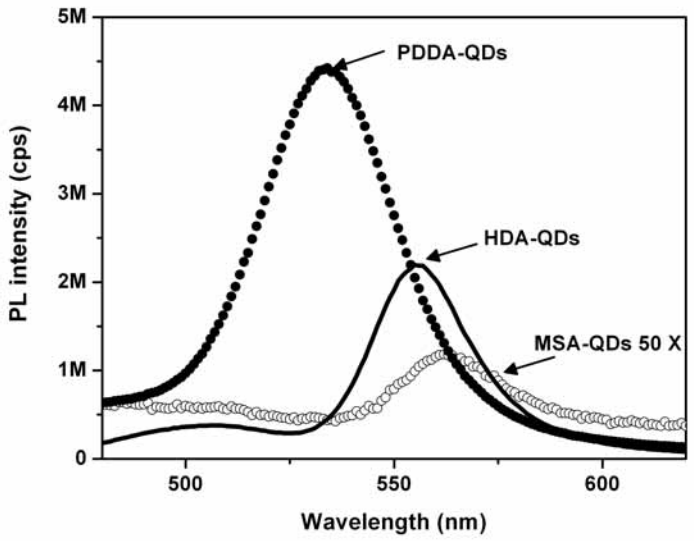

Figure 4.1 The optical characterization of different capping molecular on QDs, MSA capped (。。。); HDA capped (—); PDDA capped (●●●) under 365 nm excited.

These noticeable phenomenons in the PDDA-QDs with photoactivation can be ascribed in the QDs surface structure [16]. In accordance with the protocols of PDDA-QDs, the PDDA supplied the positive charge and were readily able to absorb on the MSA-QDs surface by van der Waals. Subsequently, the surface defects were passivated by the PDDA and the nonradiative recombination was eliminated. At the

same time, the light irradiated on the PDDA-QDs could enhance the PL and reduce the trap-state on the surfaces to improve the Q.Y from 0.2% to 48%. In order to compare the efficiency of polymer capped, a negative polyelectrolyte PSS (data not shown) was used to cape on the MSA-QDs with photoactivation. The effect of the PSS on the photoluminescence intensity and distribution of the MSA-QDs solution were very weak and aggregation easily after photoactivation. The PSS could not support well shielding and oxidizing easy on the QDs surface. Besides, Figure 4.2 depicts the time evolution of the emission intensity for PDDA-QDs and demonstrates that photoetching or photooxidation of the PDDA-QDs. In Figure 4.2 (a), the emission peak of PDDA-QDs showed blue-shifted and enhancement with photoactivation under 0 to 35 hours, and the intensity of emission peak under 35 hours photoactivation is the same with 26 hours treament. Additionally, Figure 4.2 (b) represented the experiments of the maximum emission peak and the PL as a function of photoactivation time on the PDDA-QDs. The datas were directly derived from Figure 4.2 (a). The results pointed out the characteristics of PL that could be enhanced (~ 200 folds) and blue-shifted (~29 nm) during the photoactivated through 0 to 35 hours. Therefore, after light irradiation, the probability of the electrons and holes being present on the surface as result of photooxidation is increased in the QDs with QY. This phenomenon was further verified by the surface-related emission [23]. In fact, this increasingly probability of the carriers being present on the QDs surface with high QY is a directly consequence of the optimal surface reconstruction in the sample growth process, which efficiently removes the carrier quenching defects from the surface [8,16].

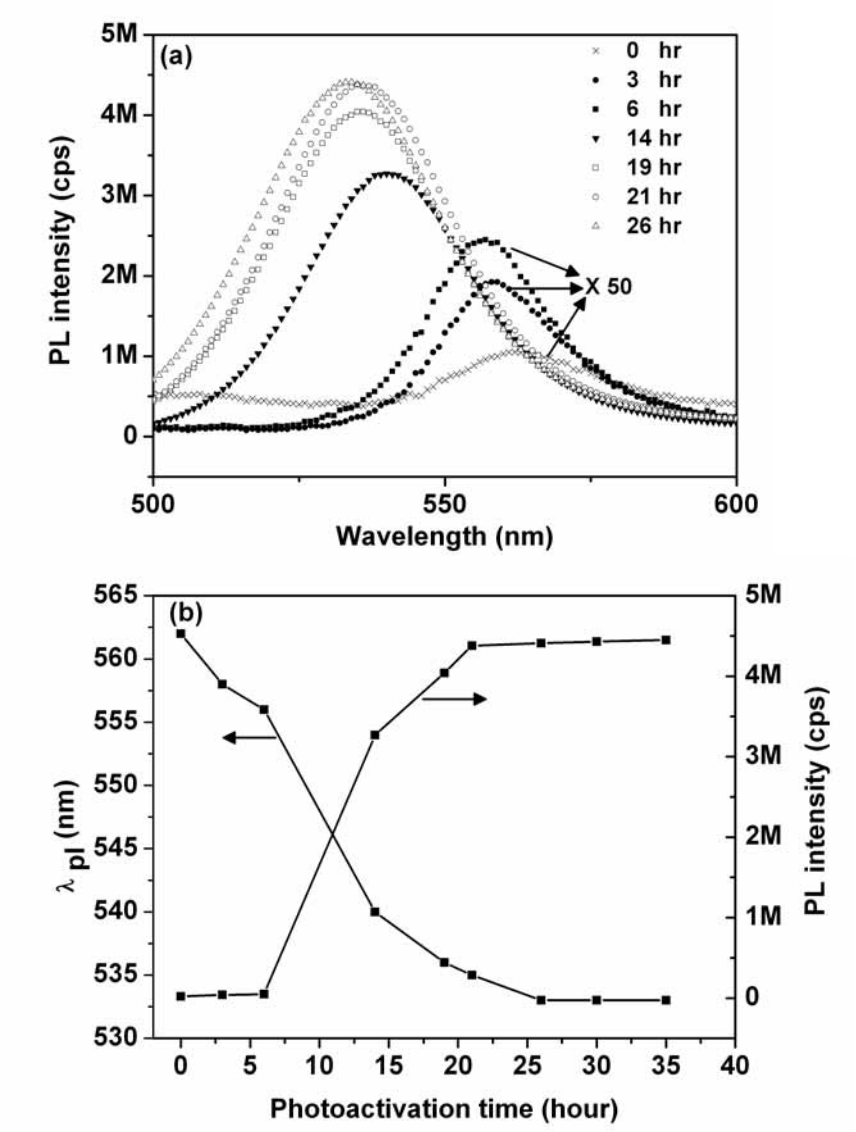

Figure 4.2 The time evolution of the emission intensity for PDDA-QDs and demonstrates that photoetching or photooxidation of the PDDA-QDs; (a) the emission peak of PDDA-QDs; (b) the experiments of the maximum emission peak and the PL as a function of photoactivation time on the PDDA-QDs.

Hence, using photoactivation on the PDDA-QDs not only improve the characterization of Q.Y and PL, but also prepare different size QDs

with various emission samples. Previous investigation reported using photoactivation, by irradiation times; control the size in the QDs. But this method cannot get almost Q.Y and photoluminescence on the different size QDs. By the new approach, it can fabricate the multicolor QDs with high PL, Q.Y, and well distribution. Figure 4.3 shows the photoluminescence and images (inset) with the multicolor of the PDDA-QDs, which emission peaks centered at 535 nm (Green), 555nm (Yellow) and 580 nm (Red), when these were excited by 365 nm.

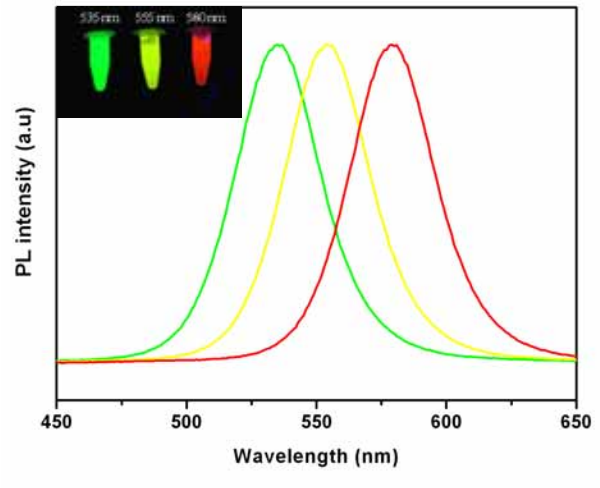

Figure 4.3 The photoluminescence and images (inset) with the multicolor of the PDDA-QDs, which emission peaks centered at 535 nm (Green), 555nm (Yellow) and 580 nm (Red), when these were excited by 365 nm.

The result indicated the multicolor PDDA-QDs have narrow full width at half maximum (FWHM) and high luminescence in virtue of the photoactivation and polymer capping rearranging the QDs surface. The similar Q.Y and PL intensity of multicolor PDDA-QDs were made by MSA-QDs with different emission ranges. Although controlling the irradiation times could make the multicolor PDDA-QDs, it cannot improve the similar Q.Y and PL intensity. It's because of the irradiation

times would affect the ratio of rearranging QDs surface and reversed the nonradiation to radiation recombination, which cause from trap electron or hole to nature band gap. Therefore, by irradiation times to fabricate the multicolor QDs is difficult to make the similar efficiency on the PDDA-QDs.

4.3.2 Surface and Size Characterization of the PDDA-QDs with photoactivation

Migration in agarose gels is a convenient technique to check the homogeneity of coated QDs in term of charge, with a good resolution in particles [24]. During gel electrophoresis in TAE buffer (Tris-Acetate-EDTA) (pH 8.3), samples migrated in a narrow predominant band, suggesting the homogeneity of the different capped agent on QDs (MSA, and PDDA capped). The migration directions of this band depend on the QDs surface charge (as shown in Figure 4.4)

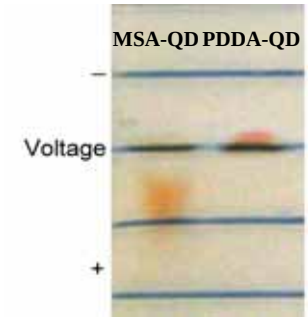

Figure 4.4 The gel electrophoresis of MSA-QD and PDDA-QD were drove by 100 V.

In the results, the migration directions in the MSA-QDs look on the positive voltage, however, the PDDA-QDs flows into negative voltage

under 100 V driving. As result of the MSA capped on the QDs surface, the carboxyl groups supported the negative charges and toward to the positive voltage under 100 V driving. On the other hand, the PDDA-QDs has positive charges on the surface; it's due to the PDDA capped on the QDs surface with MSA by electrostatic interaction, and then the photoactivation on PDDA-QDs solution could reduce the MSA absorption and support the positive charges on the surface.

TEM allows us to determine the average size; size distribution of particles with different capped agent on QDs. Figure 4.5 (a-c) indicated the multicolor of PDDA-QDs with various sizes. The size of green emission (λ_{em} 535 nm) is around 3.2 ± 0.3 nm; yellow emission (λ_{em} 555 nm) is around 3.5±0.2 nm and red emission (λ_{em} 580 nm) is around 4.6±0.2nm. As result of the PDDA capped, theses particle size distributions are well in the solution with various sizes.

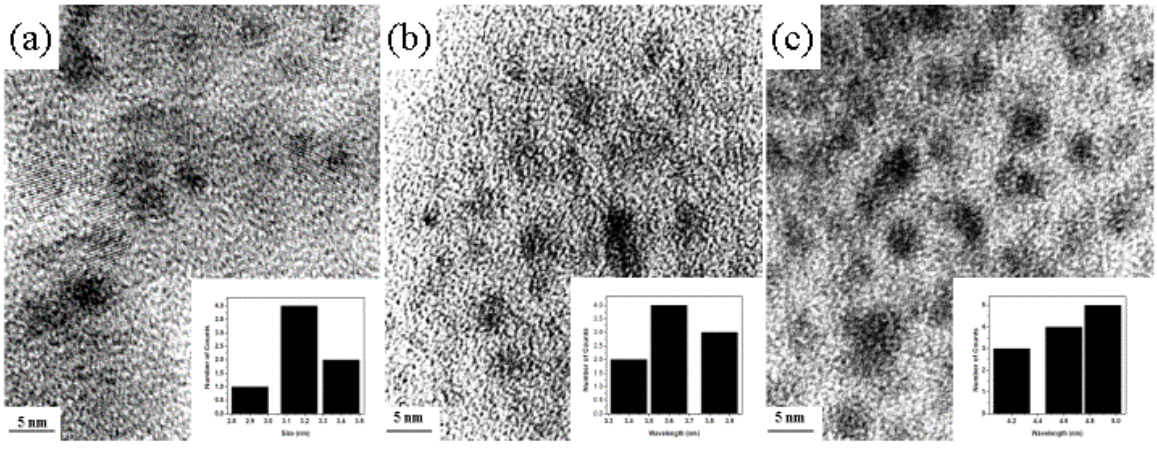

Figure 4.5 the multicolor of PDDA-QDs with various sizes. The size of green emission (λ_{em} 535 nm) is around 3.2 ± 0.3 nm; yellow emission (λ_{em} 555 nm) is around 3.5±0.2 nm and red emission (λ_{em} 580 nm) is around 4.6±0.2nm.

Multiple XPS measurements have been taken with MSA-QDs and PDDA-QDs. Typical survey spectra were obtained in 10 min using Mg Kα source.

Figure 4.6 represented the prominent peaks: Cd $3d_{5/2}$, $3d_{3/2}$; Se 3d; Zn 3S; S 2p; C 1s and O 1s from the nanocrystals and their surfaces. The survey spectra give a rough idea that photoactivation promotes the binding energy on the PDDA- QDs surface and keep the peak shifted toward to high binding energy position. As result of photoactivation on the PDDA-QDs, the intensity of binding energy is lower than MSA-QDs. The reasoning are base on following: (1) the photooxidation, goes along with photoactivation, on the PDDA-QDs surface could dissolve the dangling bonds of the surface atoms and release the Cd and Se ions to form oxidation state. Hence, the atomic component of the PDDA-QDs would be decreased, and then the binding energy intensity becomes weak. (2) The PDDA capped on the MSA-QDs surface, through the electrostatic interaction with MSA, could shelter the QDs from X-ray struck and reduce the binding energy intensity. Therefore, higher-resolution spectra were taken of the Cd and Se regions of samples with MSA-QDs and PDDA-QDs (Figure 4.7) to evidence the spectra various. The photoemission peaks from PDDA-QDs occur several electronvolts to higher binding energy of the main peak in the spectrum. Unique information about the amount and chemical state of the Cd, Se, C and O had been achieved by applying the XPS. As could be seen in Figure 4.7, the appearances of $Cd3d_{5/2}$ at 407 eV (409 eV), $Cd3d_{3/2}$ at 413.8eV (416 eV), Se 3d at 55.1eV (55.9eV), C 1s at 287 eV (288 eV) and O 1s at 533

eV(534 eV) confirmed the existence of Cadmium, selenium, carbon and oxide in both the MSA-QDs and PDDA-QDs, repecticely. For the PDDA-QDs sample, the Se 3d at 55.9 eV has slight intensity. It was worth mentioning that the intensity of the binding energy on Se 3d were reduced, due to the PDDA were capped and shield on the MSA-QDs surface, and then the atomics kept away from the PDDA-QDs surface after photoactivation. Therefore, Table 4.1 The binding energy intensity and the atomic amount of MSA-QD and PDDA-QD indicated the atomic amount of the MSA-QDs and PDDA-QDs, respectively. According to Figure 4.7 and Table 4.1 The binding energy intensity and the atomic amount of MSA-QD and PDDA-QD, the binding energy intensity and the atomic amount were also decreased in the PDDA-QDs. Consequently, the size of PDDA-QDs would be reduced after the photoactivation.

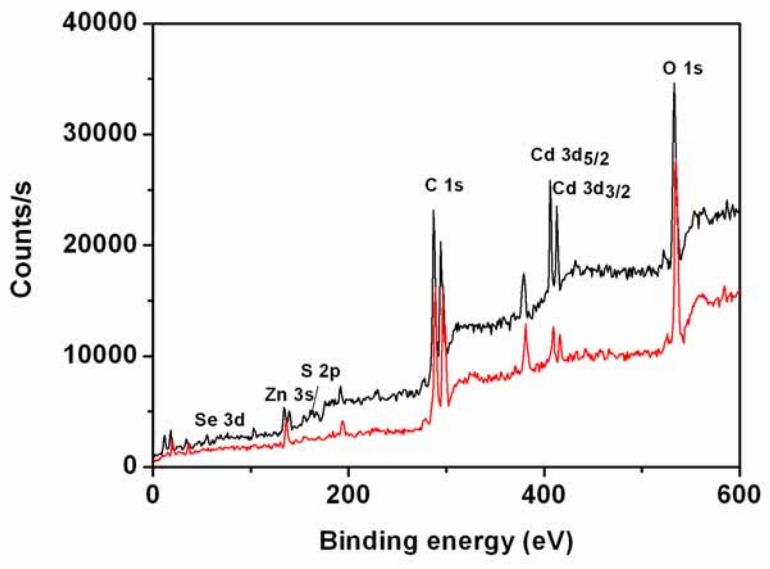

Figure 4.6 Multiple XPS measurements of MSA-QDs (Black line) and PDDA-QDs (Red line) by Mg Kα source; the prominent peaks: Cd $3d_{5/2}$, $3d_{3/2}$; Se 3d; Zn 3S; S 2p; C 1s and O 1s from the nanocrystals and their surfaces.

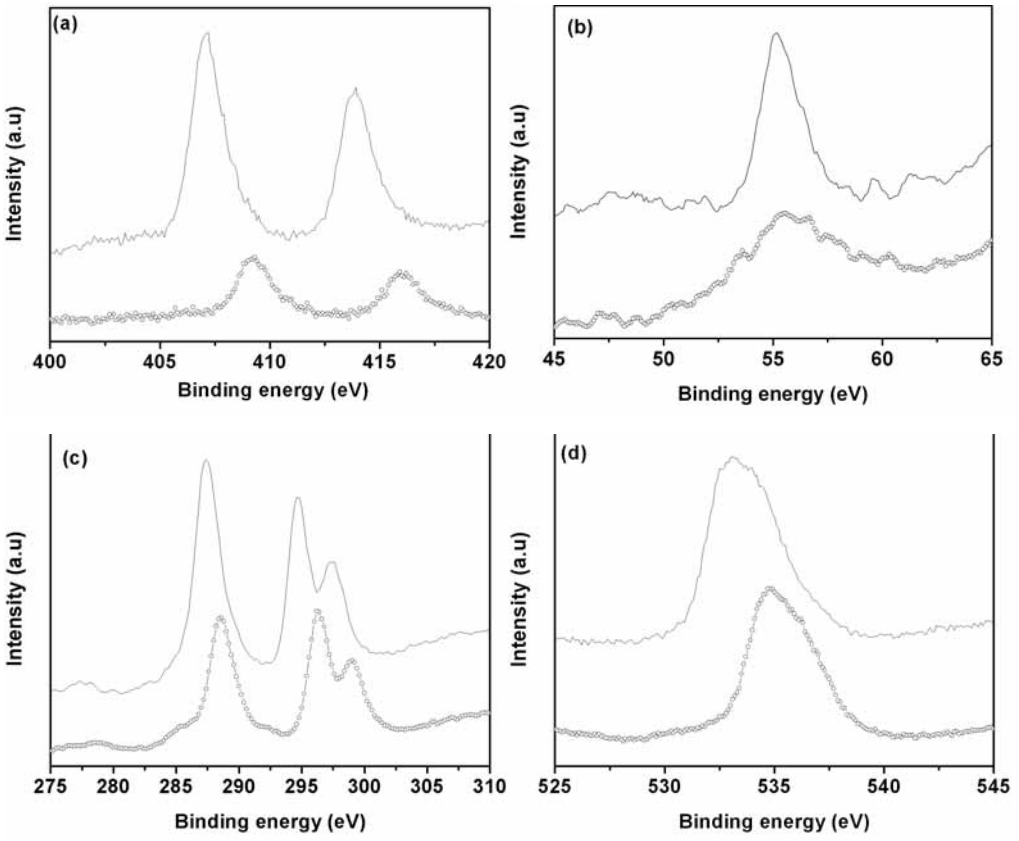

Figure 4.7 The appearances of (a) $Cd3d_{5/2}$ at 407 eV (409 eV), $Cd3d_{3/2}$ at 413.8eV (416 eV), (b) Se 3d at 55.1eV (55.9eV), (c) C 1s at 287 eV (288 eV) and (d) O 1s at 533 eV(534 eV) confirmed the existence of Cadmium, selenium, carbon and oxide in both the MSA-QDs (—) and PDDA-QDs (—。—), repecticely.

Table 4.1 The binding energy intensity and the atomic amount of MSA-QD and PDDA-QD

	Binding energy (eV)		Atom %	
	MSA-QD	PDDA-QD	MSA-QD	PDDA-QD
Se 3d	55.1	55.9	0.75	0.53
S 2p	161.5	163.2	2.7	0.25
C 1s	287.4	288.5	43.74	48.7
$Cd3d_{5/2}$	407	409	3	1.4
$Cd3d_{3/2}$	413.8	416	2.94	1.1
O 1s	533.1	534.8	33.82	40.5
Zn 3s	135	136.1	13.05	7.52

4.3.3 Fluorescence resonance energy transfer with the PDDA-QDs and SAv-Rhodamine

FRET investigated by reacting 3 μl aliquots PDDA-QDs (3.85μM) solution with 0~70 μl SAv-Rhodamine (0.95μM) in 10 mM phosphate buffer solution, pH 8.0. After 1 hour of incubation time, the reaction mixtures were diluted to 103 μl in PB buffer, and the resulting solutions were placed in 1 cm path length quartz curvettes. The PDDA-QDs and SAv-Rhodamine concentrations were ~92 nM and 0~645 nM, respectively. Figure 8 displays the emission spectra observed for these samples. An excitation wavelength of 350 nm was used for all samples. Since this excitation wavelength can provide the QDs with high efficiency luminescence, and avoid exciting directly in the Rhodamine. The strong enhancement of Rhodamine fluorescence, observed in the PDDA-QDs/ SAv-Rhodamine systems, is consistent with QD to Rhodamine FRET-due to the electrostatic binding of SAv- Rhodamine and PDDA- QDs. The result indicated that there is a clear progression in

the fluorophore emissions as a function of increasing numbers of SAv-Rhodamine; namely a progressive quenching of the QD emission and a systematic enhancement of the Rhodamine emission as the concentration of SAv- Rhodamine increase from 0~645 nM.

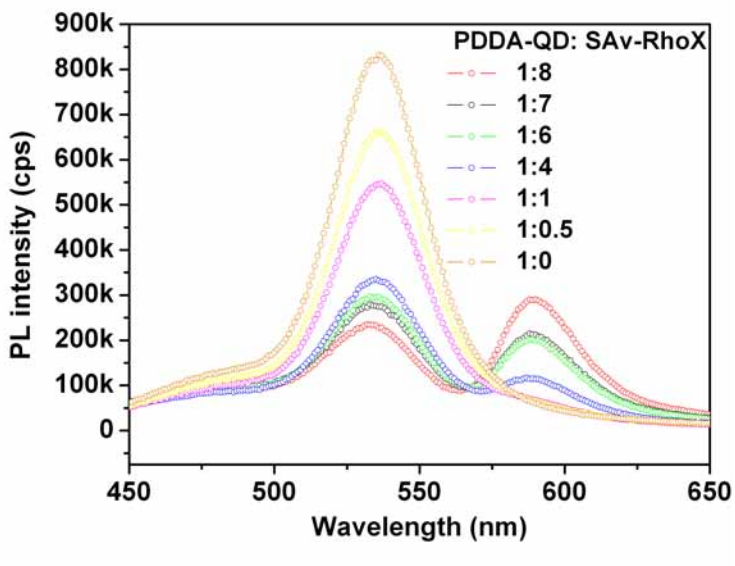

Figure 4.8 Fluorescence emission spectra from solutions containing 92 nM PDDA-QD and 0~645 nM SAv-Rhodamine by molar ratio. All solutions were prepared in 10 mM PB buffer. An excitation wavelength of 350 nm was used for all samples.

Figure 4.9 depicts the PL and FRET efficiencies as a function of the SAv-Rhodamine/PDDA-QDs molar ratio. The PL efficiency was derived from $F_{DA}/+$. F_{DA} is the integrated fluorescence intensity of the donor in the presence of acceptor(s) and F_D is the integrated fluorescence intensity of donor alone (no acceptor present). Then, the FRET efficiency can be measured experimentally and is commonly defined as following equation [25]:

$$E = 1 - \frac{F_{DA}}{F_D} \quad (1)$$

As a result of, the progressive donor quenching compared to the acceptor PL enhancement with increasing the concentration of SAv-Rhodamine adsorbed on the surface of PDDA-QDs. In additionally, the FRET efficiency provides the high-energy transfer efficiency from PDDA-QDs to SAv-Rhodamine. Then, the trends are consistent as a progressive increase in the acceptor emission follows the expected energy gain. Hence, we could distinguish from the fluorescence of SAv-Rhodamine/PDDA-QDs with molar ratio (from Figure 4.10). The FRET efficiency is determined through the fluorescence change of samples (Green to Red). Consequently, the results demonstrate the utility of using PDDA-QDs as energy donors and established the groundwork for the design and implementation of QDs-based biosensors with FRET.

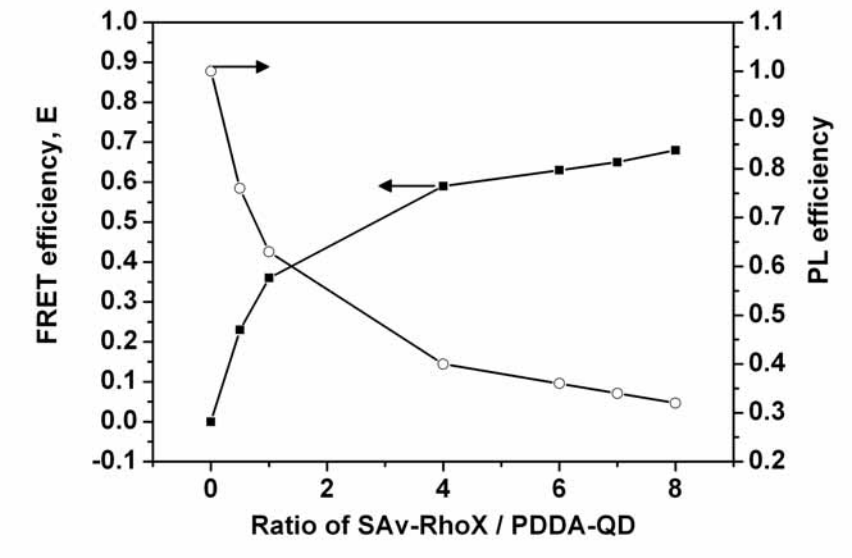

Figure 4.9 PL and FRET efficiencies as a function of the SAv-Rhodamine/PDDA-QDs molar ratio.

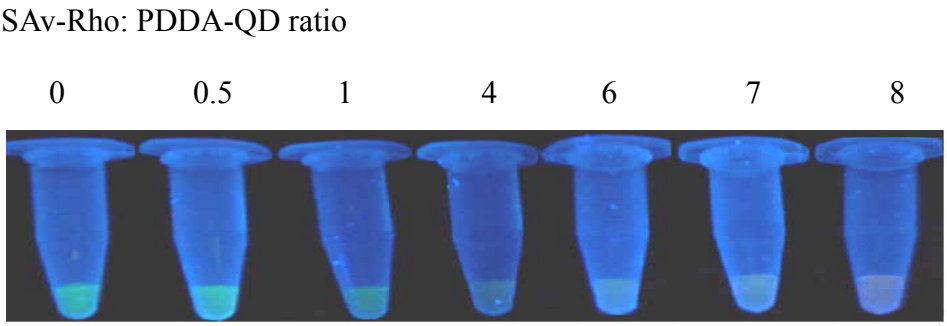

Figure 4.10 The fluorescence of SAv-Rhodamine/PDDA- QDs with molar ratio (0- 8) under 365 nm excited.

4.4 Conclusions

A new synthesis method was developed to produce high luminescence PDDA-QDs by polymer encapsulated with photoactivation under table lamp (intensity 8.5 mW/cm^2) irradiated, 26 hour, and room temperature. The PL intensity and the emission spectrum of PDDA-QDs were significantly enhancement (200 fold) and blue-shifted (29 nm) comparing with MSA-QDs. The new synthesis could fabricate the multicolor QDs with high luminescence, Q.Y, and well distribution. The TEM and Agarose Gel Electrophoresis results showed the small and homogenous size of the PDDA-QDs. The surface properties of PDDA-QDs can be monitored by XPS and analyzed the elements of the composition. Particularly, the PDDA-QDs supported the high luminescence and surface charge with Streptavidin-Rhodamine to realize the Fluorescence Resonance Energy Transfer (FRET) model with

PDDA-QDs with dye. In this study, the high throughput and high luminescence PDDA-QDs possesses many advantages, including simplicity, high luminescence, and stability.

4.5 Reference

[1] H. Zhang, C. Wang, M. Li, X. Ji, J. Zhang, B. Yang, *Chem. Mater.* 17 **(2005)** 4783.

[2] Z. Zhelev, R. Bakalova, H. Ohba, R. Jose, Y. Imai, Y. Baba, *Anal. Chem*. 78 **(2006)** 321.

[3] D. Gerion, F. Pinaud, S. C. Williams, W. J. Parak, D. Zanchet, S.Weiss, A. P.Alivisatos, *J. Phys. Chem. B*. 105 **(2001)** 8861.

[4] C. A. Constantine, K. M. Gattas-Asfura, S. V. Mello, G.Crespo, V. Rastogi, T-C. Cheng, J. J. DeFrank, R. M. Leblanc, *J. Phys. Chem. B.* 107 **(2003)** 13762.

[5] X. Ji, J.Zheng, J. Xu, V. K. Rastogi, T-C. Cheng, J. J. DeFrank, R. M. Leblanc, *J. Phys. Chem. B.* 109 **(2005)** 3793.

[6] J. A. Kloepfer, S. E. Bradforth, J. L. Nadeau, *J. Phys. Chem. B.* 109 **(2005)** 9996.

[7] S. F. Wuister, C. M. Donega, A. Meijerink, *J. Phys. Chem. B.* 108 **(2004)** 17393.

[8] T. Torimoto, S. Murakami, M. Sakuraoka, K. Iwasaki, K. Okazaki, T. Shibayama, B. Ohtani, *J. Phys. Chem. B.*110 **(2006)** 1331

[9] M. Jones, J. Nedeljkovic, R. J. Ellingson, A. J. Nozik, G. Rumbles, *J. Phys. Chem. B.* 107 **(2003)** 11346**.**

[10] J. Aldana, Y. A. Wang, X. Peng, *J. Am. Chem. Soc.* 123 **(2001)** 8844.

[11] Y. Wang, Z. Tang, Miguel A. Correa-Duarte, Isabel. Pastoriza-Santos, Michael. Giersig, Nicholas A. Kotov, L. M. Liz-Marza´n, *J. Phys. Chem. B.* 108 **(2004)** 15461.

[12] W. G. J. H. M. Sark, P. L. T. M. Frederix, D. J. V. Heuvel, H. C. Gerritsen, *J. Phys. Chem. B.* 105 **(2001)** 8281.

[13] L. Manna, E. C. Scher, L-S. Li, A. P. Alivisatos, *J. Am. Chem. Soc.* 124 **(2002)** 7136.

[14] J. A. Gaunt, A. E. Knight, S. A. Windsor, V. Chechik, *J. Coll. Inter. Sci.* 290 **(2005)** 437.

[15] S. R. Cordero, P. J. Carson, R. A. Estabrook, G. F. Strouse, and S. K. Buratto, *J. Phys. Chem. B.* 104 **(2000)** 12137.

[16] S. Zhang, J. Yu, X. Li ,W. Tian, *Nanotechnology* . 15 **(2004)** 1108.

[17] A. T. R. Williams, S. A. Winfield, J. N. Miller, *Analyst*, 108 **(1983)** 1067.

[18] X. G. Peng, L. Manna, W. D.Yang, J. Wickham, E. Scher, A. Kadavanich, and A. P. Alivisatos, *Nature.* 404 **(2000)** 59.
[19] W. C. W. Chan and S. M. Nie, *Science.* 281 **(1998)** 2016.
[20] C. Bullen , P. Mulvaney, *Langmuir* 22 (**2006)** 3007.
[21] X. Wang, L.Qu, J. Zhang, X. Peng, M. Xiao, *Nano Lett.,* 3 (**2003)** 1103.
[22] N. Myung, Y. Bae, A.J. Bard, *Nano Lett.,* 3 **(2003)** 747.
[23] S. Maenosono, N. Eiha, and Y. Yamaguchi, *J. Phys. Chem. B.* 107 **(2005)** 2645.
[24] A. R. Clapp, I. L. Medintz, J. M. Mauro, B. R. Fisher,M.G. Bawendi, H. Mattoussi, *J. Am. Chem. Soc.* 126 **(2004)** 301.
[25] C. Luccardini, C. Tribet, F. Withl, V. Marchi-Artzner, M. Dahan, *Langmuir*, 22 **(2006)** 2304.

Chapter 5 FRET-based biosensing system with PDDA-QDs/KSI and Cholic acid-TMR

Abstract:

In this study, we have explored the potential of PDDA-QDs as fluorescent donors in a FRET based assay. A tetramethylrhodamine (TMR), serving as the energy acceptor, is covalently labeled to Δ 5-3-ketosteroid isomerase (KSI), and this dye-enzyme complex was immobilized on the PDDA-QDs surface with electrostatic interaction. Using this configuration, we explored the effects of varying the ratio of dye-labeled enzymes attached to the PDDA-QDs. These results show the progressive quenching of the PDDA-QDs emission and subsequent enhancement of the dye PL signal with increasing number of dye-labeled enzymes immobilized on the QDs surface. Then, we extend our sensor design beyond the initial prototype and demonstrate a self-assemble PDDA-QDs based FRET sensor for the detection of Cholic acid (Cholic acid). A dyelabeled Cholic acid bound in the PDDA-QDs/ KSI and quenches the luminescence of QDs with proximity induced FRET. This result could support the binding constant (K_D) of Cholic acid-TMR with KSI from FRET efficiency between QDs with TMR. Then, we also demostrate the competition reaction between Cholic-TMR and 4-Estren-17b-OL-3-ONE (19NT) based on the FRET system with the PDDA-QDs/KSI. The FRET based system of PDDA-QDs/KSI could assay ~1.86 μM (19NT) under various concentration of Cholic-TMR (0.135μM ~ 0.894μM). Consequently, the FRET based sensing system has some advantages, such as non-immobilized enzyme; high throughput and low cost, to apply into the biosensor designing.

5.1 Introduction

Accurate and sensitive detection of water-soluble analytes, such as toxins, small molecule explosives, carbohydrates, ionic species, and various biomolecules including DNA, proteins, and peptides is a highly explored scientific goal with ramifications in healthcare, safety, and defense applications [1-2]. The interaction of a target molecule (analyte) with a protein receptor in a biological recognition process is often associated with a change in the protein conformation as a response to the binding matrix. Therefore, designing and developing recognition-based sensing systems that can account for such changes with a transduction signal in a medium of interest are the focus of many research groups [1,3-6]. Previous researchers suggest that utilizing Forster resonance energy transfer (FRET) between a fluorescent donor molecule bound to the target and an acceptor attached to a receptor protein have been widely used to study receptor-ligand interactions and changes in protein conformation upon binding to a target analyte or used as a response to changes in the solution conditions (temperature, pH conditions, ets.) [1]. While FRET has already been used extensively for biological application; difficulties still remain when using conventional organic dyes as the interacting donor-acceptor pair. Because of organic dyes have some shortcomings in the donor-acceptor FRET designing, including narrow absorption spectra, broad emission with long tailing, very low photobleaching thresholds, and low Stockes shifts. While the overall energy transfer may be efficient in these systems, there is often significant emission overlap that indefinites the individual behavior of the

donor or acceptor and leads to complications in data analysis [1]. For that reason, colloidal QDs have unique optical and spectroscopic properties that possess several inherent advantages over organic dyes and can offer a compelling alternative to traditional fluorophores in several fluorescence-based assay applications. Furthermore, QDs show size dependent and tunable absorption and photoemission properties due to quantum confinement of the charge carriers (electron-hole pairs) [1,7-10]. The broad absorption spectra would allow flexibility in choosing the desired excitation wavelength in FRET system where direct excitation of the acceptor molecules can be substantially reduced.

Δ5-3-ketosteroid isomerase (KSI) [11-12] catalyzes allylic isomerization of the 5,6 double bond of 5-3-ketosteroids to the 4,5 position at a rate approaching the diffusion limit by an intramolecular transfer of a proton with a dienolate intermediate (Figure 5.1). In the isomerization reaction catalyzed by KSI, Asp-38 acts as the base responsible for shuttling the 4α-proton to the 6α-position in the steroid substrate [13-14], and a dienolate intermediate generated during catalysis is stabilized by two electrophilic catalysts, Tyr-14 and Asp-99 [15-16]. While it has been generally agreed that both Tyr-14 and Asp-99 contribute to catalysis by stabilizing the intermediate through hydrogen bonding, the exact mechanism and the nature of the stabilization by these residues have been rather controversial until recently [11,15]. Cholic acid (CA) and 4-Estren-17b-OL-3-ONE (19NT), product analogues, have served as a useful probe for investigating the active site of isomerase and for measuring the enzymesteroid binding affinity.

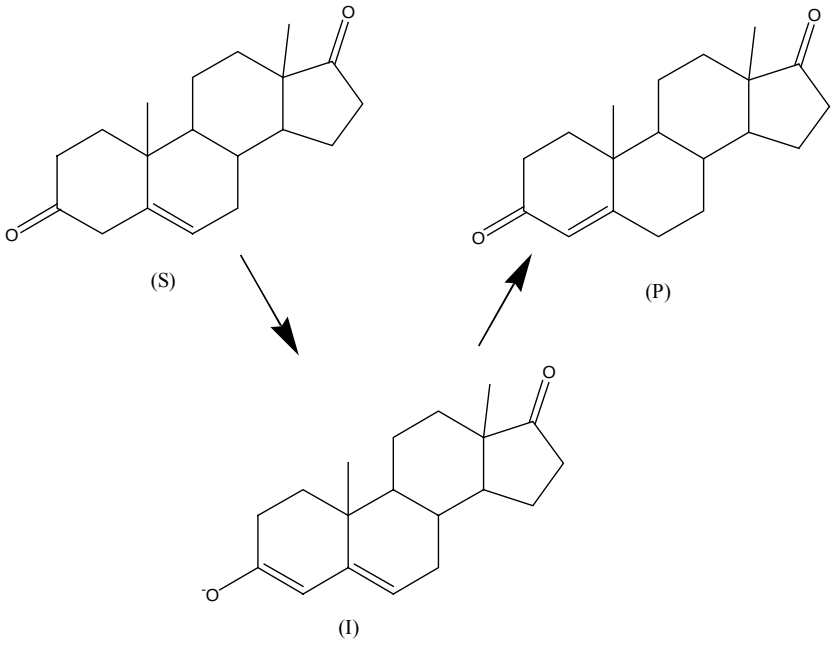

Figure 5.1 Reaction catalyzed by ketosteroid isomerase. The α proton at C-4 is transferred to the α side of C-6 during the isomerization reaction. The substrate (**S**), 5-androstene-3, 17-dione, is converted to the product (**P**), 4-androstene-3,17-dione, with the dienolate intermediate (**I**) [11].

In the present study, we have explored the potential of PDDA-QDs as fluorescent donors in a FRET based assay. A tetramethylrhodamine (TMR), serving as the energy acceptor, is covalently labeled to a Δ 5-3-ketosteroid isomerase (KSI), and this dye-enzyme complex was immobilized on the QDs surface with electrostatic interaction. Using this configuration, we explored the effects of varying the ratio of dye-labeled enzymes attached to the PDDA-QDs. We also found that the measured FRET efficiency for a fixed acceptor dye increased substantially with increasing number of dye-labeled enzymes during a titration sequence. This results from progressive quenching of the PDDA-QDs emission and subsequent enhancement of the dye PL signal with increasing number of

dye-labeled enzymes immobilized on the QDs surface. Then, we extend our sensor design beyond the initial prototype and demonstrate a self-assemble PDDA-QDs based FRET sensor for the detection of CA. A dyelabeled CA bound in the KSI/PDDA-QDs and quenches the luminescence of QDs with proximity induced FRET. This result could support the binding constant (K_D) of CA-TMR with KSI from FRET efficiency between QDs with TMR. Continuously, we also demostrate the competition reaction between Cholic-TMR and 19NT based on the FRET system with the PDDA-QDs/KSI. The FRET based system of PDDA-QDs/KSI could assay ~1.86 μM (19NT) under various concentration of CA-TMR (0.135μM ~ 0.894μM).

5.2 Materials and Methods

5.2.1 Instruments and chemicals

A Jobin-Yvon Spex Fluolog-3 spectrophotometer were used to investigate the fluorescence characteristics of the samples. The detail synthesis protocols of PDDA-QDs were described on ***Chapter 4 (materials and Methods)***. The KSI and CA-TMR were prepared by ***Ko Shing Chang (Prof. Li's Lab)***.

5.2.2 Assay condition of the FRET between PDDA-QDs with KSI-TMR

FRET investigated by reacting 10 μl aliquots PDDA-QDs (6.6 μM) solution with 0~100 μl KSI-Rhodamine (19.8 μM) in 20 mM phosphate buffer solution, pH 7.5. After 1 hour of incubation time, the reaction mixtures were diluted to total 200 μl in PB buffer, and the resulting

solutions were placed in 1 cm path length quartz curvettes for photolumiscence measurement.

5.2.3 Assembly of the KSI-Bound Dye-Labeled analogue with QDs and FRET Quenching Assays

20μl of KSI solution (2.99 $\times 10^{-5}$M) and 10μl PDDA-QDs (9.9 $\times 10^{-6}$ M) were mixed together and incubated for 1 hour, 4°C in the dark. Phosphate buffer solution (20 mM, pH 7.5) was added to each tube to give a final volume of 120μl. To these solutions were added varying amounts of CA-TMR (0~ 70μl of 2.55×10^{-6}M, the concentration were calculated by A_{550}, ε = 65000 cm-1M^{-1}), and the mix was incubated at 4° C for about 15 min. These solutions were further adjusted by adding phosphate buffer solution (20 mM, pH 7.5) to each tube to final values of 200μl, and the resulting solutions were placed in 1 cm path length quartz curvettes for photolumiscence measurement. The assay model was shown in Figure 5.2.

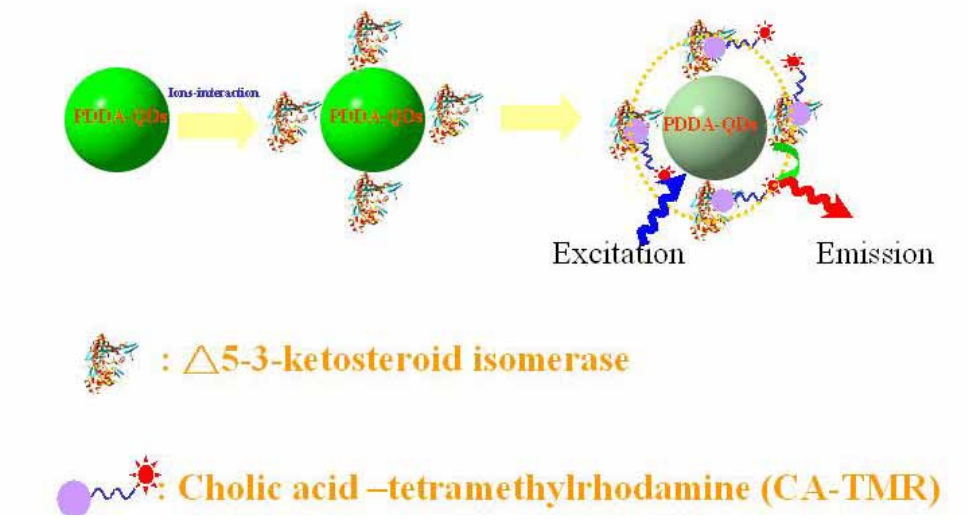

Figure 5.2 FRET-based biosensing model with PDDA-QD/KSI and CA -TMR.

5.2.4 Condition of Sensor Function and Determination of 19NT Concentration

20μl of KSI solution (2.99 $\times 10^{-5}$M) and 10μl PDDA-QDs (9.9 $\times 10^{-6}$ M) were mixed together and incubacted for 1 hour, 4°C in the dark. Phosphate buffer solution (20 mM, pH 7.5) was added to each tube to give a final volume of 120μl. To these solution were added with the mixed solution, which obtain varying amounts of CA-TMR (0~0.894μM) and 19NT (0~1.865μM), and the mixture was incubated at 4°C for about 15 min. These solutions were further adjusted by adding phosphate buffer solution (20 mM, pH 7.5) to each tube to final values of 200μl, and the resulting solutions were placed in 1 cm path length quartz curvettes for photolumiscence measurement.

5.3 Results and discussion

5.3.1 Spectra

We prepare two emission properties of PDDA-QDs (530 nm, 543 nm), and red emission organic dye (TMR) with absorption ranges around 500 to560 nm. Figure 5.3 display absorption and emission spectra obtained from solution of the PDDA-QDs and CA-TMR sample used in these experiments. The PDDA-QDs sizes were chosen so as to maximize the spectral overlap of the donor-acceptor emission and absprption spectra while still maintaining good spectral resolution of the donor and acceptor emission.

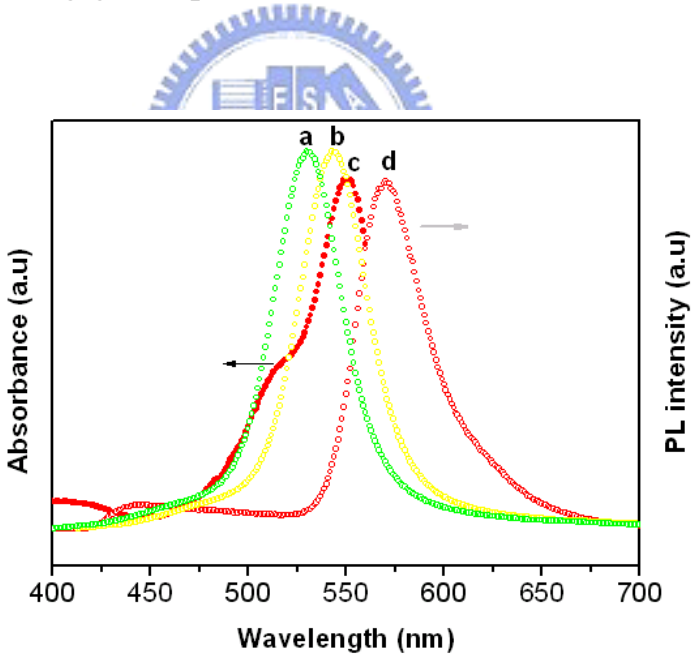

Figure 5.3 Normalized spectra of (a) emission of PDDA-QDs (530 nm) (b) emission of PDDA-QDs (543 nm) (c) absorption of CA-TMR (d) emission of CA-TMR (580 nm) excited 400 nm. All spectra were recorded in PB (20 mM, pH 7.5).

5.3.2 FRET efficiency between PDDA-QDs with KSI-TMR

Figure 5.4 shows the PL spectrum of the PDDA-QDs (530 nm) donor and TMR dye (580nm) acceptor for each ratio (in titration series KSI-TMR) for the PDDA-QDs-due pairs used. In all cases, raw PL spectra were corrected to account for direct excitation of the acceptor and deconcentrated to provide separate signals characteristics of the QD and TMR fluorophores. Although the acceptor absorption was minimized under excitation at 400 nm (within the valley of TMR absorption spectrum), the appreciable PL signal could be measured in the case. The result showed that there is a clear progression in the fluorophore emission as a function of increasing number of KSI-TMR, namely a progressive quenching of the PDDA-QDs emission and a systematic enhancement of the TMR emission as the number of dyes surrounding the PDDA-QDs increased from 0 to 30.

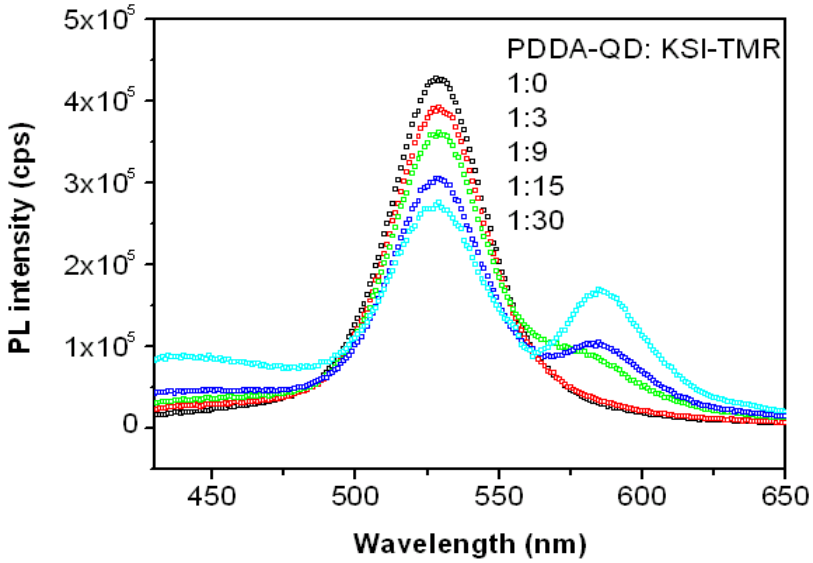

Figure 5.4 PL spectrum of the PDDA-QDs (530 nm) donor and TMR dye (580 nm) acceptor for each ratio (in titration series KSI-TMR) for the PDDA-QDs-due pairs used.

Figure 5.5 depicts the integrated PL signals for the 530 nm emitting PDDA-QDs, as a function of the KSI-TMR/PDDA-QDs ratio. We also reported the values for the expected acceptor integrated PL intensity extracted from the FRET efficiency (E). In the case, the trends are consistent as a progressive increase in the acceptor emission follows the expected energy gain. These results strongly suggest that FRET is the primary mechanism for the reported observations.

Figure 5.6 displays the emission spectrum observed from a sample containing 0.33 μM PDDA-QDs, 0.33μM PDDA-QDs/ 2.1μM KSI-TMR and 2.1μM KSI-TMR under 400 nm excited. The result indicated that the KSI-TMR could not be excited efficiency under 400 nm excited. However, this should be compared with the 3-fold enhancement in the TMR fluorescence observed for the 0.33μM PDDA-QDs/ 2.1μM KSI-TMR solution, which confirms that the enhanced fluorescence in this solution is due to PDDA-QD-TMR FRET.

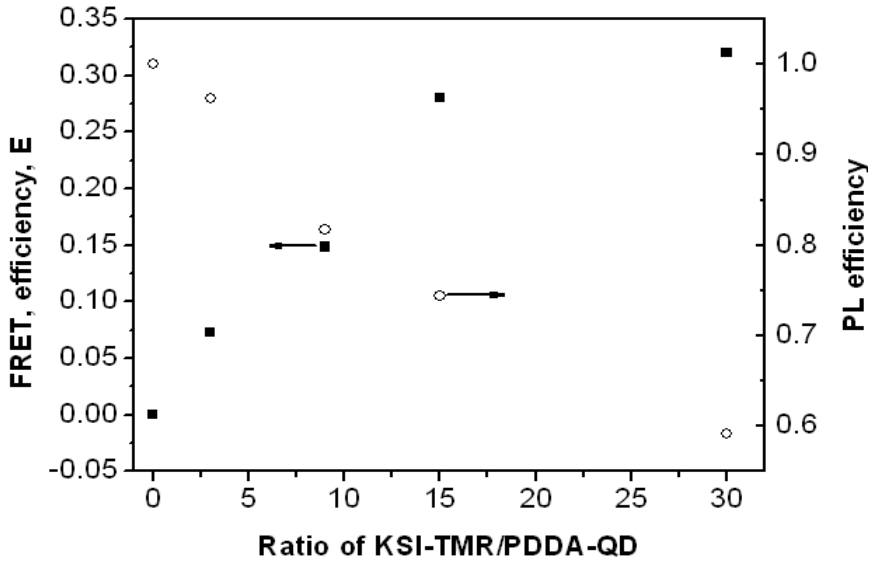

Figure 5.5 PL and FRET efficiencies as a function of the KSI-TMR /PDDA-QDs molar ratio.

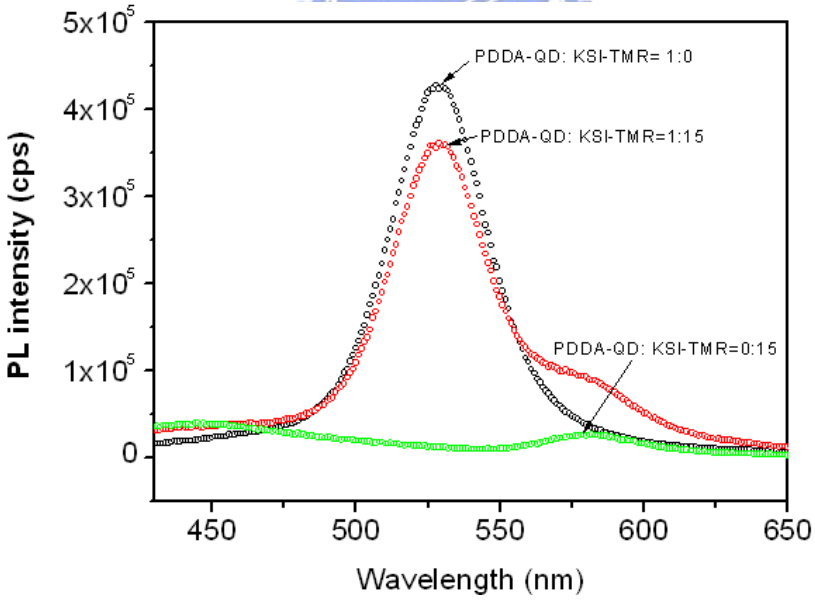

Figure 5.6 The emission spectrum observed from a sample containing 0.33 μM PDDA-QDs, 0.33μM PDDA-QDs/ 2.1μM KSI-TMR and 2.1μM KSI-TMR under 400 nm excited.

5.3.3 Assembly of the KSI-Bound Dye-Labeled analogue with QDs and FRET Quenching Assays

In order to improve the FRET efficiency between PDDA-QDs and TMR, we choice the PDDA-QDs with 543 nm emission, which could be increased efficiency energy transfer area. Binding assays conditions were described by ***Material and Method***. The binding constant of Cholic acid (K_D = 0.268 μM), a product analogue, has served as a useful probe for the active site of isomerase and for measuring the enzymesteroid binding affinity. When Cholic acid binds to isomerase, which are assembled on PDDA-QDs surface, a progressive and substantial QD populations quenched in the energy transfer efficiency with increasing number of CA-TMR attached to a single nanocrystal. Figure 5.7 displays the emission spectra observed for these samples. Emission spectra obtain from 0.495μM PDDA-QDs/ 2.99μM KSI and varying amounts of CA-TMR (0 to 3.5μM) are also shown for comparison. An excitation wavelength of 400 nm was used for all samples. At this wavelength, PDDA-QDs excitation occurs with high efficiency, while direct TMR excitation is minimal (see Figure 5.3). The strong enhancement in the TMR fluorescence observed for the PDDA-QDs-KSI/CA-TMR solution is consistent with PDDA-QDs and TMR FRET due to binding of CA-TMR and QD-KSI. However, when PDDA-QDs (0.495μM) mixed with CA-TMR (0~0.77μM) in the phosphate buffer (20 mM, pH 7.5), there are not apparent quenched phenomenon on the PDDA-QDs (as shown in Figure 5.9). As a result of KSI do not assemble on the PDDA-QDs, and serve the bridge of energy transfer between donor and acceptor. Therefore, the FRET-based model is suitable for biomolecule

assay. Figure 5.8 indicated that the FRET efficiency between PDDA-QDs-KSI and CA-TMR are obtained from Figure 5.7. The K_D (0.25 μM) value of CA-TMR was derived from the FRET efficiency of PDDA-QDs. Therefore; the FRET-based biosensing model could achieve

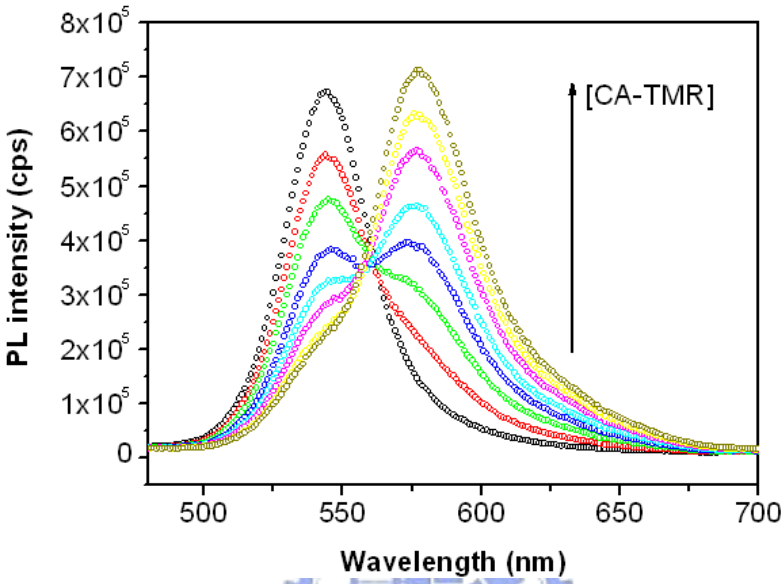

high sensitivity in assay biomolecule and monitor the enzyme activity.

Figure 5.7 Emission spectra obtain from 0.495μM PDDA-QDs/ 2.99μM KSI and varying amounts of CA-TMR (0 to 0.89μM) are also shown for comparison. An excitation wavelength of 400 nm was used for all samples.

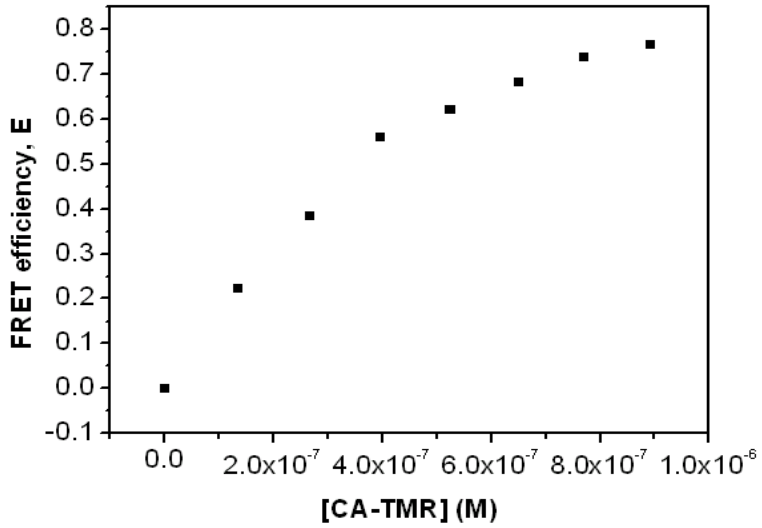

Figure 5.8 The FRET efficiency between PDDA-QDs-KSI and CA-TMR are obtained from Figure 5.7.

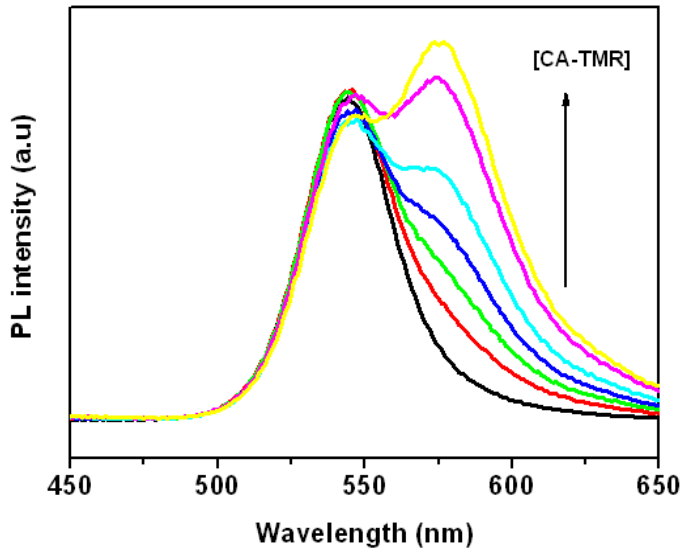

Figure 5.9 Emission spectra obtain from 0.495μM PDDA-QDs and varying amounts of CA-TMR (0 to 0.77μM) are also shown for comparison. An excitation wavelength of 400 nm was used for all samples.

5.3.4 Sensor Function and Determination of 19NT Concentration

We examined the ability of the PDDA-QDs/KSI conjugates to assay 19NT concentration in the mixture solutions (CA-TMR with 19NT solutions). The scheme of sensing model was shown in Figure 5.10. Starting from samples made of PDDA-QDs/KSI conjugates mixed with various concentration CA-TMR and 19NT, the FRET efficiency was monitored at 543 nm PDDA-QDs. Figure 5.11 shows a typical experiment examining changes in the FRET efficiency of 543 nm emitting PDDA-QDs with increasing concentrations of above mixed solutions. The data show a systematic recovery of the FRET efficiency of donor with increasing 19NT concentration, indicating a progressive concentration-dependent loss of FRET between the PDDA-QDs and the 19NT as the target analyte concentration was increased. These results prove that the added 19NT displaced the analogue acceptor away (CA-TMR) from KSI, reducing the rate of FRET, which indicates the ability of our designed PDDA-QDs/KSI/19NT assembly to function as an effective sensor based on FRET. According the results, the FRET based sensing system could assay 1.86 μM 19NT under various concentration of CA-TMR. These observations confirm our finding with the prototype solution-phase PDDA-QDs/KSI sensor assembly where we showed that surface assembled KSI maintained their affinity toward their 19 NT substrate.

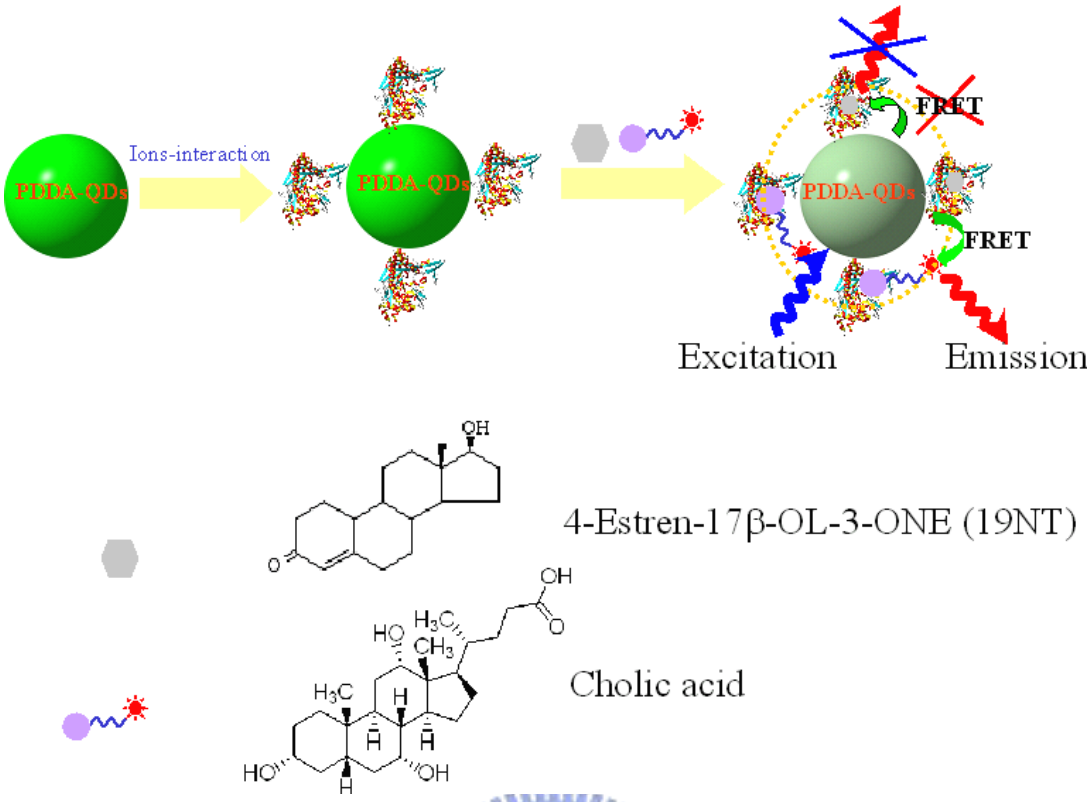

Figure 5.10 The scheme of sensing model with PDDA-QDs/KSI in the mixed solution (CA-TMR and 19NT).

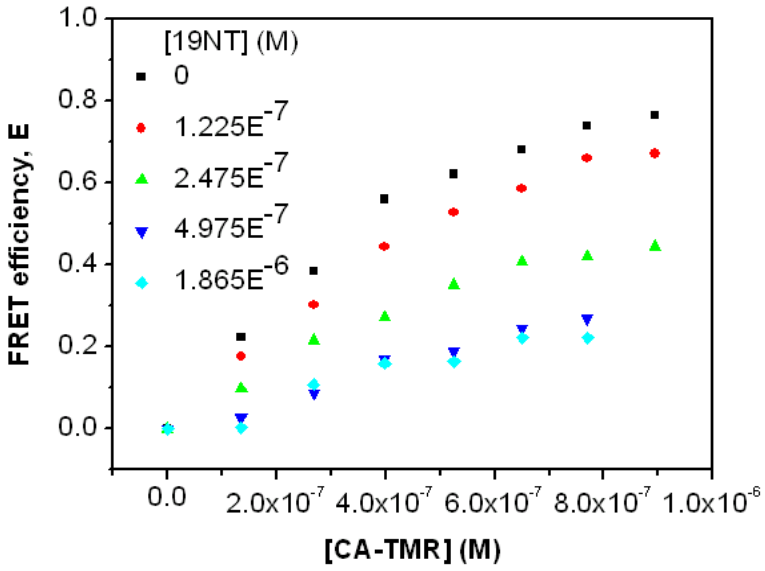

Figure 5.11 shows a typical experiment examining changes in the FRET efficiency of 543 nm emitting PDDA-QDs with increasing concentrations of mixed solutions (CA-TMR and 19NT).

5.4 Conclusion

PDDA-QDs/ KSI and CA-TMR system demonstrated a FRET-based biosensing. We could turn the emission spectrum of PDDA-QDs to achieve high-energy overlapping efficiency with TMR organic dye. In order to realize the FRET system, first, we used PDDA-QDs (donor) and KSI-TMR (acceptor) to study the energy transfer efficiency. Although the FRET efficiency are not high percentages, we also could see the energy transfer between QD and TMR. However, we turn the emission spectrum of PDDA-QDs to improve the FRET efficiency and realized the biosensing with the FRET-based system. We have shown that the binding constant of CA-TMR (0.25 μM) was derived from the FRET efficiency of PDDA-QDs. Therefore, the FRET-based biosensing system could realize by PDDA-QDs and organic dye interaction with constant distance. Furthermore, the competition reaction, which obtains CA-TMR and 19NT, based on the FRET efficiency could assay 1.86 μM 19NT by PDDA-QDs/KSI. These observations confirm our finding with the prototype solution-phase PDDA-QDs/KSI sensor assembly where we showed that surface assembled KSI maintained their affinity toward their 19 NT substrate. Consequently, the FRET based sensing system has some advantages, such as non-immobilized enzyme; high throughput and low cost, to apply into the biosensor designing.

5.5 Reference

[1] Aaron R. Clapp, Igor L. Medintz, J. Matthew Mauro, Brent R. Fisher, Moungi G. Bawendi, Hedi Mattoussi, *J. Am. Chem. Soc.* 126 **(2004)** 301.

[2] S. S. Iqbal, M. W. Mayo, J. G. Bruno, B. V. Bronk, C. A. Batt, J. P. Chambers, *Biosens. Bioelectron.*15 (**2000)** 549.

[3] D. E. Benson, D. W. Conrad, R. M. de Lorimer, S. A. Trammell, H. W. Hellinga, *Science* 293 (**2001)** 1641.

[4] P. J. O Connell, G. G. Guilbault, *Anal. Lett.* 34 (**2001)** 1063.

[5] H. W. Hellinga, J. S. Marvin, *Trends Biotechnol.* 16 **(1998)** 183.

[6] L. L. Looger, M. A. Dwyer, J. J. Smith, H. W. Hellinga, *Nature* 423 **(2003)** 185.

[7] C. B. Murray, D. J. Norris, M. G. Bawendi, *J. Am. Chem. Soc.*115 (**1993)** 8706.

[8] L. Qu, Z. A. Peng, X. Peng, *Nano Lett.* 1 (**2001)** 333.

[9] S. V. Gaponenko, *Optical Properties of Semiconductor Nanocrystals*; Cambridge University Press: Cambridge, **(1998).**

[10] A. P. Alivisatos, *Science* 271 **(1996)** 933.

[11] G. Choi, N-C Ha, S.W. Kim, D-H Kim, S. Park, B-H Oh, K. Y. Choi, *Biochemistry* 39 (**2000)** 903.

[12] J. M. Schwab, B. S. Henderson, *Chem. Rev.* 90 **(1990)** 1203.

[13] A.Kuliopulos, A. S. Mildvan, D. Shortle, P. Talalay. *Biochemistry* 28 **(1989)** 149.

[14] L. Xue, A. Kuliopulos, A. S. Mildvan, P. Talalay, *Biochemistry* 30 **(1991)** 4991.

[15] Q. Zhao, C. Abeygunawardana, A. G. Gittis, A. S. Mildvan, *Biochemistry* 36 **(1997)** 14616.

Chapter 6 Conclusion

In this work, we achieve several goals as below: ***At First, the CdSe/ZnS QDs surface has been modified to contain carboxyl group and applied to detect urea and glucose based on luminescence properties of QDs.*** We demonstrate that the water-soluble QDs are fabricated through mercaptosuccinic acid ligand exchange with various emission spectra, which depend on the size. Then, the luminescence properties of MSA-QDs, which confide the acid or base in the environment, can be utilized as a reliable agent for the enzymatic determination of urea and glucose concentration. The MSA-QDs exhibite linear response in PL intensity, whose urea concentration is from 0.01 to 100 *m*M. Additionally, this new approach, glucose can be successfully analyzed with wide concentration range. As compared to other urea and glucose sensors (indicator) presented in the literatures, the MSA-QD-based biosensor exhibits several advantages, such as the ease of its fabrication, low cost, no enzyme immobilization process required, high flexibility, and good sensitivity. It offers a persuasive way to determine the urea and glucose concentration without using complicate instrumental application. ***Second, the quantum efficiency of water-soluble QDs (MSA-QDs)has been improved to suit for lipid (triglyceride) assay, where the MSA-QDs must be photoactivated through fluorescent lamp and more hydrophobic sites on the QDs surface have to been created to soluble the triglyceride.*** In this work, the fluorescent lamp is employed as photoactivation source, which contains

wide band spectra, and easily gets high performance luminescence POD-QDs with low aggregation phenomena. This study demonstrates an assay system containing POD-QDs and lipase for the quantitative analysis of triglyceride. With this novel approach, triglyceride in a wide range of concentration can be successfully analyzed. As compared to traditional triglyceride assay methods, the POD-QDs-based detection exhibits several advantages, such as ease of reagent preparation, low cost, no enzymatic immobilization, high flexibility, and good sensitivity. The newly developed method can quantitatively determine triglyceride without using multiple enzymes and/or complicated instrument setup.

Third, the quantum efficiency of water-soluble QDs (MSA-QDs) has been improved with PDDA capped and photoactivation realized the FRET-based biomolecule assay. A simple method is proposed to improve QDs luminescence, which contains the photoactivation and polymer (PDDA) capped under the fluorescent lamp irradiation. A new synthesis method is developed to produce high luminescence PDDA-QDs by polymer encapsulated with photoactivation under table lamp (intensity 8.5 mW/cm^2) irradiated, 26 hour, and room temperature. The PL intensity and the emission spectrum of PDDA-QDs are significantly enhancement (200 fold) and blue-shifted (29 nm) comparing with MSA-QDs. The novel synthesis can fabricate the multicolor QDs with high luminescence, Q.Y., and well distribution. The TEM and Agarose Gel Electrophoresis results show the small and homogenous size of the PDDA-QDs. The surface properties of PDDA-QDs can be monitored by XPS and analyzed the elements of the composition. Particularly, the PDDA-QDs supports the high luminescence and surface charge with Streptavidin-Rhodamine

to realize the Fluorescence Resonance Energy Transfer (FRET) model with PDDA-QDs with dye. Additionally, the emission spectrum of PDDA-QDs is turned to achieve high-energy overlapping efficiency with TMR organic dye. To complete the FRET system, the PDDA-QDs (donor) and KSI-TMR (acceptor) are employed to study the energy transfer efficiency. Although the FRET efficiency is not high percentages, the energy transfer is observed between QD and TMR. However, the emission spectrum of PDDA-QDs is turned to improve the FRET efficiency and realize the biosening with the FRET-based system. The binding constant of CA-TMR (0.268 μM) is derived from the FRET efficiency of PDDA-QDs. Furthermore, the competition reaction, which obtain CA-TMR and 19NT, based on the FRET efficiency can assay 1.86 μM 19NT by PDDA-QDs/KSI. These observations confirm our finding with the prototype solution-phase PDDA-QDs/KSI sensor assembly where we show that surface assembled KSI maintain their affinity toward their 19 NT substrate. Consequently, the FRET-based biosensing system can be realized by PDDA-QDs and organic dye interaction with constant distance. In this study, the high throughput and high luminescence PDDA-QDs have many advantages, including simplicity, high luminescence, and good stability. Finally, we summarized characterizations of our research areas in Figure 6.1.

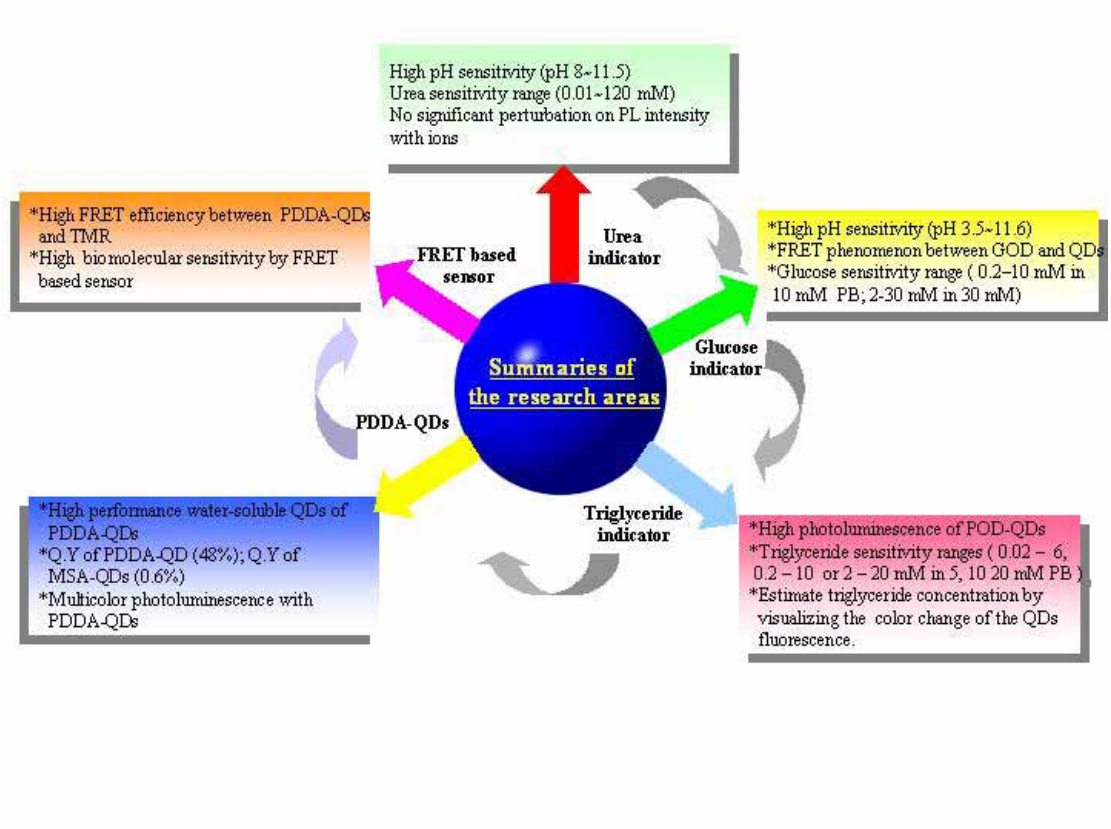

Figure 6.1 Summaries of the research areas.